1994-03

Life cycle cost/cost-effectiveness analysis of U.S. Army Recruits : high quality versus low quality

Funk, David M.

Monterey, California. Naval Postgraduate School

NAVAL POSTGRADUATE SCHOOL
Monterey, California

THESIS

Damage and Compressive Failure of
Unbalanced Sandwich Composite Panels
Subject to a Low-Velocity Impact

by

L. Bryant Fuller

March 1994

Thesis Advisor: Young W. Kwon

Approved for public release; distribution is unlimited

REPORT DOCUMENTATION PAGE

Form Approved OMB No. 0704

1. AGENCY USE ONLY	2. REPORT DATE 17 March 1994	3. REPORT TYPE AND DATES COVERED Master's Thesis

4. TITLE AND SUBTITLE Damage and Compressive Failure of Unbalanced Sandwich Composite Panels Subject to a Low-Velocity Impact

5. FUNDING NUMBERS

6. AUTHOR(S) *FULLER, L. Bryant*

7. PERFORMING ORGANIZATION NAME(S) AND ADDRESS(ES)
Naval Postgraduate School
Monterey, CA 93943-5000

8. PERFORMING ORGANIZATION REPORT NUMBER

9. SPONSORING/MONITORING AGENCY NAME(S) AND ADDRESS(ES)

10. SPONSORING/MONITORING AGENCY REPORT NUMBER

11. SUPPLEMENTARY NOTES The views expressed in this thesis are those of the author and do not reflect the official policy or position of the Department of Defense or the U.S. Government.

12a. DISTRIBUTION/AVAILABILITY STATEMENT
Approved for public release; distribution is unlimited.

12b. DISTRIBUTION CODE
*A

13. ABSTRACT

An unbalanced sandwich composite structure consisting of titanium and glass reinforced plastic (GRP) facesheets with a phenolic honeycomb core will be used for construction of a surface ship mast. Principle areas of concern in using these composites in primary load-bearing applications are the response due to compressive loads and the effects of low-velocity impact damage. This research focuses on experimental studies of the compressive strength after impact (CAI) of unbalanced sandwich composite beams. The beams, in simply supported configurations, are impacted transversely and then subjected to a compressive axial loads. Samples are impacted on both the titanium and GRP sides. Additionally, the composites are statically loaded on each side. This study investigates initiation and progress of damage in the unbalanced sandwich beams caused by various impact loads. In addition, effects on the compressive failure load resulting from the various impact loadings are examined.

14. SUBJECT TERMS
Unbalanced sandwich composite, low-velocity impact, compressive strength after impact, damage

15. NUMBER OF PAGES 106

16. PRICE CODE

17. SECURITY CLASSIFICATION OF REPORT	18. SECURITY CLASSIFICATION OF THIS PAGE	19. SECURITY CLASSIFICATION OF ABSTRACT	20. LIMITATION OF ABSTRACT
Unclassified	Unclassified	Unclassified	UL

NSN 7540-01-280-5500

Standard Form 298 (Rev. 2-89)
Prescribed by ANSI STD. 239-18

Approved for public release; distribution is unlimited.

Damage and Compressive Failure of
Unbalanced Sandwich Composite Panels
Subject of a Low-Velocity Impact

by

L. Bryant Fuller
Lieutenant, United States Navy
B.S., University of Tennessee, 1984

Submitted in partial fulfillment
of the requirements for the degree of

MASTER OF SCIENCE IN MECHANICAL ENGINEERING

from the

NAVAL POSTGRADUATE SCHOOL
March 1994

Author: [redacted]
L. Bryant Fuller

Approved by: [redacted]
Dr. Young W. Kwon, Thesis Advisor

[redacted]
Matthew D. Kelleher, Chairman
Department of Mechnical Engineering

ABSTRACT

An unbalanced sandwich composite structure consisting of titanium and glass reinforced plastic (GRP) facesheets with a phenolic honeycomb core will be used for construction of a surface ship mast. Principle areas of concern in using these composites in primary load-bearing applications are the response due to compressive loads and the effects of low-velocity impact damage. This research focuses on experimental studies of the compressive strength after impact (CAI) of unbalanced sandwich composite beams. The beams, in simply supported configurations, are impacted transversely and then subjected to compressive axial loads. Samples are impacted on both the titanium and GRP sides. Additionally, the composites are statically loaded on each side. This study investigates initiation and progress of damage in the unbalanced sandwich composite beams caused by various impact loads. In addition, effects on the compressive failure load resulting from the various impact of loadings are examined.

TABLE OF CONTENTS

LIST OF FIGURES

LIST OF TABLES

ACKNOWLEDGEMENT

I would like to express my sincerest appreciation to Professor Young W. Kwon for his expert guidance, excellent instruction and patience during the course of this thesis.

Second, my thanks to Jim Scholfield and Tom Christian for the outstanding assistance and support in helping assemble and operate the all the experimental equipment and instrumentation required to conduct this study.

Finally and most importantly, I wish to express my gratitude to my wife, Candace, for her support, assistance and understanding over the past several months. After countless hours of listening to discussions concerning impact testing and unbalanced sandwich composites, she deserves a Master's degree herself.

I. INTRODUCTION

Sandwich composites are becoming increasingly more attractive for use as primary structural members. These composites are constructed of two, thin, strong sheets separated by a thick, light, weaker core. The sheets are adhesively bonded onto the core to enable load transfer between the components. The resultant product is a stiff, lightweight member capable of replacing monolith materials in many load-bearing applications. Some principle areas of concern in using these composites in primary load-bearing applications are the response due to compressive loads and effects of impact damage. Due to delamination and core shearing, sandwich composites have considerably reduced compressive strength under edge-wise loading. Impacts, even at low velocities, can significantly reduce the load carrying capability of a composite structural member further. A study conducted by Murphy [Ref. 1] addressed the buckling stability of unbalanced sandwich composites. The results and methods of this study are an integral part of this investigation.

The purpose of this study is to support the Navy's research and development of an Advanced Performance Mast System (APMS). The APMS project is sponsored by the Naval Surface Warfare Center (NSWC), Annapolis, Maryland, Carderock Division. The composite configuration studied in this paper

is an unbalanced sandwich composite. The term unbalanced means that the facesheets are each made of two different materials. In this case, the composite consists of Titanium 6AL-4V and glass reinforced plastic (GRP) facesheets and a phenolic, Nomex fiber reinforced honeycomb core.

It is well known that low-velocity impacts on composites can cause significant damage. Such damage can be hardly detectable by visual examination, but can cause considerable reductions in the strength and stiffness of the materials. This study consists of a two-pronged investigation of the effect of impact damage on the buckling stability of the unbalanced sandwich composite. The first portion of the experimental procedure involves subjecting the composite, while in simply supported beam configuration, to a low-velocity impact using a mass-slider mechanism. After impact the sandwich column is subjected to an edgewise compressive load and tested for buckling stability in the same manner as was done in Ref. 1.

The primary focus of this study is to predict the force/energy required to cause core damage due to a low-velocity impact; develop a quantitative and/or qualitative correlation between impact parameters and resulting compressive load carrying strength; determine if the response of the composite is the same for an equivalent static force application; observe differences in sample responses due to loading on different skin sides and determine the failure

loads which will cause buckling instability once the core has been damaged. The composite samples were impacted and statically loaded on both the GRP and titanium sides. Differences in specimen response and subsequent properties were analyzed. Secondary objectives of this study are investigation of other damage mechanisms possible; acquisition of component response data for use in future modeling efforts; and refining of the experimental techniques required for future impact testing of composites.

II. BACKGROUND

Reviewing the research literature, it is noted that a large and increasing amount of effort is being devoted to the impact response of composites. Most of the studies are focused on laminate composites, but a considerable amount involves sandwich composites. To the author's knowledge, however, not many studies have been focused on unbalanced sandwich composites.

Although little has been done with unbalanced sandwich plates/beams, a literature survey of current relevant research findings is summarized below. Most of the information pertains to experiments conducted on laminate and balanced sandwich composites, but many of the results are applicable for this paper. Kim and Jun [Ref. 2] found that for low speed impact the damage of a composite plate is usually invisible to the naked eye and spread over a large region inside the plate. A portion of the applied impact energy is converted into elastic deformation and the remaining part is absorbed by the specimen to result in permanent deformation and damage such as matrix cracking, delamination, fiber breakage and fiber matrix debonding. With sandwich composites, additional damage to the core, such as core crushing and shear deformation, can occur. Since sandwich structures have the additional energy absorbing mechanism, core deformation, the facesheets of sandwich plates

have smaller delamination areas than laminates. It is also quite possible that the core can be damaged with no delamination area present on the facesheets. The damage modes occurring for sandwich panels depends on the material properties of the components, the thicknesses of cores and facesheets, and facesheet-core interfaces. It was found that Nomex honeycomb specimens appear to have a damage threshold below which there is no facesheet damage but there is core damage.

In the work done by Nemes and Simmonds [Ref. 3] it was noted impact force is a function of many parameters including dimensions of the plate, flexural properties, dimensions of the impactor and local contact stiffness of the plate. When peak displacements greater than 1/100th of the facesheet thickness occur in sandwich composites containing a lightweight core, the contact deformations of such composites are dominated by the deformation of the core, rather than deformation of the face plates. Since the deformations occurring in the core beneath the point of contact are large, the portion of the total deformation due to transverse shear deformation of the core is quite significant. Normal stresses that exist in the contact region are predominantly compressive, therefore, core shear failure is postulated to occur due to the transverse shear stresses that exist.

Lee, Huang and Fann [Ref. 4] found that because of the response of the core, the impacted face of a sandwich

composite behaves differently from the opposite one. The transverse deflection of the cross section of the sandwich plate is not the same throughout the thickness. The transverse deflections of the two facesheets are different under concentrated static or dynamic load. The core transmits transverse shear as well as transverse normal deformations. For points far away from the impacted point, dynamic responses are dominated mainly by the bending effect of the whole sandwich plate. It was also found that the contact force caused by the impactor is proportional to the impact velocity, but the duration of contact is insensitive to it. A heavier impactor mass will increase the impact force as well as the contact time.

From the paper by Sorblom, Hartness and Cordell [Ref 5.] the conclusion can be made that the impact force history is a more relevant measure of a material's characteristics than is the total kinetic energy of the impactor. The response of a structure depends on geometry, material and velocity of both the impactor and a target portion of the structure. The term low-velocity means an impact velocity low enough to neglect the inertia effect of the response of the structure. Furthermore, since so many variables affect the composite's response it is safe to conclude that impact test results will, at best, be difficult to relate to the basic material properties.

Kelkar, Craft and Sandhu [Ref. 6] quantified impact velocities into three velocity domains:

(a) High velocity or ballistic impact where the velocity $v > 1500$ ft/sec or (457.2 m/sec)

(b) Intermediate velocity impact (40 ft/sec $< v <$ 1500 ft/sec) or (12.19 m/sec $< v <$ 457.2 m/sec)

(c) Low velocity impact ($v <$ 40 ft/sec) or ($v <$ 12.19 m/sec)

Based on the mass of the sliding-mass impactor used in this experiment (6.85 kg or 15.1 lb.), the impactor energy range corresponding to a low velocity impact can be considered as 0-506 Joules (0-373 ft-lb). It would be more appropriate to classify the impact based on the impact energy level because the impact depends on both the mass of the impactor and its velocity.

III. EXPERIMENTAL PROCEDURES

This section provides a detailed description and illustrations of the experimental apparatus and procedures used in conducting the testing part of this study.

A. APPARATUS

All tests were conducted at the Naval Postgraduate School, Monterey, California, in an ambient temperature of 18.0° ± 2.0° C with an average relative humidity equal to 40% ± 6%.

All impact and static bending tests, as well as, axially loaded compressive tests were performed on samples of an unbalanced, sandwich construction consisting of Titanium 6Al-4V and glass reinforced plastic (GRP) facesheets and a phenolic resin, Nomex fiber reinforced honeycomb core. Nominal dimensions for each specimen tested were as follows: length = 0.3058 m (12.0 in.), width = 0.06985 m (2.75 in.), thickness = 0.02997 m (1.18 in.). The titanium facesheet had a nominal thickness of 0.00254 m (0.1 in.) and the GRP facesheet had a nominal thickness of 0.00203 m (0.08 in.). The core thickness was 0.0254 m (1.0 in.). Material properties of the given composite components are listed in Table I.

For each impact test a sliding-mass impact mechanism as illustrated in Figure 1 was used. The mass of the impactor

was 56.7 kg (125 lbs.). The drop height varied from 0.0127 m (0.5 in) to 0.1016 m (4.0 in.). Impact velocities ranged from 0.5 m/s (1.67 ft/s) to 1.412 m/s (4.632 ft/s). Impactor potential energies varied from 7.06 J (5.21 ft-lbs) to 56.51 J (41.67 ft-lbs).

TABLE I. MATERIAL PROPERTIES OF SANDWICH COMPONENTS

	Titanium	GRP	HRH-10 Core
Shear Strength (Mpa)	500	-	$1.76^{l}/0.965^{t}$
Posisson's Ratio	.342	.15	0
Young's Modulus (Gpa)	113.7	20.7	59.3/32.4 (MPa)
Thickness (m)	0.0027	0.0254	0.0021

^{l} - longitudinal direction, ^{t} - transverse direction

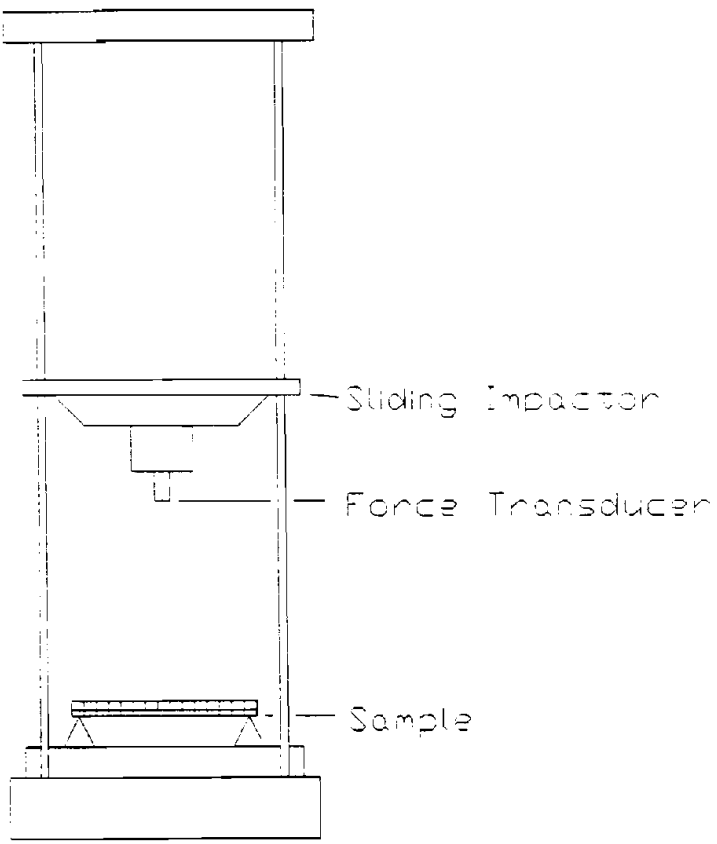

Figure 1. Sliding-Mass Impact Mechanism

A fixture was designed to hold the composite beam in a simply supported configuration. The fixture prevented both lateral and vertical motion of the specimen during impact. Each sample was positioned underneath the impactor so as to ensure the impact force occurred at the center of the beam. The fixture was then solidly attached to the mechanism baseplate. Since the impactor head was of a cylindrical shape, a thin strip of brass, 0.069 m x 0.15 m x 0.003 m, (2.75 in x 0.6 in x 0.125 in) was secured to the center of the impacted facesheet to spread out the contact load over the

width of the beam. This was done in order to cause the impact to be more representative of a two-dimensional nature rather than three-dimensional.

The actual impactor, attached to the sliding plate, was a PCB Impact Force Transducer (Model # 200A04 or Model # 200A05) capable of measuring peak impact forces of 4488.2 N (1000 lbs.) and 22,241 N (5000 lbs.), respectively. The sliding mass was also equipped with a PCB accelerometer (Model # 302B02) to measure changes in acceleration of the impactor. Each composite sample was instrumented with five CEA-06-250UN-350 precision strain gages, gage factor 2.100 + 0.5%. The number of gages was limited to five for the impact test since the bridge amplifier only had five channels available. As shown in Figure 2, two strain gages were placed at the quarter length points on the impacted facesheet and three strain gages were placed on the opposite side. Two were placed at the quarter length points and one at the center. One of the samples used in a static bending test was instrumented with nine strain gages in order to more accurately measure the strain response of the beam under load. In this case, strain gages were place at two inch increments on the backside and at two inch increments with the center position vacant on the loaded side. For impact tests, the strain gages were connected to a Ectron amplifier bridge (Model # E513-6A-M997). Figure 3 is an illustration of the composite beam sample in its impact test configuration.

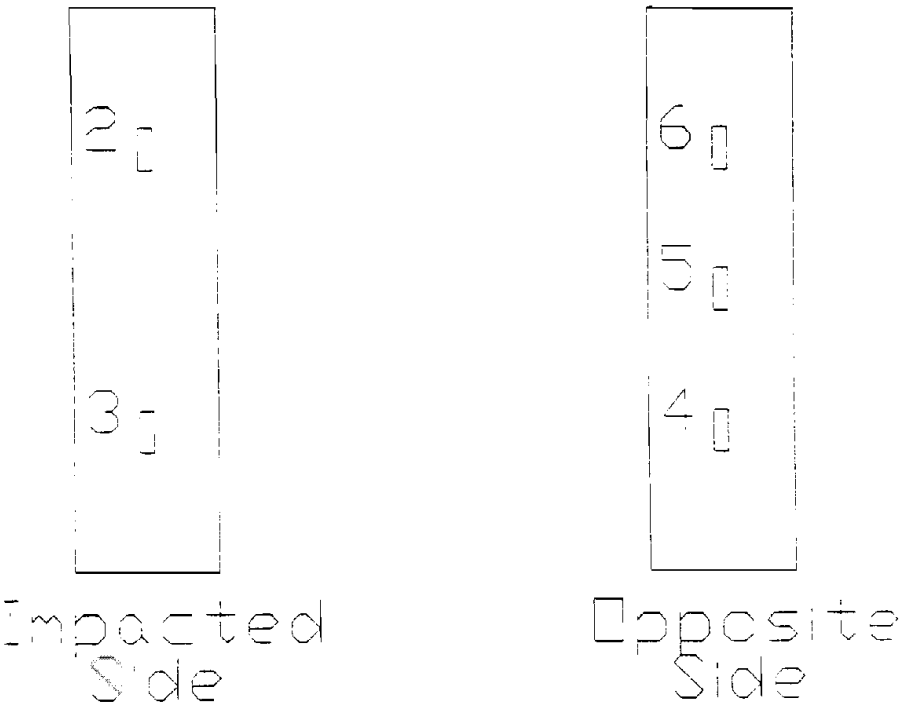

Figure 2. Strain Gage Placement

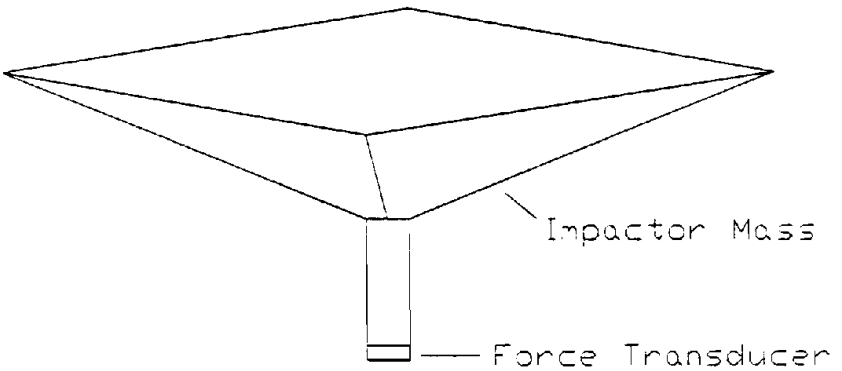

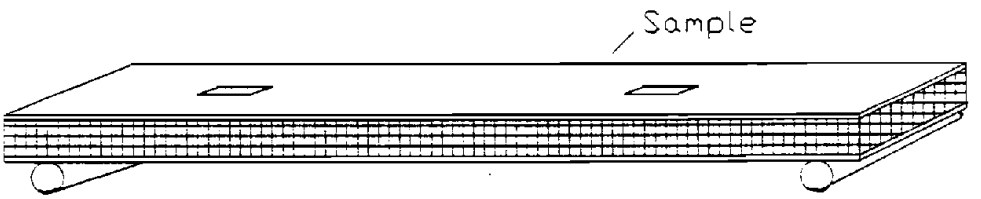

Figure 3. Sample Impact Configuration

All seven instruments were connected to an analog to digital computer board and a computer with a data acquisition program sampled each channel during the experiments. Outputs from each instrument could also be displayed on an oscilloscope. Due to computer program limitations sampling frequency of each channel was limited to 3500 Hz when sampling seven channels. Analysis prior to the beginning of experimentation, however, indicated that a sample frequency of 2500 Hz would be sufficient for the purposes of this study.

Some samples were loaded statically for comparison with the results from the low-velocity impact tests. The same fixture used in the impact tests was employed to achieve a simply supported condition. The tests on these samples were done with the MTS material testing machine. The MTS machine provided readings and a force-displacement print-out for the applied contact force and a measurement of the displacement of the sample. Strain gage outputs were read manually as was done in the axially compressive load tests. Additionally, each sample was instrumented in the exact same manner with five strain gages. The only difference being that the load was applied to the center of each beam in a slow, controlled manner instead of being imparted by a free-falling mass.

For the compressive buckling portion of this experiment the same configuration as used by Murphy [Ref. 1] was used. An axial compressive load was applied using the Riehle Material testing machine, with a capacity of 533,784 Newtons

(120,000 lbf.). A testing fixture was designed to provide simply supported end conditions on the loaded surfaces of each beam; the unloaded side surfaces were unconstrained. The simply supported condition was accomplished using two 0.0762 m (3 in.) diameter, 0.2794 m (11 in.) long, Rycase (1117) low carbon, high manganese steel round shafts machined with keyways for holding specimens and shims. Each shaft was mounted in two Dodge unisphere 0.0762 m (3 in.) pillow blocks. The shafts were free to rotate 360 in the bearings. The bearings were bolted to aluminum plates fixed to the Riehle testing machine. The strain gage outputs were connected to a Measurements Group SB-10 Switch & Balance Unit, and readouts, in microstrain, provided by Measurements Group P-3500 Strain Indicator. Deflection in the center of the beam was measured with a Starrett 1.000" dial indicator. A distance transducer, Colesco, model # DV301-6020-111-1110 was mounted vertically and attached to the upper aluminum baseplate to measure axial contraction in inches. Figure 4 illustrates the compressive test machine and sample configuration.

The samples were mounted in the test fixture so that loading could be applied directly on the neutral axis. The neutral axis was calculated, neglecting the effect of gluing materials, to be approximately 0.002 m (0.085 in.) inward from the titanium facesheet and core interface. Shims were used to position the composite sample to ensure loading was not eccentric.

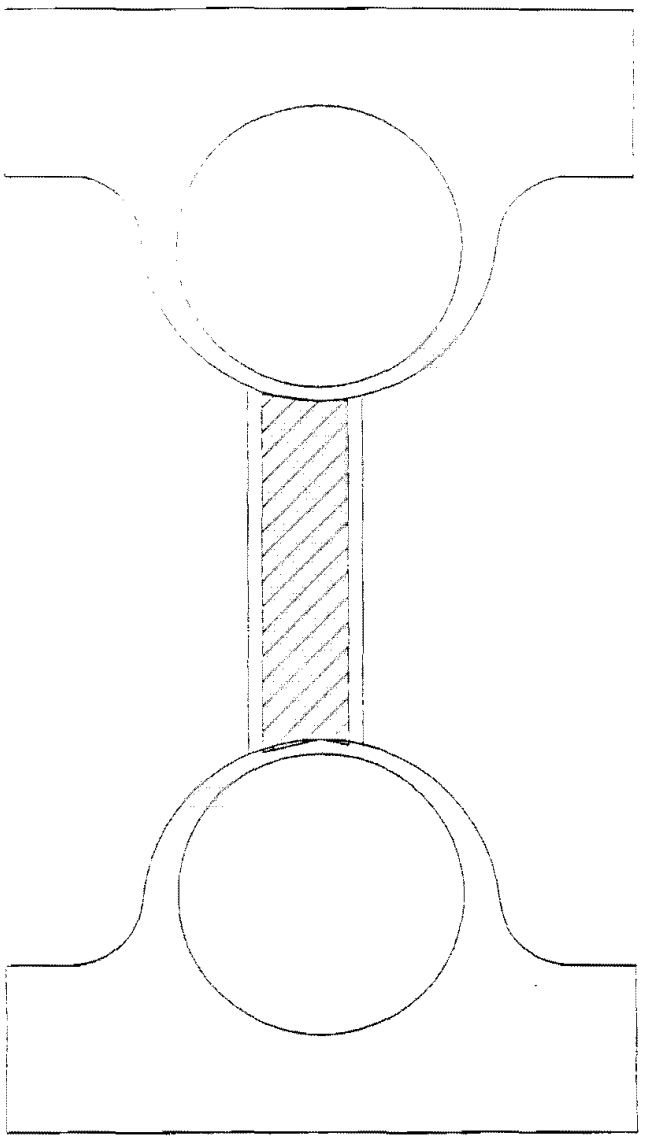

Figure 4. Compressive Failure Test Fixture

B. PROCEDURES

The first procedure performed on each specimen prior to the axially compressive loading test was the application of either a dynamic or static point load. Each contact load was applied to the center of the composite beam in a simply supported configuration. For the impact tests, the sample was positioned to ensure the impactor would strike the center of the beam. The height of the force transducer for each drop was carefully set using pre-cut blocks used as measurement standards. The sliding-mass mechanism was configured to allow the impactor mass to slide freely down the guide rods after release.

Each of the seven instruments on the impactor and sample was assigned a data acquisition channel on the computer. Since the time from impactor release to impact with the beam was very short, the computer was triggered to begin acquiring data immediately after release. One second of data was taken at sampling frequencies of 1600 Hz or 2500 Hz for each channel. This ensured a complete picture of the impact event was captured. None of the signals were filtered.

Once the impact signals were recorded a simple computer routine converted the voltages in the appropriate physical parameters of pounds, g units and microstrain. After the voltage to force conversions were made, the force versus time information was then used to determine the acceleration, energy, velocity and distance versus time information. Simple

algorithms, based on the same ones used by Crane and Juska [Ref 7.], were used as follows.

The force recorded by the impact force transducer is the total contact force imparted on the composite beam (mass times the acceleration of the impactor). The acceleration of the impactor is obtained from Newton's second law:

$$mg - F = ma \tag{1}$$

where F is the force measured from the transducer and mg is the force due to gravity of the impactor.

In equation (1), the only unknown is the acceleration, a, of the impactor. By rearranging equation (1), the acceleration can be solved for as

$$a = g - (F / m) \tag{2}$$

or substituting in the weight of the sliding mass, w, equation (2) becomes

$$a = (1 - (F / w)) \times g \tag{3}$$

Using equation (3), the acceleration of the impactor is determined each time the impactor contact force is measured. For this study, the force is sampled every 0.0004 or 0.000625 seconds.

The initial velocity of the impactor at the instant before it strikes the composite can be easily calculated from the simple formula

$$v = (2gh)^{0.5} \tag{4}$$

average acceleration during the sampling time interval, t_i and t_{i-1}. The velocity, then, is given by

$$v_i = v_{i-1} + ((a_i + a_{i-1}) / 2) \times \delta t \qquad (5)$$

where δt is the time interval between data points.

The displacement of the composite during each time interval can be determined from the velocities. The displacement is calculated by taking the average velocity multiplied by the time increment added to the previous displacement and is given as

$$x_i = x_{i-1} + ((v_i + v_{i-1})) / 2) \times \delta t \qquad (6)$$

MATLAB was used to execute the conversion algorithm and produce the plots of the signal outputs.

For the static three-point bending tests, the samples were placed in the simply supporting fixture and positioned in the MTS machine to ensure loading at the center of the beam. The load was applied in 222.4 N (50 lbf.) increments. At each increment the deflection at the center as well as the reading for each strain gage was recorded. Loading was increased until the deformation rate of the specimen exceeded the loading rate of the MTS machine. Failure, due to core crimping and shearing, occurred prior to this point. In one case the loading rate was increased so as to cause more damage to the core and observe the effect on the subsequent compressive failure load. Readings of deflection and strain were also taken after the beam was unloaded.

For the compressive load failure tests each specimen was placed in the fixture with shims to ensure the line of loading would be on the neutral axis. The specimen ends were held securely in the fixtures, but the fixtures themselves were still free to rotate to ensure a simply supported configuration was maintained. After the samples were placed in the fixture and the machine adjusted to be ready to begin applying a compressive load, strain gages were balanced out and initial length and center deflection readings were taken. The compressive load was then applied, initially, in 2224.1 N (500 lbf.) increments. At each increment the force applied, strain gage output, amount of deflection and change of axial length were recorded. As the loading approached the failure limit the increments were decreased to 444.8 N (100 lbf.) or 889.6 N (200 lbf.) between readings. In each case in which the core had been damaged during either the impact or static test, failure was manifested by core crimping/shearing. In the case which the core was not previously damaged, core crimping/shear and column buckling occurred virtually simultaneously.

IV. EXPERIMENTAL RESULTS

This section presents the results as obtained from the individual experiments. While some description of the results is provided, a more detailed explanation and physical interpretation of the results are given in the next chapter. Similar data was taken for all three types of tests, impact, static and compressive loadings. For the impact tests all data readings were automated, but for the static and axial compressive tests the readings were obtained manually. In order to ensure consistency in recording loading responses, samples were instrumented as uniformly as possible with strain gages in the same relative positions, the same force transducer used for every impact and the same procedures were employed for each separate test. Results are presented graphically and in tabular form. Where necessary similar outputs are presented together to allow for direct comparison.

A. IMPACT RESULTS

For each impact test the following one second of data was recorded: output for five strain gages, a force transducer and an accelerometer. After the output voltages were converted to more readily usable signals, the complete impact event was plotted on a hardcopy printout and an output table could be produced. Table II provides a summary of all impacts

performed and lists some key features of each drop test.

Figures 5 and 6 are the force plots for impacts from 0.0254 m (1 in.) on the GRP and titanium facesheets, respectively. The relatively smooth curve produced by the force indicates that no damage occurred in the sample. Figures 7 and 8 are the force plots for impacts from 0.0381 m (1.5 in.) on the GRP and titanium sides, respectively. The sudden change in the force output indicates that failure in the sample has occurred. In this study failure always resulted from damage to the core in the form of core crimping/shearing. The results from drop heights of 0.0508 m (2 in.) are similar. Figures 9 and 10 represent impacts on the corresponding GRP and titanium facesheets, respectively.

Before damage is initiated in the core, the magnitude of peak force increases and the contact time of impact lengthens for higher drop heights. Once damage occurs in the core, the contact time continues to greatly increase for higher drop heights, but the magnitude of the peak force remains almost constant. For the GRP side impact from 0.1016 m (4 in.) the peak force actually less than the resulting force for GRP side impact from 0.0254 m (1 in.). Due to the higher initial velocity of the impactor, more energy is imparted to the composite in a shorter period of time. This results in a earlier failure of the core, or loss of beam stiffness, and therefore the magnitude of the force applied by the composite on the force transducer is smaller.

Peak force values as well as the durations of impact are functions of the stiffness of the impacted sandwich beam. These values depend on the global beam stiffness, the stiffness of the facesheet impacted, sample geometry and mass of impactor. In all cases, except for the drop from 0.0127 m, the peak force is greater and the contact time is shorter for impacts on the GRP side. Figures 11 and 12 clearly show that up until failure occurs the force response is very nearly the same for each side impacted. Failure occurs at a lower force level for titanium side impact. After failure occurs the titanium impact force signal is basically the same shape as that for GRP impact, but the plateau for the titanium impact force lasts a slightly longer period.

TABLE II. SUMMARY OF IMPACT TESTS

Drop Height (m)	Impact Side	Peak Force (N)	Contact Time (s)	Energy Imparted (J)	Damage Location*
0.0127	GRP	2860	0.0360	5.89	-
0.0127	Ti	3132	0.0332	4.41	-
0.0254	GRP	3825	0.0332	10.17	-
0.0254	Ti	3545	0.0356	10.96	-
0.0381	GRP	3874	0.0492	21.58	2/6
0.0381	Ti	3496	0.0548	19.81	2/6
0.0508	GRP	3950	0.0570	31.20	3/4
0.0508	Ti	3514	0.0706	30.52	2/6
0.1016	GRP	3608	0.1112	65.0	3/4

* Damage location is based on strain gage location.

See Figure 2 for gage location numbers.

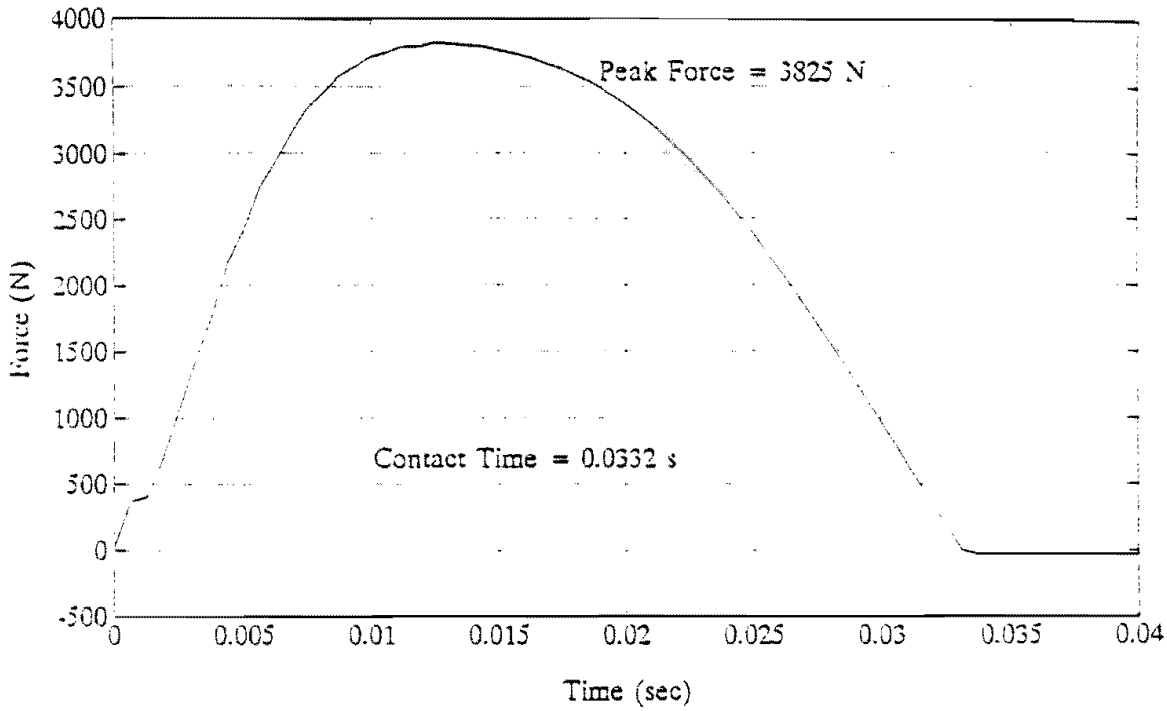

Figure 5. Force Plot for Impact on GRP From 0.0254 m

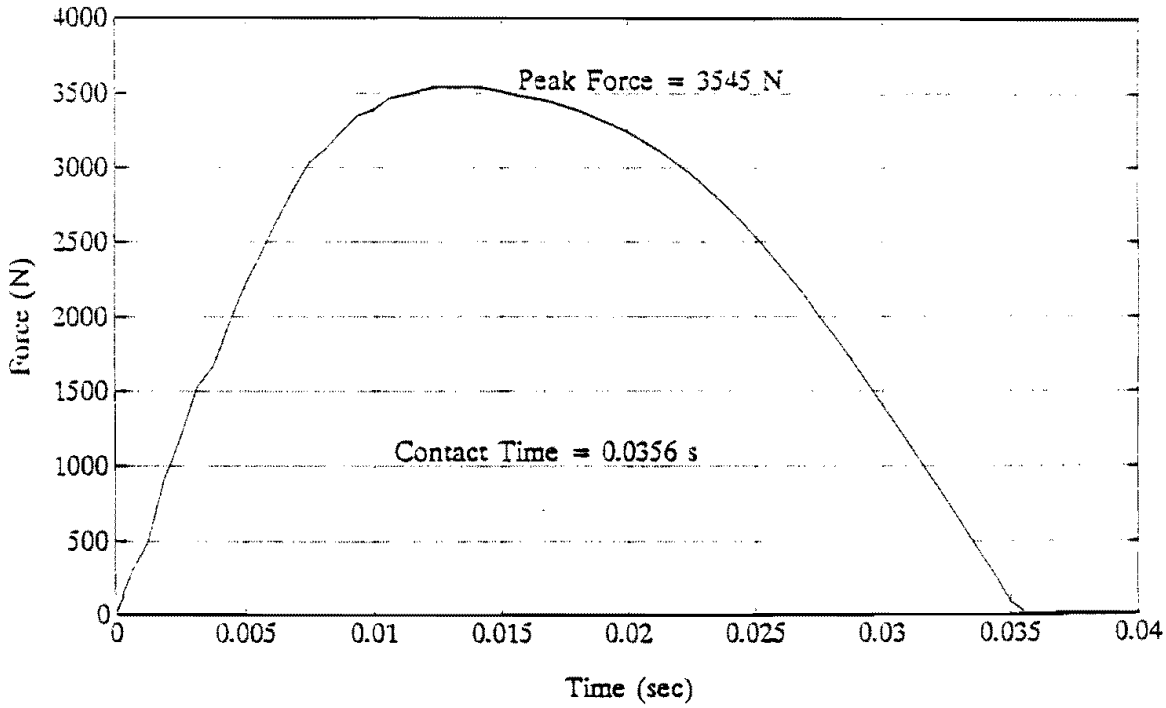

Figure 6. Force Plot for Impact on Titanium From 0.0254 m

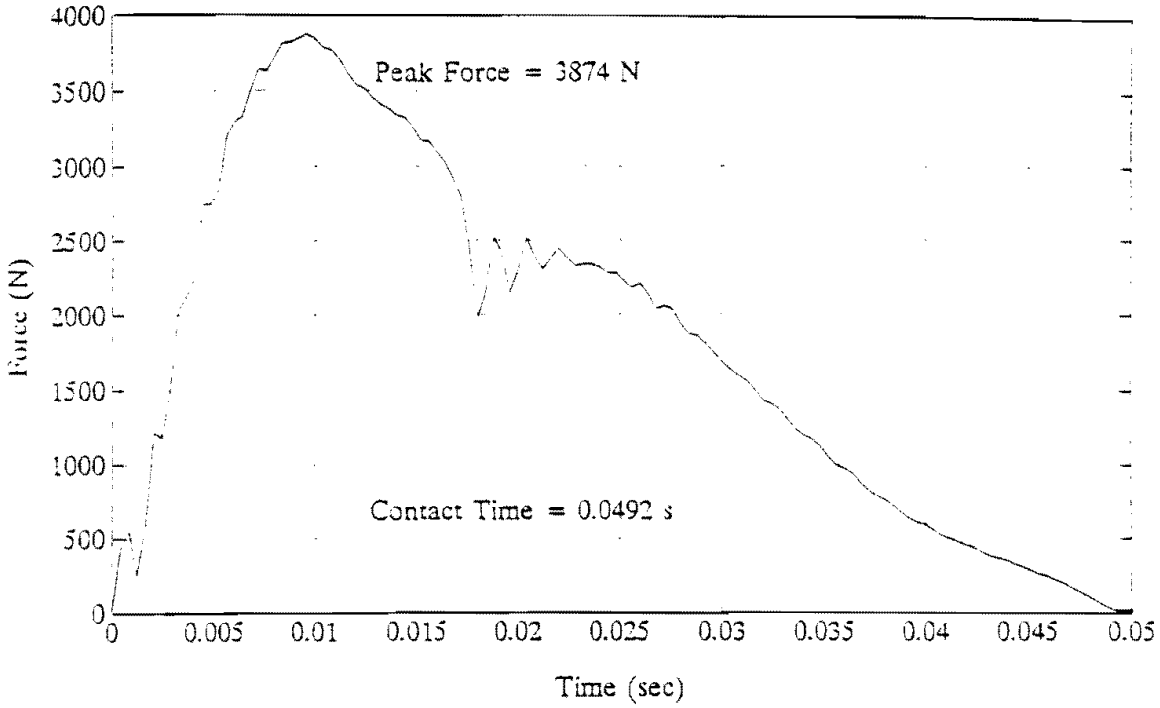

Figure 7. Force Plot for Impact on GRP From 0.0381 m

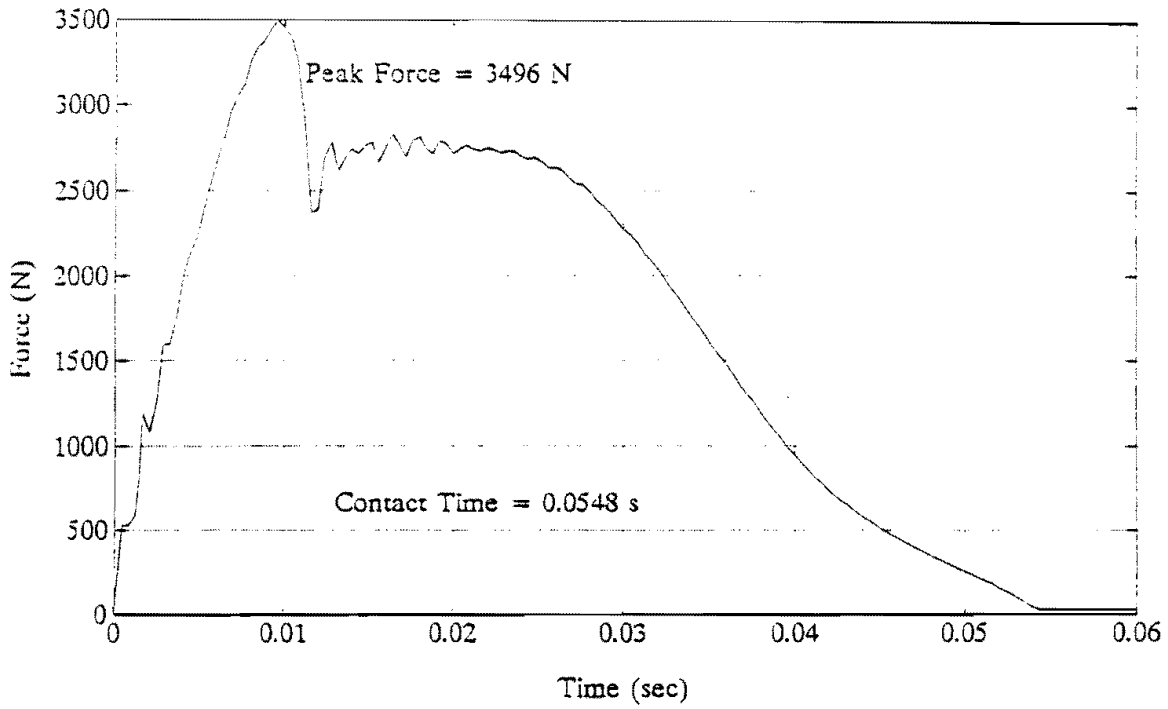

Figure 8. Force Plot for Impact on Titanium From 0.0381 m

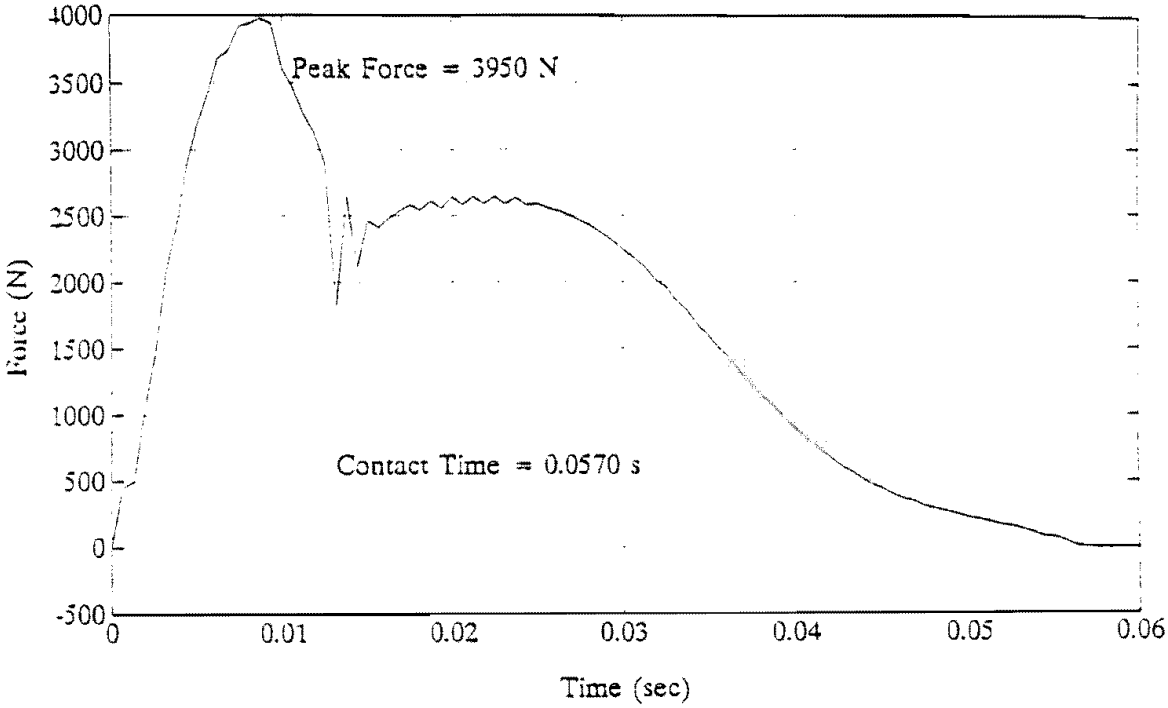

Figure 9. Force Plot for Impact on GRP From 0.0508 m

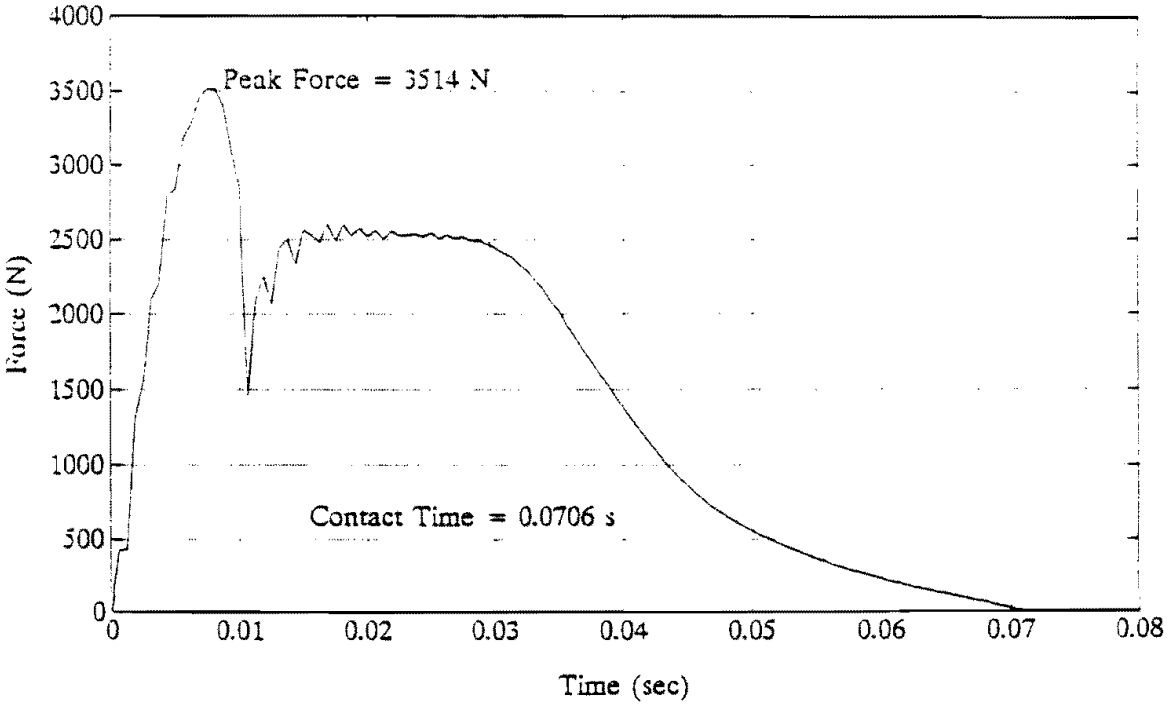

Figure 10. Force Plot for Impact on Titanium From 0.0508 m

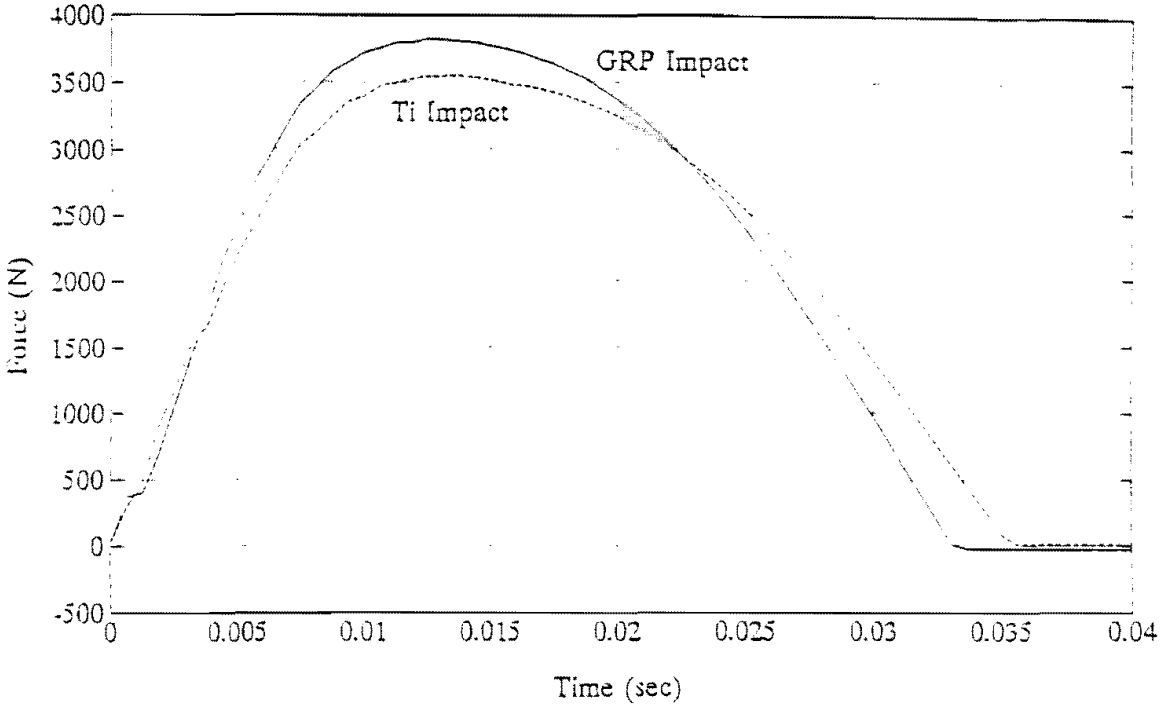

Figure 11. Force Plots for Impacts From 0.0254 m

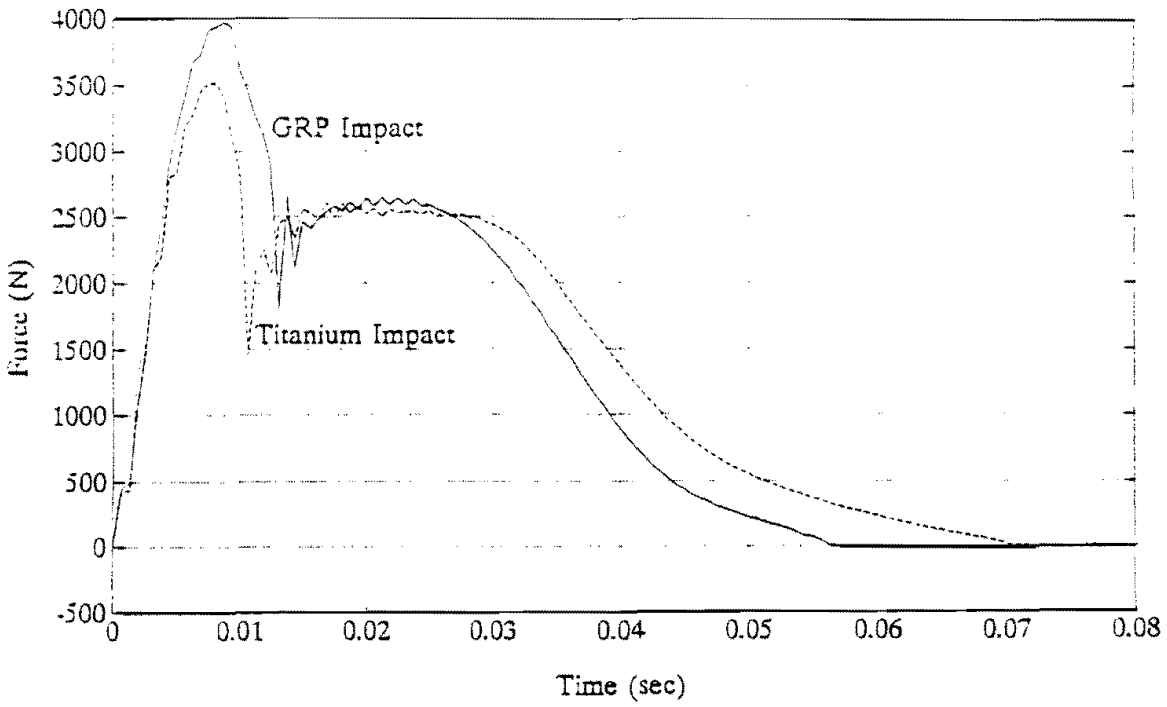

Figure 12. Force Plots for Impacts From 0.0508 m

The strain response caused by impact behaves in a similar manner. Figures 13 and 14 are the strain responses from impacts from 0.0254 m (1 in.) on the GRP and titanium sides, respectively. Once again, the relatively smooth traces indicate that no damage has occurred in the sample. Figures 15 and 16 are the strain signals for impacts from 0.0381 m (1.5 in.) on the GRP and titanium facesheets, respectively. The sudden change in the strain response represents the point at which damage occurred within the composite. By noting which strain gages showed the rapid changes, it is easy to determine at what location damage in the core has occurred. For example, on Figure 15 gage locations 2 and 6 are the sites of core damage. The strain responses for drop heights of 0.0508 m (2 in.) are, likewise, similar. Figures 17 and 18 represent impacts on the GRP and titanium sides for these drop heights, respectively.

Using the values calculated for displacement of the sample during contact with the impactor, force versus displacement plots can be generated. Figures 19 and 20 are representative of the outputs produced impacts from a drop height of 0.0254 m (1 in.) and a drop height of 0.0508 m (2 in.) on the GRP side, respectively. From the force-displacement plot for each impact test a simple trapezoidal rule algorithm was employed to integrate area under the hysterisis curve produced. This calculated value represents the amount of work done on the sample by the impactor during impact. As indicated in Table

II, the amount of energy imparted to each composite increases as the drop height increases. Examination of the energy amounts for drops from 0.0254 m (1 in.) on both the GRP and titanium sides indicates an approximate value of 11 J (100 lb-in) is close to the maximum amount of energy which can be imparted to the composite without damage occurring. The energy amount associated with a 0.0254 m (1 in.) impact appears to be a threshold value. Once this energy level is exceeded damage in the core is initiated and begins to propagate. By subtracting the threshold energy of 11 Joules from the area of the plot in which damage does occur, one may determine the amount of energy used in deforming the core.

The appendix contains complete outputs of all plots generated for each impact test performed during this study. For each test performed graphical plots corresponding to force-time, velocity-time, displacement-time and force-displacement data are included.

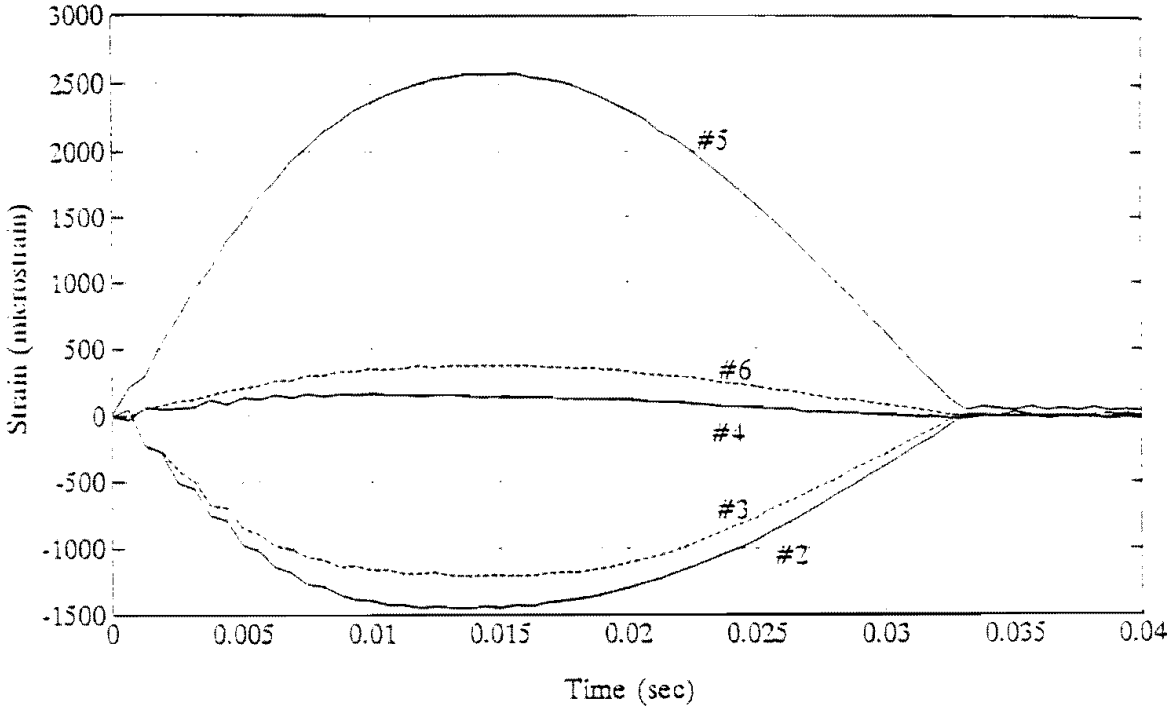

Figure 13. Strain Response for Impact on GRP From 0.0254 m

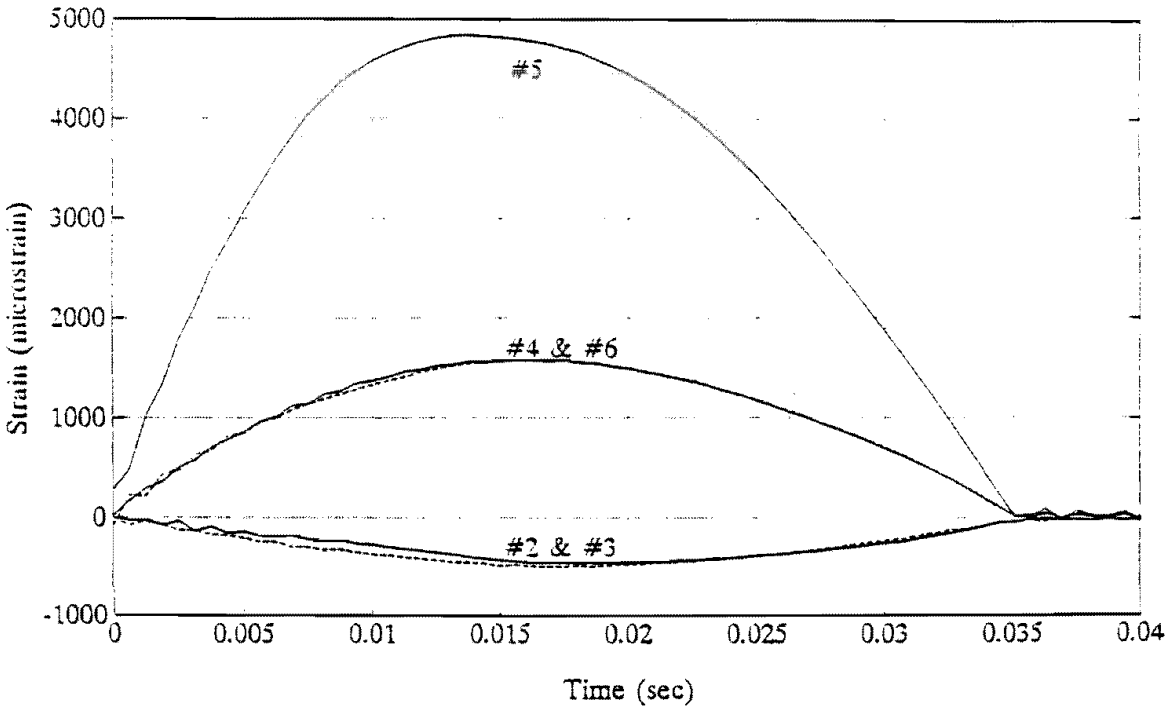

Figure 14. Strain Response for Impact on Ti From 0.254 m

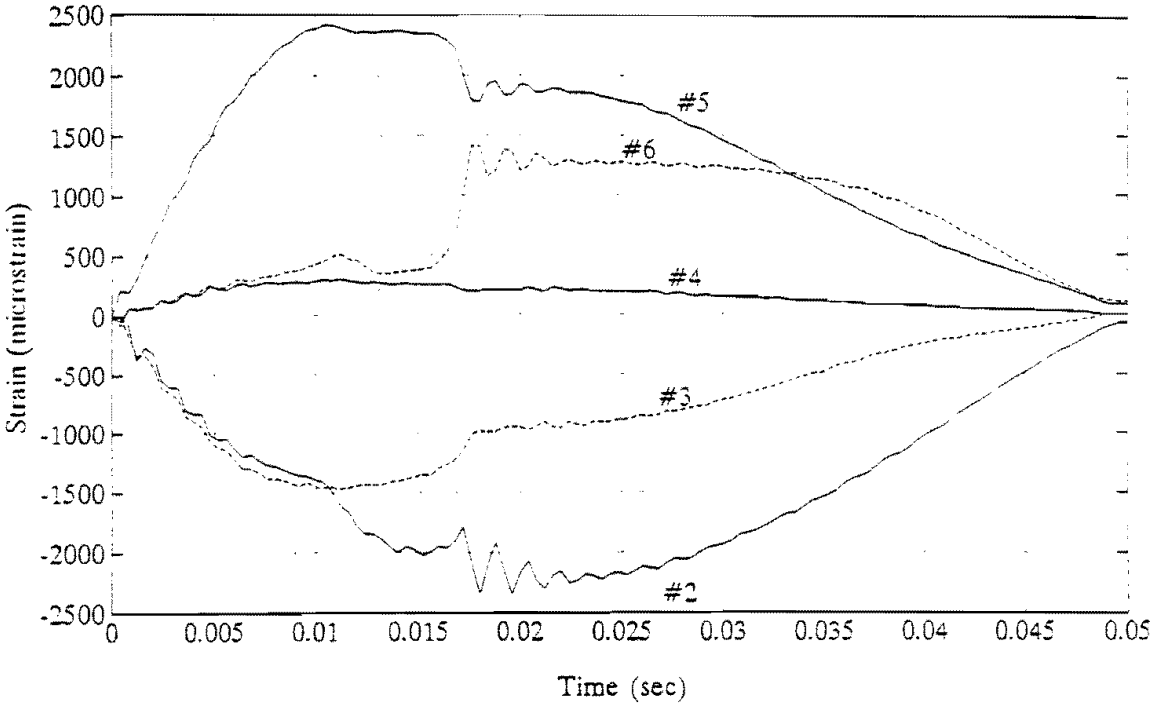

Figure 15. Strain Response for Impact on GRP From 0.0381 m

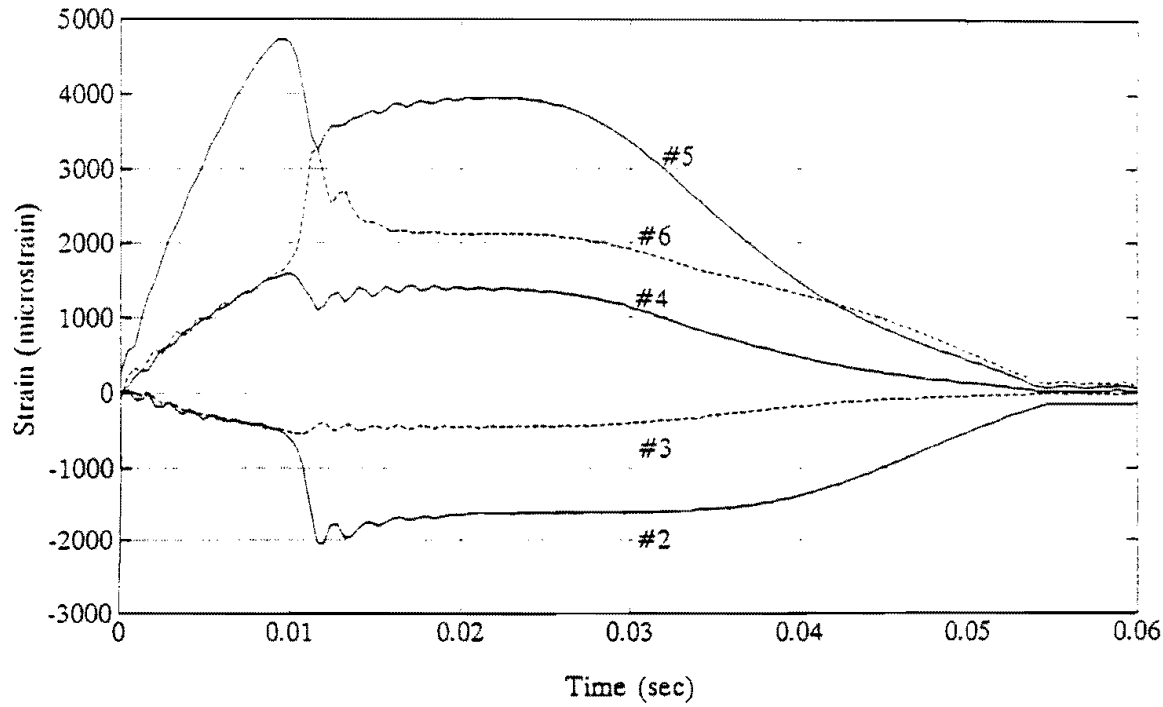

Figure 16. Strain Response for Impact on Ti From 0.0381 m

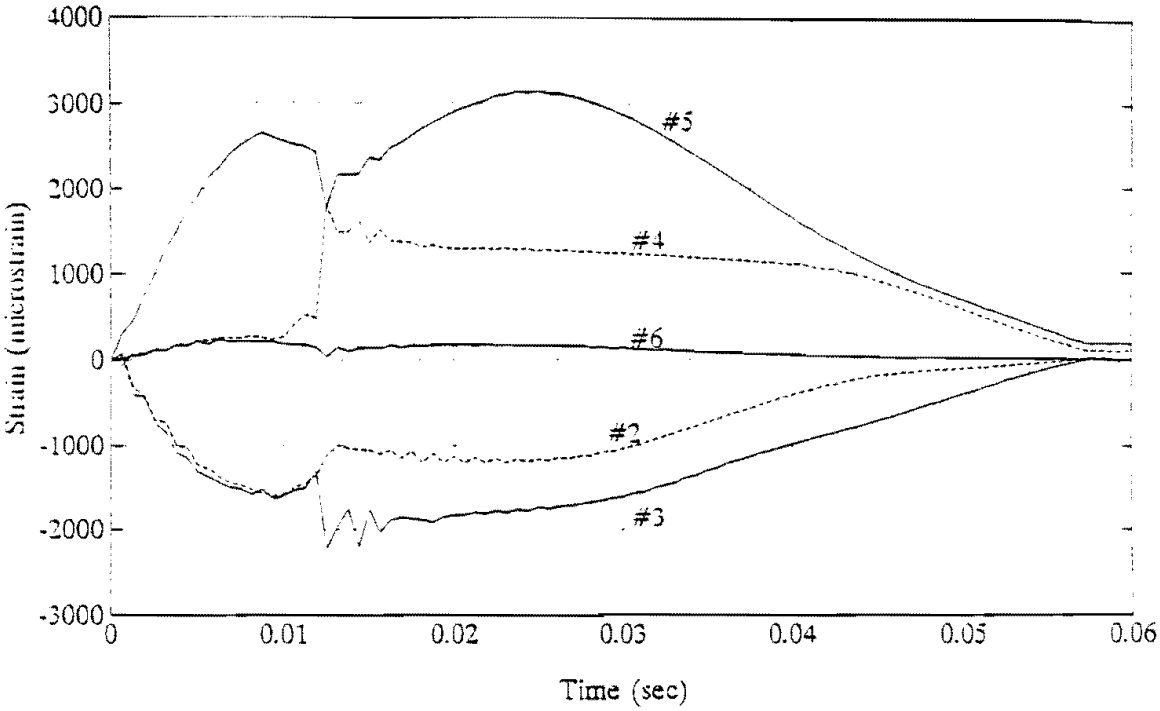

Figure 17. Strain Response for Impact on GRP From 0.0508 m

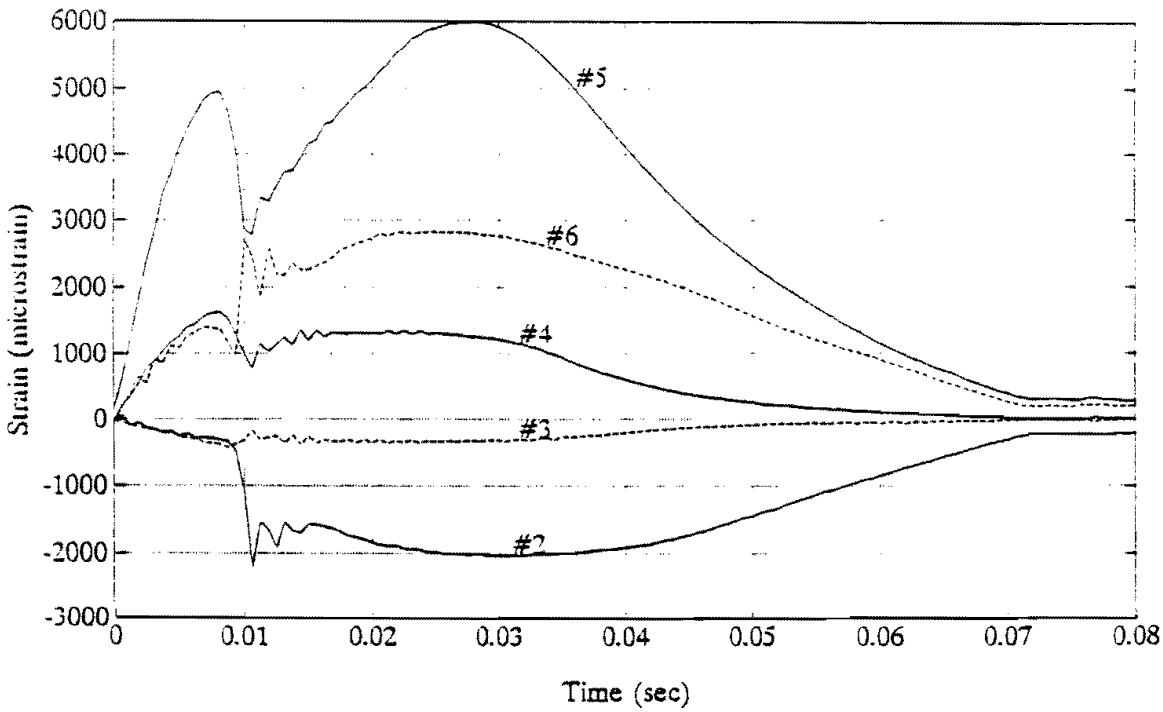

Figure 18. Strain Response for Impact on Ti From 0.0508 m

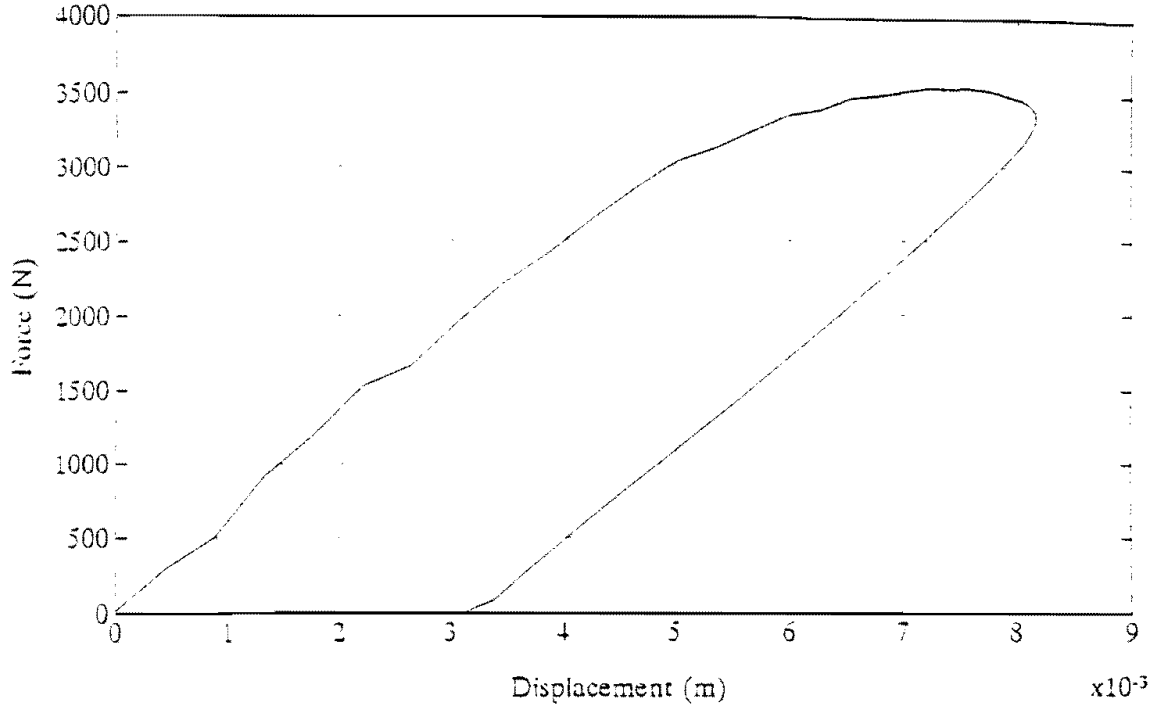

Figure 19. Force-Displacement, Impact on GRP From 0.0254 m

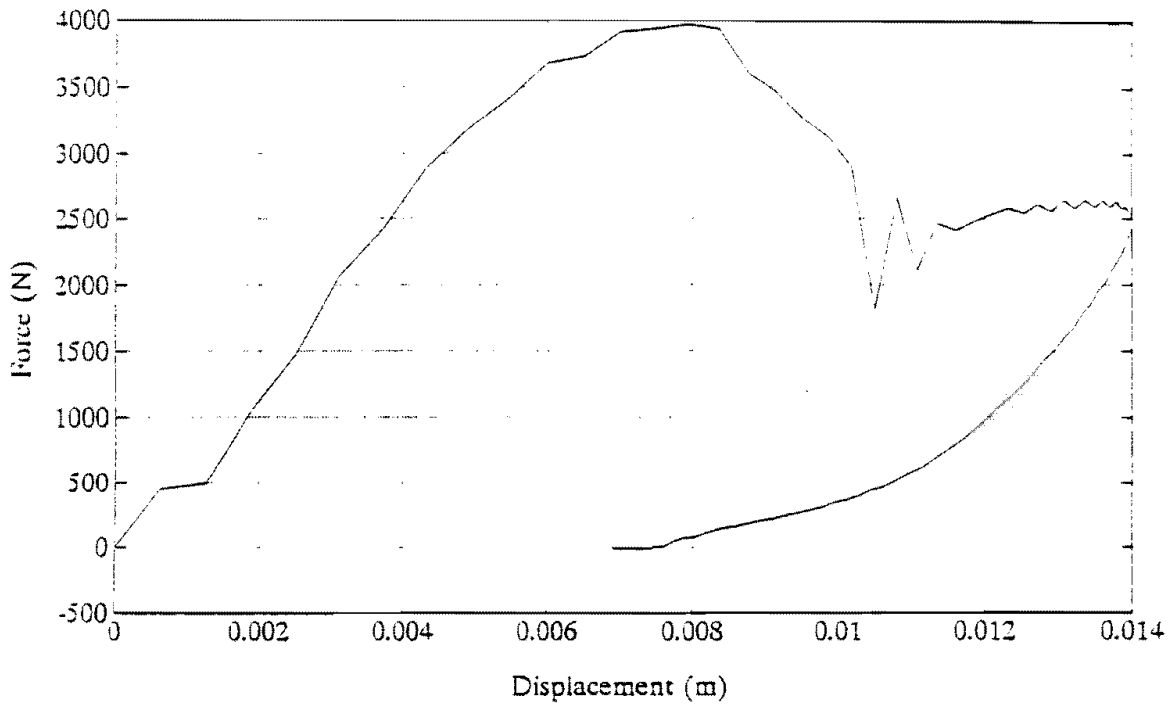

Figure 20. Force-Displacement, Impact on GRP From 0.0508 m

B. STATIC LOADING RESULTS

The static loading tests were three point bending tests with the load applied in increments. During each test the MTS machine was used to determine the force applied and the displacement of the beam under load. As a result, a force-displacement plot was produced. The load was applied in approximately 222.4 N (50.0 lbf.) increments. At each load level strain gage outputs, amount of force and sample deflection readings were recorded. Tables III and IV provide average values for specimen strain and deflection responses for the three point bending tests conducted.

Each static loading test was carried out until the composite failed due to core damage. The peak force achieved during each test corresponded to failure of the sample due to rapid deformation. The most readily noticeable difference between the composite responses for dynamic and static loadings is that the force levels required to cause core damage for the static tests is approximately 444.8 N (100 lbf.) or approximately 11% less than those for the dynamic tests. Additionally, statically loaded samples failed symmetrically in two locations, at each quarter point, instead of a single location. More detailed analysis and comparison sample responses will be considered in the Discussion and Summary section of this paper.

TABLE III. AVERAGE RESPONSE FOR STATIC LOADING ON GRP SIDE

Force (N)	Strain Gage Readings (microstrain)				
	#2	#3	#4	#5	#6
463	-158	-186	30	271	28
903	-329	-368	60	534	57
1343	-493	-551	92	802	86
1784	-659	-735	125	1084	120
2006	-745	-832	140	1234	134
2211	-816	-922	157	1386	157
2438	-902	-1031	180	1568	174
2647	-971	-1136	205	1775	196
2878*	-1120	-1306	263	2005	228
3078*	-1125	-1328	565	2333	248

* Failure has occurred.

TABLE IV. AVERAGE RESPONSE FOR STATIC LOADING ON TITANIUM SIDE

Force (N)	Strain Gage Readings (microstrain) #1	#2	#7	#8	#9
400	-6	-44	408	214	78
939	-19	-110	985	510	182
1366	-28	-165	1444	745	261
1815	-36	-228	1944	1011	345
2006	-38	-262	2168	1120	375
2237	-39	-310	2430	1265	418
2442	-33	-369	2672	1406	449
2660	-23	-449	2922	1566	482
2891*	2	-566	3225	1765	528
3149*	29	-724	3560	2003	602

* Failure has occurred.

Due to the symmetric response of the composite beam, only half the strain gage readings are listed in the above table. Figure 21 illustrates the strain gage placement for these static loading tests.

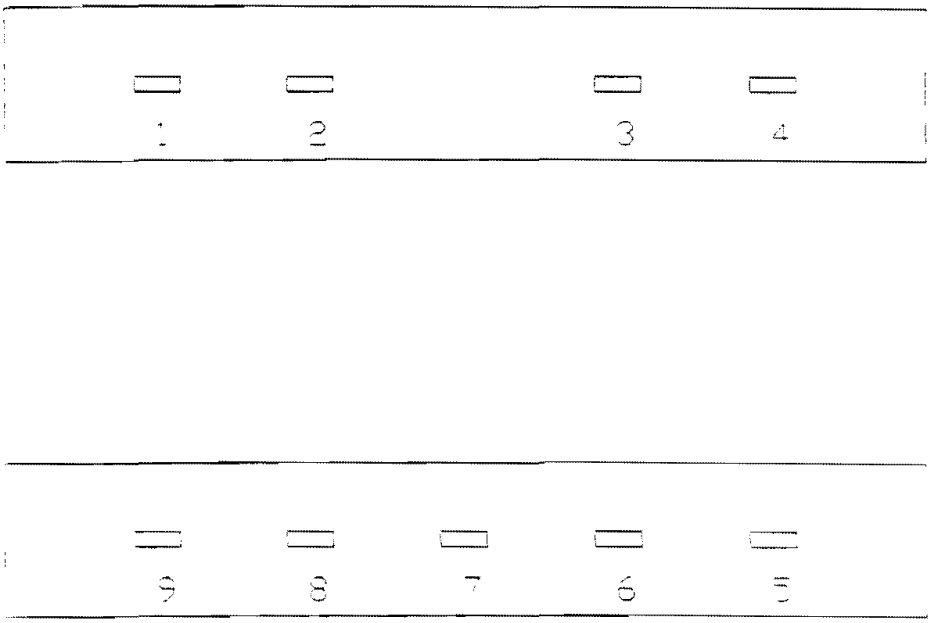

Figure 21. Strain Gage Placement for Static Loading on Titanium Side

C. COMPRESSIVE LOADING FAILURE TESTS

After each sample was either impacted or statically loaded, the composite was placed in the compressive test fixture and an axial compressive load was applied. The load was applied in 2224 N (500 lbf.) or smaller increments until failure occurred. Again, the mode of failure was core crimping/shear. At each load increment strain gage outputs, change in axial length and deflection of the center of the sample measurements were recorded. Table V provides a summary of the results of the compressive loading tests.

From the test results it is apparent that as the level of force imparted to the composite increases, the axial compressive failure load decreases. Figure 22 graphically illustrates there exists a threshold value. When an impact force exceeds the threshold value, it results in a significant reduction in load carrying capability under compression. This threshold value corresponds the force level required to initiate core damage in the composite. As the amount of force continues to increase and damage in the core becomes bigger, the compressive failure load decreases further. A compressive failure test was also conducted on a sample which, after repeated impact and compressive loadings, had severe damage in the core and had suffered delamination between the GRP and core on one end. The failure load for this sample was found to 6672 N (1500 lbf.). This value could be considered to

represent the minimum compressive load carrying capability of the samples even after catastrophic damage has occurred.

TABLE V. COMPRESSIVE LOADING TEST RESULTS

Peak Force (N)	Impact Side	Energy Absorbed (J)	Compressive Failure Load (N)
2860	GRP	5.89	43370
3132	Ti	4.41	43370
3545	Ti	10.96	43370
3825	GRP	10.17	43370
3496	Ti	19.81	15035
3874	GRP	21.58	21351
3514	Ti	30.52	10676
3950	GRP	31.20	14590
3608	GRP	65.0	9341

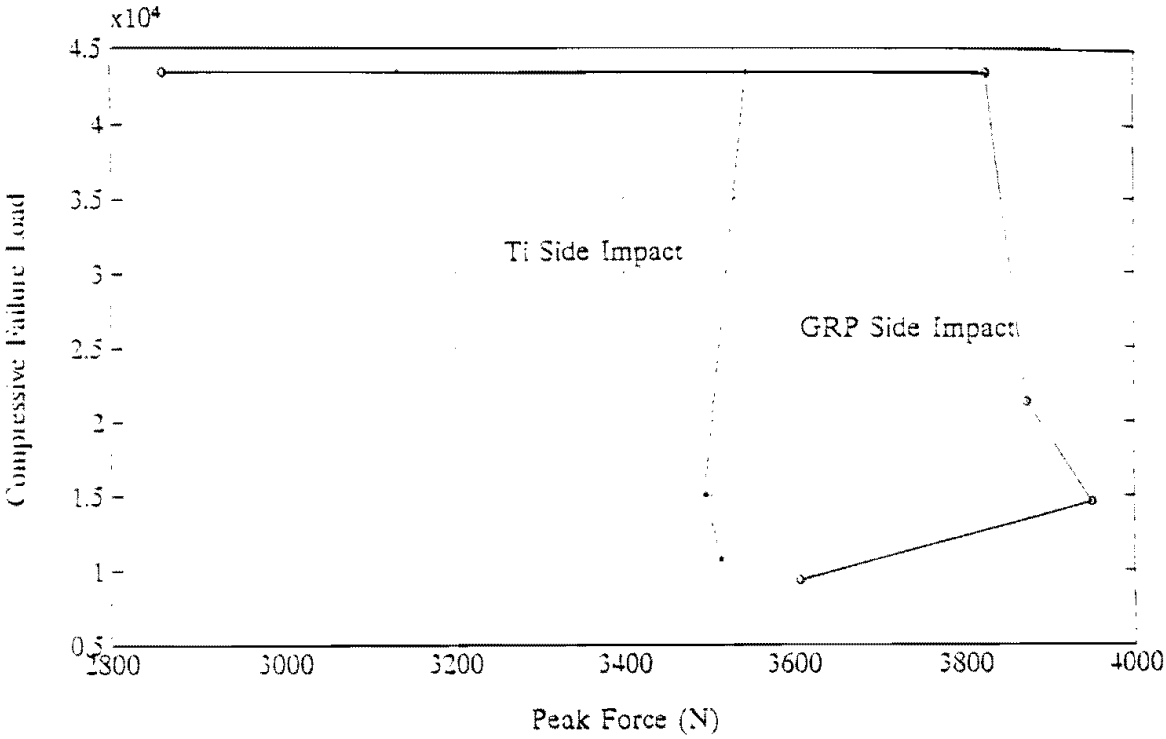

Figure 22. Impact-Compressive Failure Loads

V. DISCUSSION

It was originally assumed that many of the observed responses of the unbalanced sandwich composite samples could have been predicted using intuition and modeling the specimen using the beam theory. Several experimental results, however, proved to be different than expected. This underscores the importance of performing experimental tests in order to understand the complex responses with a structure such as an unbalanced sandwich composite.

A. TRANSVERSE LOADING RESPONSE

Tables VI and VII provide a listing of the average force and strain response outputs for different impacts from 0.0254 m (1 in.) to 0.0508 m (2 in.) on the GRP and titanium facesheets, respectively. From statics, the resultant moment at the center of a simply supported beam is twice the moment at the quarter point. For the linear elastic deformation, the strain is proportional to bending moment. Neglecting the effect of transverse shear deformation, it is expected the strain to be two times greater at the center than the quarter point. Due to positioning of the samples on the support device, the configuration actually had an overhang of approximately 0.0127 m (0.5 in.) on each end of the beam. Considering this, it would be expected for the moment, and

therefore, strain to be a factor of 2.2 times greater at the center than at the quarter point, neglecting the transverse shear effect. The data in Tables VI and VII indicates for impacts on the GRP side the strain at the center is almost 9.5 times greater than at the quarter point, and for titanium impacts it is approximately 3.4 times greater. Correcting for the effect of core shear deformation can account for some deviation from expected values, however, increases in ratios by a factor of 9.5 were not expected and are highly unusual.

Analysis of strain gage readings and videotape recordings of the impact tests and of the static loading tests, shows that the radius of curvature of the beam is quite different from that expected. A much greater amount of curvature takes place in the local vicinity of the point of load application.

TABLE VI. AVERAGE STRAIN VALUES FOR GRP SIDE IMPACT

Force (N)	Strain Gage Readings (microstrain)				
	#2	#3	#4	#5	#6
427	-5.2	-5.6	-14.6	275	-2.0
694	-274	-264	48	546	78
1059	-461	-417	73	735	86
1463	-620	-630	103	962	117
2122	-774	-798	129	1240	167
2424	-986	-986	163	1472	191
2882	-1074	-1083	187	1715	216
3176	-1154	-1154	195	1854	239
3358	-1247	-1245	220	2007	261
3656	-1329	-1287	223	2192	297
3825	-1387	-1431	215	2407	362

TABLE VII. AVERAGE STRAIN VALUES FOR TITANIUM SIDE IMPACT

Force (N)	Strain Gage Readings (microstrain)				
	#2	#3	#4	#5	#6
512	25	21	122	617	169
943	-61	-69	357	1326	393
1085	-127	-85	432	1484	515
1268	-115	-127	534	1737	532
1561	-129	-137	657	2187	610
1748	-209	-193	734	2371	696
1979	-167	-199	791	2689	774
2197	-209	-224	925	3088	869
2411	-213	-247	949	3230	931
2673	-244	-274	1047	3550	1055
2860	-210	-275	1155	3881	1069
3136	-271	-324	1289	4218	1239
3323	-323	-372	1424	4539	1364
3407	-340	-399	1478	4675	1403

Another important deviation from the classical beam theory for the unbalanced sandwich composite, as compared with a monolith material, is the shear deformation of the core material. If the beam is considered to be made of steel or aluminum, the presence of a shear stress of approximately 1.1 Mpa (160 psi) would result in negligible shear deformation for the monolith material with a large shear modulus. However, the composite core (HRH-10) in this study has a shear modulus of only 1 Mpa (140 psi). Clearly, the effect of shear deformation in the composite cannot be neglected and contributes significantly to the response of the beam.

When the samples were subjected to static transverse loads, the results in the strain responses were not markedly different from the impact results. For the samples which were statically loaded on the GRP side the strain gage arrangements were exactly the same as for the GRP impact tests. Once again, the ratio of strains at the mid-point and quarter points should have been 2.2 based on the actual configuration of the tests, neglecting the shear deformation. As can be seen in Table VIII, the actual strain ratio is approximately 8.6.

When the loading was applied to the titanium side the strain gage arrangement was modified in order to provide a more detailed picture of the strain response of the beam. In this case strain gages were placed at the one-third, two-third and center points of the specimen. The beam still had a

0.0127 m (0.5 in.) overhang on each end. Based on the classical theory the ratios of strains between the one-third and middle points should be 3.67, between the two-third and middle points should be 1.57 and between the one-third and two third points should be 2.33. Experimental results listed in Table IX show these ratios to be approximately 5.1, 1.85 and 2.85, respectively. Due to the symmetric bending of the composite beam under static load, up to failure of the core, the strain gage readings on one side are reported in Table IX.

While these ratios are certainly closer to the classical theory values, a discrepancy which cannot necessarily be attributed to experimental errors still exists. In both cases when the samples are either dynamically or statically loaded on the titanium side, the deviations from beam bending theory are smaller. When loading is applied to the GRP side, however, the ratios significantly vary.

TABLE VIII. AVERAGE RESPONSE FOR GRP STATIC LOADING

Force (N)	Deflection (m)	Strain Gage Readings (microstrain)				
		#2	#3	#4	#5	#6
463	0.0006	-158	-186	30	271	28
903	0.0012	-329	-368	60	534	57
1343	0.0019	-493	-551	92	802	86
1784	0.0025	-659	-735	125	1084	120
2006	0.0029	-745	-832	140	1234	134
2211	0.0033	-816	-922	157	1386	157
2438	0.0039	-902	-1031	180	1568	174
2647	0.0044	-971	-1136	205	1775	196
2878	0.0054	-1120	-1306	263	2005	228
3078	0.0064	-1125	-1328	565	2333	248

TABLE IX. AVERAGE RESPONSE FOR TITANIUM STATIC LOADING

Force (N)	Deflection (m)	Strain Gage Readings (microstrain) #1	#2	#7	#8	#9
400	0.0005	-6	-44	408	214	78
939	0.0012	-19	-110	985	510	182
1366	0.0018	-28	-165	1444	745	261
1815	0.0025	-36	-228	1944	1011	345
2006	0.0028	-38	-262	2168	1120	375
2237	0.0032	-39	-310	2430	1265	418
2442	0.0036	-33	-369	2672	1406	449
2660	0.0042	-23	-449	2922	1566	482
2891	0.0049	2	-566	3225	1765	528
3149	0.0060	29	-724	3560	2003	602

In order to more fully understand the mechanics of these strain responses, a four point bending test was performed. For this four point bending test the load was applied to both the GRP and titanium sides at the quarter points or 0.0762 m (3 in.) from each end. The composite was placed on the simple support fixture with the same 0.0127 m (0.5 in.) overhang and instrumented with ten strain gages placed (five on each facesheet) at 0.0254 m (1 in.) increments along the length of

the beam. The location where the load was applied was left vacant. Due to the symmetric response of the sample for static loads only one half of the composite was instrumented. Strain gage placement is shown in Figure 23. In the four point bending test the moment in the section between the applied loads is constant and the shear is zero. Since there is no transverse shear force and a constant bending moment in the center section, it would be expected for all the strains in this region to be the same for a given load. Strain amounts for the gages on the GRP facesheet remained almost constant. Strain amounts on the titanium facesheet, however varied by amounts up to 100% for most loads. The reason for this deviation is unclear.

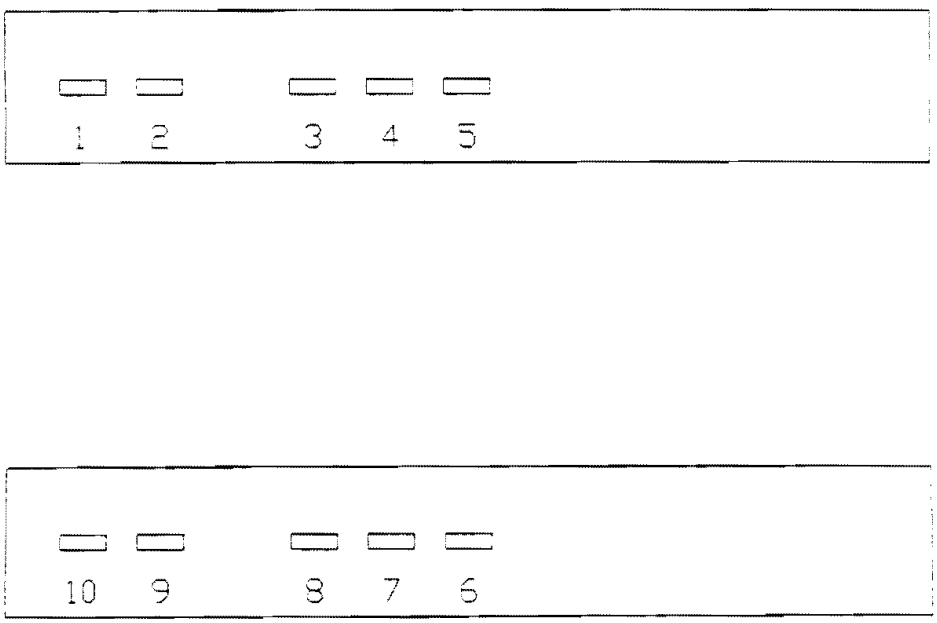

Figure 23. Strain Gage Locations for Four-Point Bending

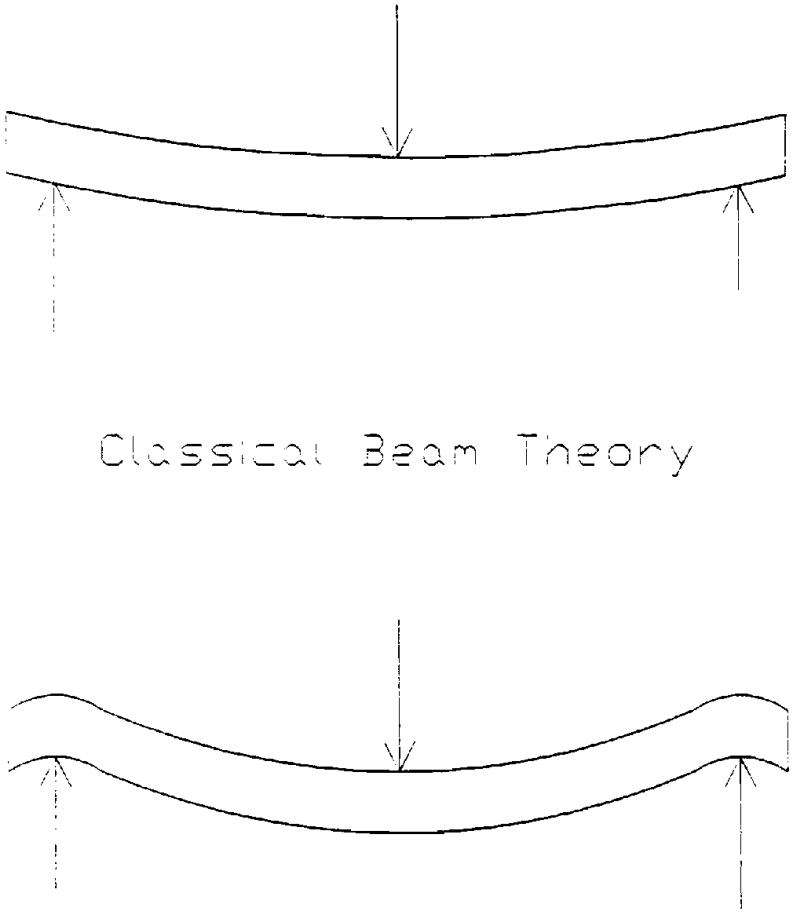

Figure 24. Beam Bending Shapes

Figure 24 illustrates the shape resulting from both three point and four point loading tests. For both cases it is clear from observations made during the tests and when reviewing the videotapes afterward that the deformed shape was very different from what was expected from the beam bending theory. Strain gage readings for the location 0.0254 m (1 in.) from the end actually show the top facesheet to be in

tension and the bottom facesheet to be in compression instead of the opposite states expected from classical beam bending theory. It can be argued that the samples used in this study are actually "short" beams and therefore classical beam theory does not strictly apply. While to a limited extent this may be correct, there is clearly more physics involved than can be explained away by the "short" beam effect. In order to gain a more complete understanding of the mechanisms at work in this and similar unbalanced sandwich composites, more research needs to be done using different sample geometries and support configurations.

Other interesting points discovered from the experimental data comes by comparing the force, strain and deflection at the center of the beam responses for the various loading configurations. Even though transversely applied failure loads can vary depending on which side is impacted or whether or not the load is dynamically or statically transmitted, there are many similarities up to the failure point for each test. Figures 25 and 26 show the force transducer outputs for impacts from 0.0254 m (1 in.) and 0.0508 m (2 in.), respectively, on the GRP and titanium facesheets. Up to the point of failure the force traces practically coincide with one another.

Table X lists the average center deflections for impact loadings on both the GRP and titanium facesheets. Average center deflections for static tests are included in Tables

VIII and IX. Figure 27 shows that the average deflections of the center of the beam do not vary significantly, up to the failure, when the beam is loaded either by impact or statically. The deflection traces, again, nearly coincide with one another (only vary by approximately 1 mm (0.04 in.)) up to the failure load. Once failure has occurred in the core, however, the static loading deflections increase significantly compared to the impact tests. This is because static loading causes core damage at both ends and impact loading only cause damage at one location.

One composite response parameter, however, appears to be independent of the manner in which the sample was loaded. Examination of the data for impacts on both the GRP and titanium sides, as well as, static loadings on both sides reveals that failure in the core always occurs near the quarter length points. Additionally, the magnitudes of the strains in the facesheets at the failure points are fairly constant. Figures 28 and 29 show the strains at the failure point for impacts from 0.0508 m (2 in.) for the GRP and titanium facesheet gages, respectively.

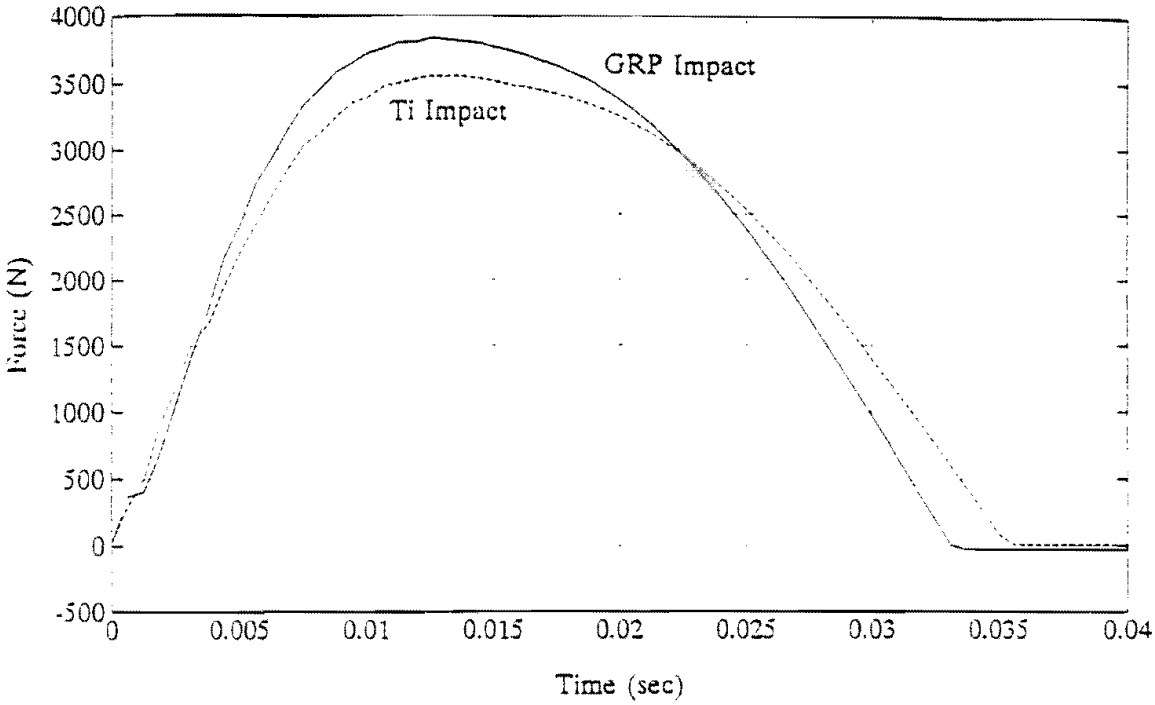

Figure 25. Impacts on GRP and Titanium Sides from 0.0254 m

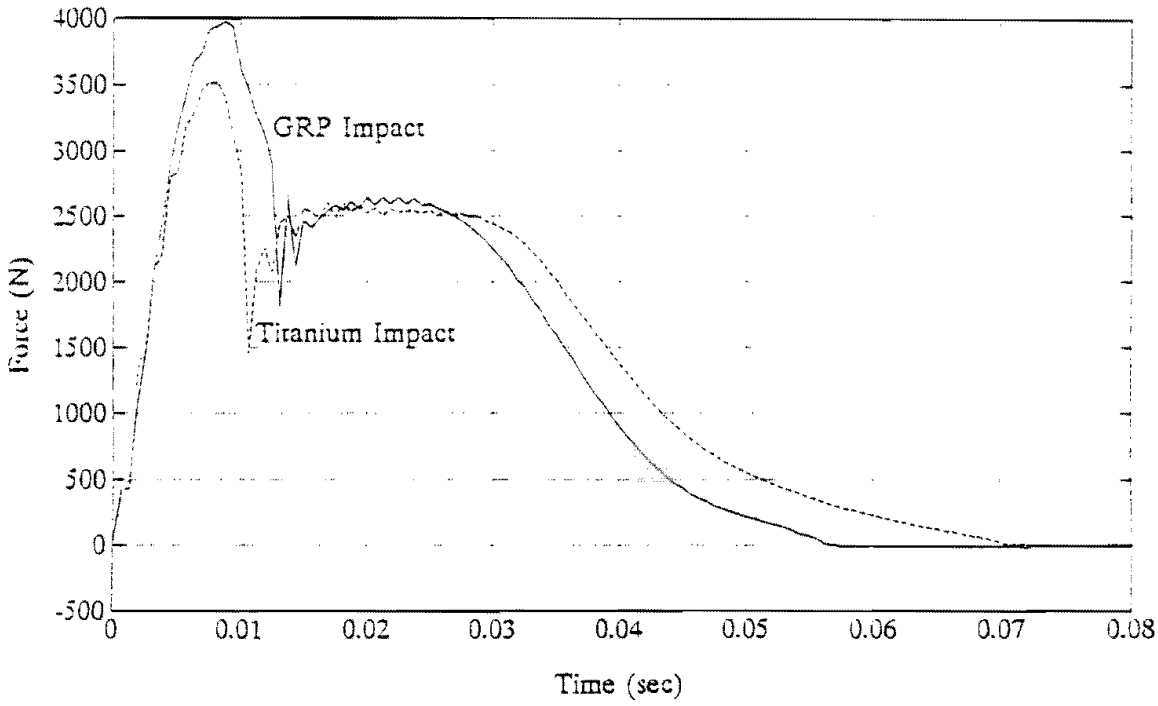

Figure 26. Impacts on GRP and Titanium Sides from 0.0508 m

TABLE X. AVERAGE CENTER DEFLECTIONS FOR IMPACT LOADING

Force (N)	GRP Side (m)	Titanium Side (m)
445	0.0007	0.0008
890	0.0015	0.0013
1335	0.0022	0.0020
1780	0.0026	0.0029
2225	0.0033	0.0041
2670	0.0037	0.0045
2893	0.0043	0.0051
3115	0.0046	0.0055
3338	0.0051	0.0063
3560	0.0056	-

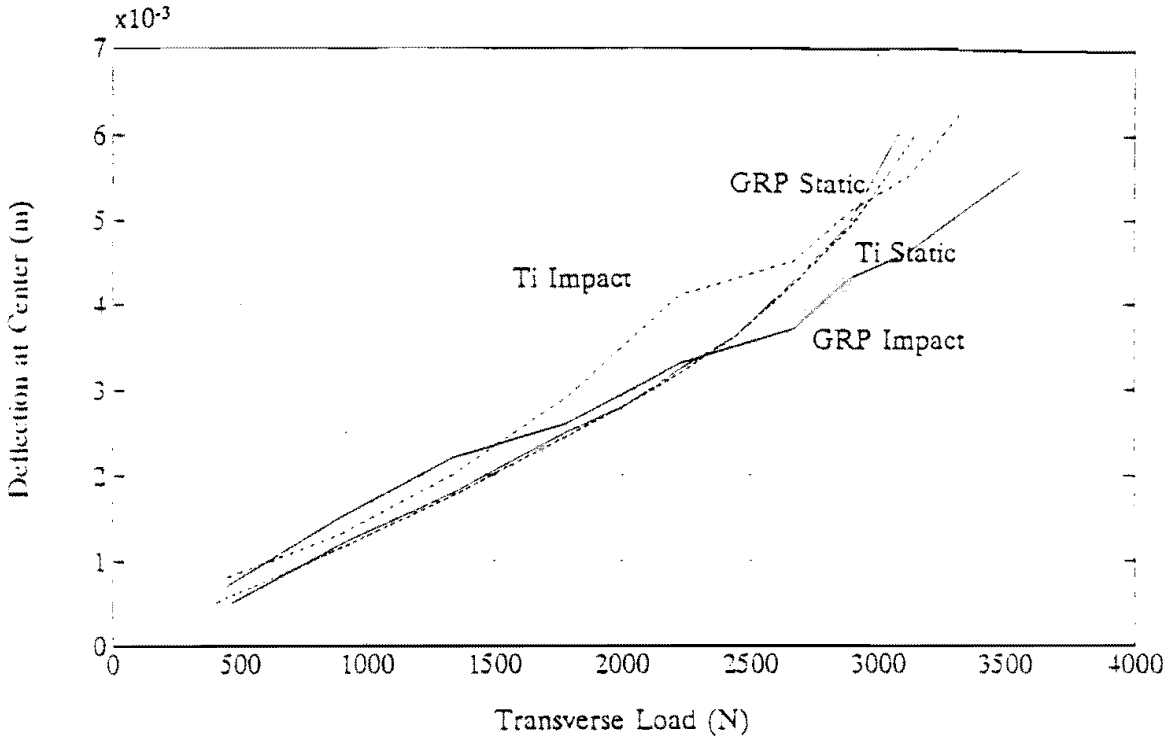

Figure 27. Deflection for Static and Impact Loads

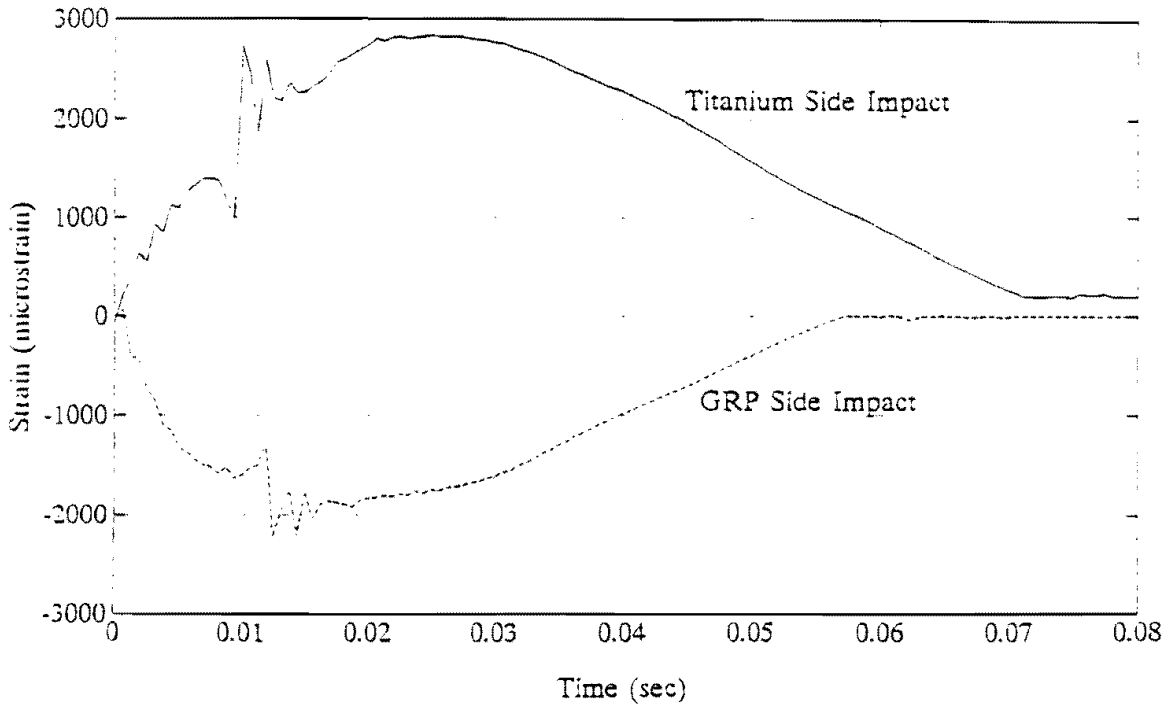

Figure 28. Strains at Failure Point (GRP Gages)

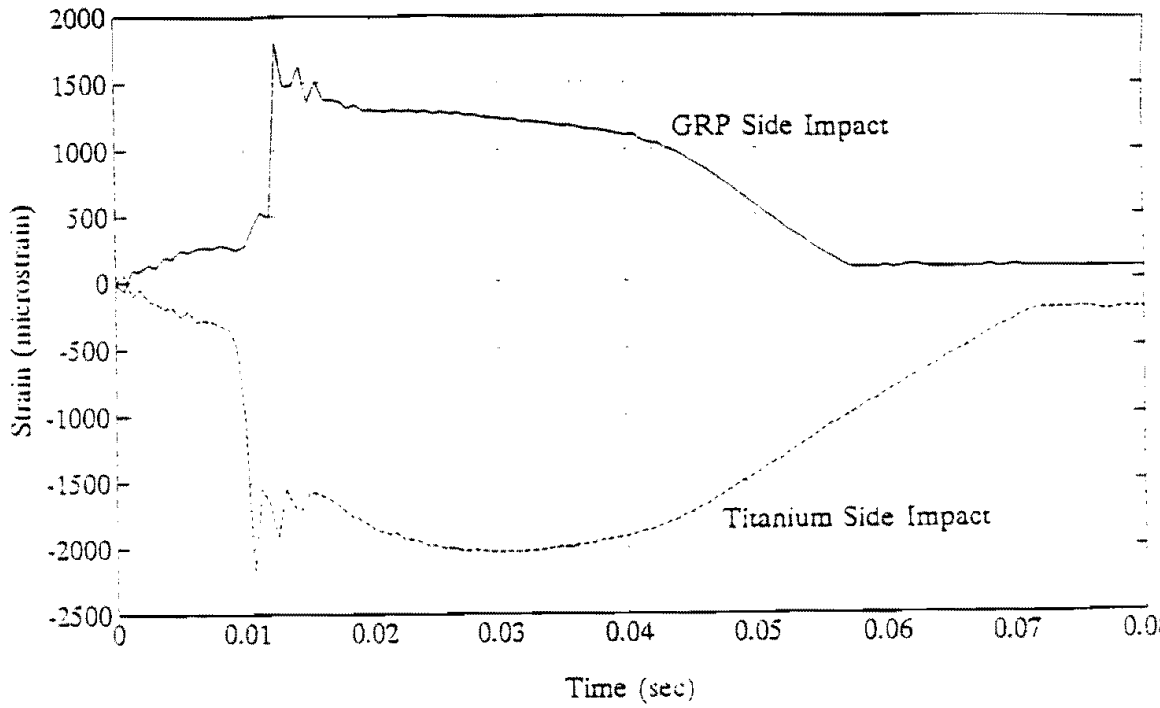

Figure 29. Strains at Failure Point (Ti Gages)

From the data it appears that when the strain magnitudes near the quarter point on the beam simultaneously reach approximately 1500 microstrain for the GRP facesheets and approximately 250 microstrain for the titanium facesheets, failure in the core occurs. This failure always occurs near the beam's quarter length point. Examination of the beam under load reveals that the greatest amount of change in curvature occurs in this region. Intuitively, this indicates that the shear should also be greatest in this vicinity. The large amount of shear stress in the core results in failure at the quarter points.

It was also observed that failure for impacted samples occurred at one location, but the statically loaded samples failed at two locations. These two locations were at each end near the quarter points. Similar to a monolith material, failure initiates at an internal point of discontinuity or weakness. Once damage is initiated, increasing the amount of absorbed energy due to loading causes the damage to propagate throughout the local vicinity until the structure is sufficiently weakened so that failure on a global scale of the component occurs. This type of failure mechanism is a time dependent function. In the impacted specimens, failure occurred only at one end. Once failure occurred at one location the deformation in that region rapidly increased as the core lost stiffness. The massive deformation in this one region sufficiently precluded failure at another location during the extremely short time interval of the impact.

When the composites were statically loaded, however, the loading process took a much longer time to complete. In this case, the force level was built up incrementally and sufficient time was available for damage to occur and propagate at more than one location. All statically loaded samples were damaged by core crimping/shear at two locations. This time dependent behavior may also be the reason the magnitude of force required for failure in the static loading case is approximately 444.8 N (100 lbf.) less than the failure load in the impact tests.

B. COMPRESSIVE STRENGTH AFTER IMPACT

One of the objectives of this study at the onset was the development of a relation which would correlate the amount of damage inflicted in the composite to the residual compressive strength of the sample. The initiation and degree of propagation of damage is a function of load applied to the composite. Primary indicators of this applied load are peak impact force, work done on the sample by the impactor, the momentum imparted to the sample and the change of kinetic energy experienced by the impactor. From the force plots it was obvious that the failure force was dependent on the manner the force was applied and the side of the composite which was loaded. As illustrated in Figure 22, peak contact force levels do not provide consistent indications of residual compressive strength. The absorbed energy, however, provides a more independent indicator.

Since peak force does not provide a good indication, other loading parameters available from the experimental results were considered. As detailed earlier the area under the force displacement curve provides a measure of the amount of work done by the impactor on the composite. A simple trapezoidal rule integration can be used to calculate this amount of energy. Likewise, the area under the force versus time plot is equal to the amount of momentum imparted to the sample ($M = \int F dt$). A simple trapezoidal rule integration can be again employed to determine this amount. Another

energy parameter which can be easily determined from the data is the change in kinetic energy of the impactor. By using the relation:

$$K.E. = \frac{1}{2} m (v_i^2 - v_f^2)$$

where v_i is the impactor velocity immediately prior to impact and v_f is the rebound velocity of the impactor, the change in kinetic energy occurring during the impact can be determined.

Table XI lists the peak forces, momentum, energy imparted, change in kinetic energy values and the resulting compressive failure strengths for each impact test. Note that although the peak forces generated for the same drop heights vary by at least 444.8 N (100 lbf.), the energy amounts and momentum values vary by less than 10%. For this reason, the energy levels and momentum are the principal indicators which need to be considered. Figures 30, 31 and 32 graphically illustrate the residual compressive strength relationships between energy imparted, change in kinetic energy and change in momentum, respectively. Based on deviations for each side impacted, momentum values appear to be the most consistent indicators.

A comparison of energy imparted ratios and compressive failure load ratios (using the drop height figures from 0.0254 m (1 in.) in the denominator each time) suggests some type of one-to-one correlation for the GRP impacts. The energy ratios

for drops from 0.0381 m (1.5 in.) and 0.0508 m (2 in.) are 2.12 and 3.07, respectively. The corresponding compressive failure load ratios are 2.03 and 2.97, respectively. Unfortunately, when the same ratios are compared for the titanium impacts a good correlation is not readily apparent. The energy ratios are 1.8 and 2.78, respectively, while the compressive failure load ratios are 2.88 and 4.06, respectively. It is clear that in order to develop a more definitive quantitative relation, further experiments need to be performed. With more data available, a more reliable correlation between energy levels and the resulting reduction in compressive load carrying capability can be developed.

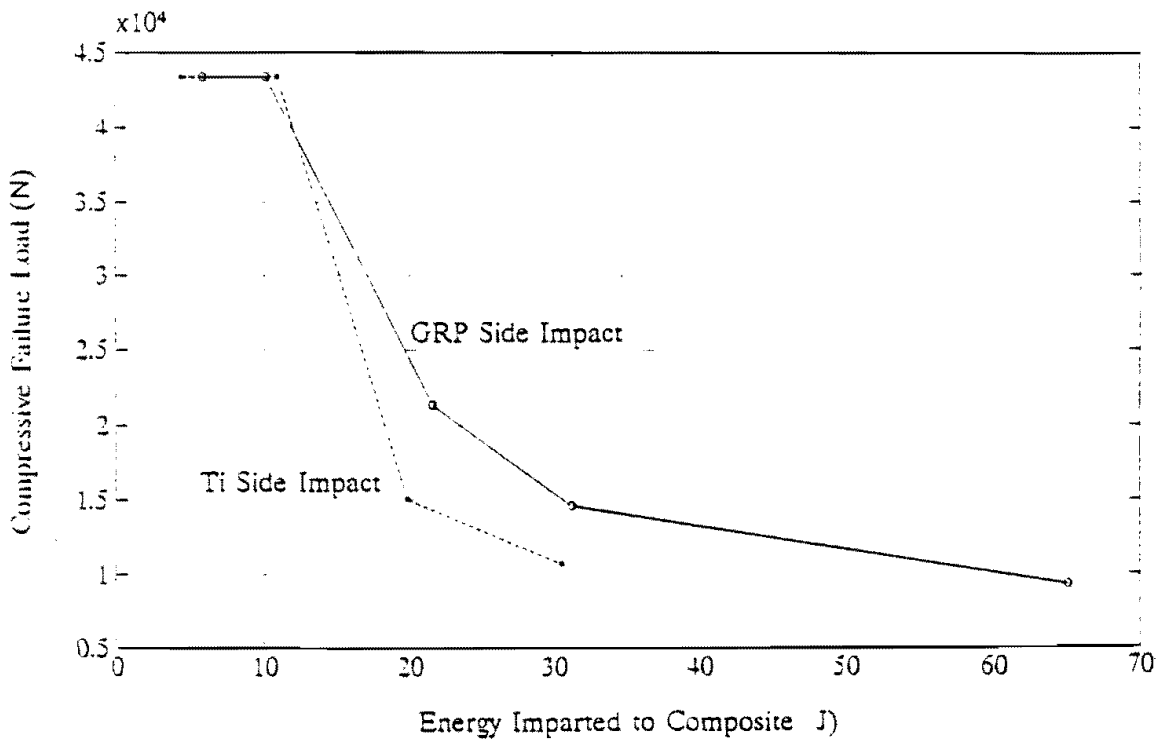

Figure 30. Energy Imparted vs Compressive Failure Load

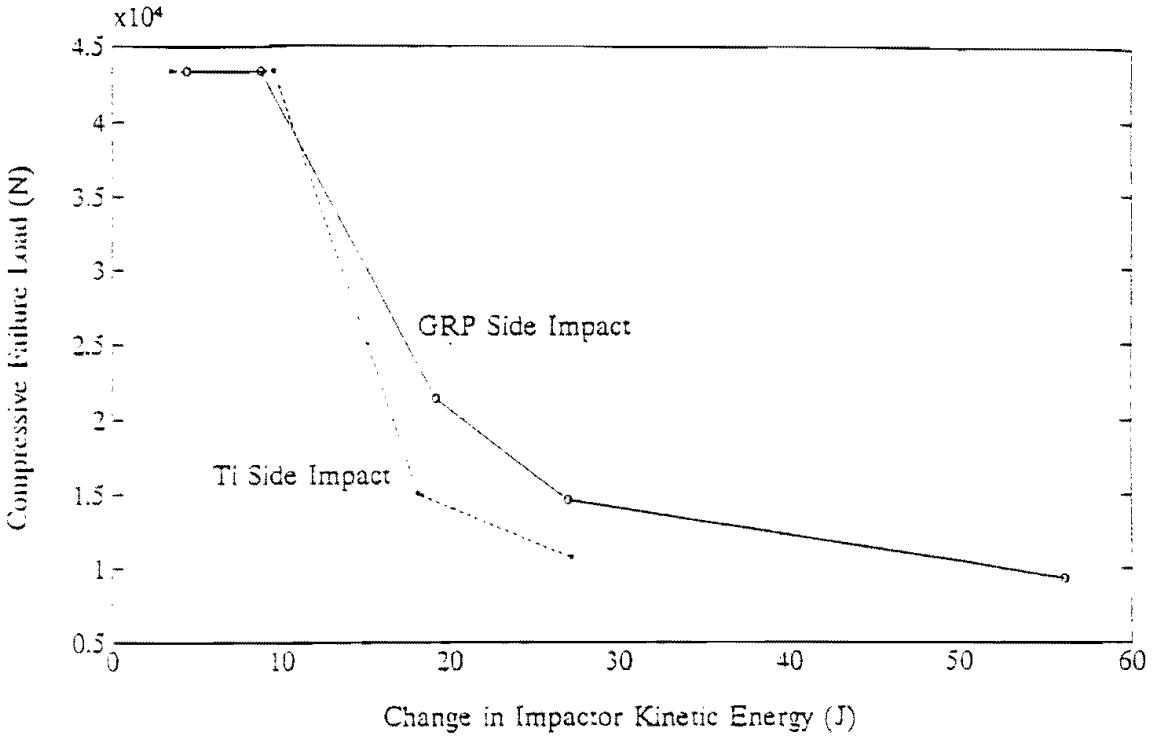

Figure 31. Change in Impactor Kinetic Energy vs Compressive

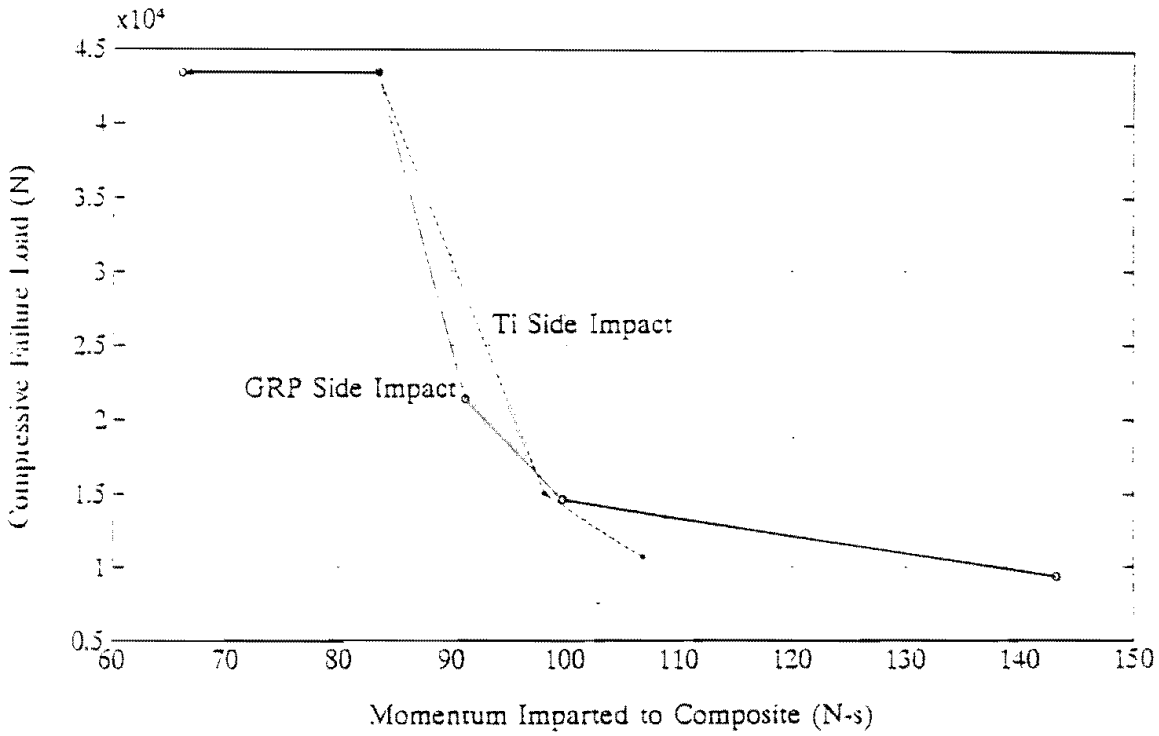

Figure 32. Change in Momentum vs Compressive Failure Load

TABLE XI. COMPRESSIVE STRENTGH TESTS

Peak Force (N)	Impact Side	Energy Imparted (J)	Kinetic Energy Change (J)	Momentum Change (N-s)	Compressive Failure Load (N)
2860	GRP	5.89	4.36	66.06	43370
3132	Ti	4.41	3.41	66.80	43370
3545	Ti	10.96	9.53	83.39	43370
3825	GRP	10.17	8.80	83.48	43370
3496	Ti	19.81	18.10	98.22	15035
3874	GRP	21.58	19.20	91.22	21351
3514	Ti	30.52	27.20	106.83	10676
3950	GRP	31.20	27.0	99.85	14590
3608	GRP	65.0	56.23	143.31	9341

It is noted that the same mode of failure which occurred in Murphy's study [Ref 1] of undamaged composites, also took place in the damaged samples in this study. In each case core crimping occurred at a region near the end, the sample would then rapidly deform, creating a "S" bend shape in the vicinity of the core crimping. Failure in each sample would, of course, occur in the same region which crimped

during impact or static loading. Table XII provides data for each of the statically loaded samples and the corresponding compressive failure loads.

From the data it appears that in the case of static loading, the resulting compressive failure load is independent of the side loaded. It should be noted that the compressive failure load for the second GRP side loaded sample was lower. In this case, once failure occurred at 3292 N (740 lbf.) the loading rate of the MTS machine was increased in order to cause more damage in the core and determine if the load magnitude could be further increased. The sample responded by increasing its deformation rate so that the 3292 N level was not exceeded. This did result, though, in more core damage which led to a reduced compressive load carrying capability by approximately 8896 N (2000 lbf.).

TABLE XII. COMPRESSIVE FAILURE LOADS FOR STATIC LOAD SAMPLES

Force (N)	Side Loaded	Compressive Failure Load (N)
3292	GRP	25444
3292	GRP	17793
3403	Ti	27490

VI. CONCLUSIONS

The response of an unbalanced sandwich composite subjected to either low-velocity impact or static transverse loads is complex. The results discovered during the experimental portion of this study underscores the requirement for performing numerous tests in order to be able to accurately understand how the composite behaves. Often times it was found that unexpected responses occurred for the various loading configurations. More tests are still required to be better able to understand and predict the mechanisms involved in the behavior of these unbalanced sandwich composites.

Several key findings from this study are listed below:

- Classical beam bending theory cannot be applied to model this composite.
- Transverse shear forces in the core cannot be neglected and have significant effects on the facesheet strain response.
- The compressive load carrying capability of an unbalanced sandwich composite is very sensitive to core damage. Once a threshold value is exceeded a small amount of damage occurs in the core. This small amount of damage leads to a significant reduction (50%-60%) in compressive load carrying strength.
- For impacts from the same height, impacts on the titanium side result in 30%-40% greater reductions in compressive strength.
- External work performed by the impactor on the composite, the change of impactor kinetic energy and the amount of momentum imparted to the sample are all better indicators to be used as a parameter to predict residual compressive strength. Of these three, momentum may be the best indicator.

- Failure occurs at the quarter points of the beam. Failure occurs at one location for impact loads and at both quarter points for static loads.

- Onset of core damage occurs at the same magnitude of strain, approximately 300 microstrains for titanium and 1500 microstrains for GRP, regardless of type of loading or side loaded. This indicates failure occurs, as expected, at the same stress levels and can, therefore, be used as a good failure criteria.

As stated previously more research needs to be focused on the behavior of this unbalanced sandwich composite and other similar composite. It will be important to perform tests on samples involving different geometries and support configurations. With the gathering of more data, more accurate predictions concerning structural responses due to low-velocity impact and compressive loads can be made. Additional data will also enable verification of any finite element model designed to analyze this type of composite.

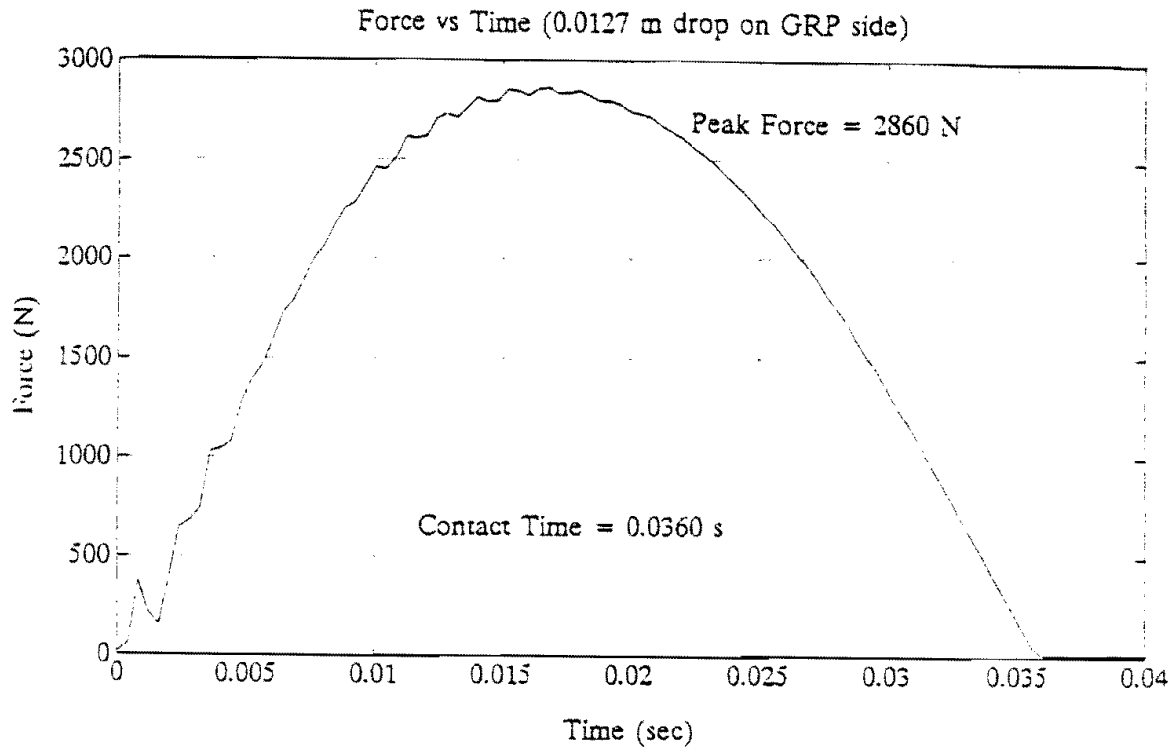
Force vs Time (0.0127 m drop on GRP side)
Peak Force = 2860 N
Contact Time = 0.0360 s
Force (N)
Time (sec)
3000
2500
2000
1500
1000
500
0
0.005
0.01
0.015
0.02
0.025
0.03
0.035
0.04

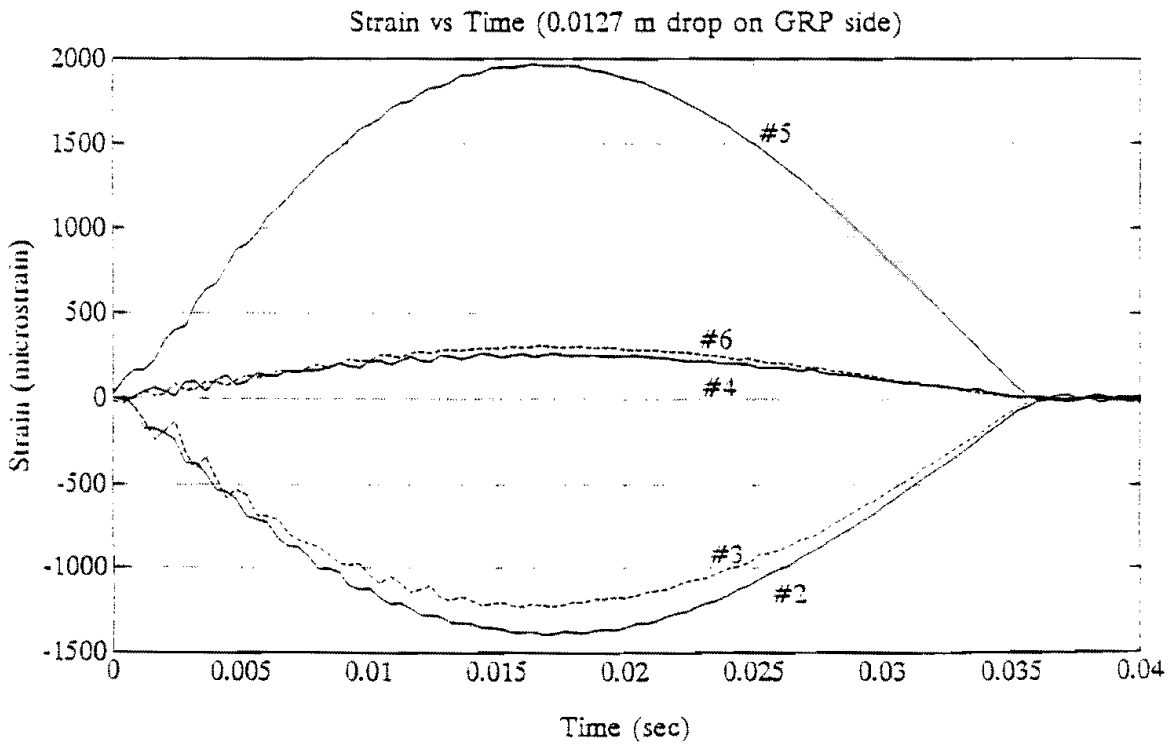
Strain vs Time (0.0127 m drop on GRP side)
#5
#6
#4
#3
#2
Strain (microstrain)
Time (sec)
2000
1500
1000
500
0
-500
-1000
-1500
0.005
0.01
0.015
0.02
0.025
0.03
0.035
0.04

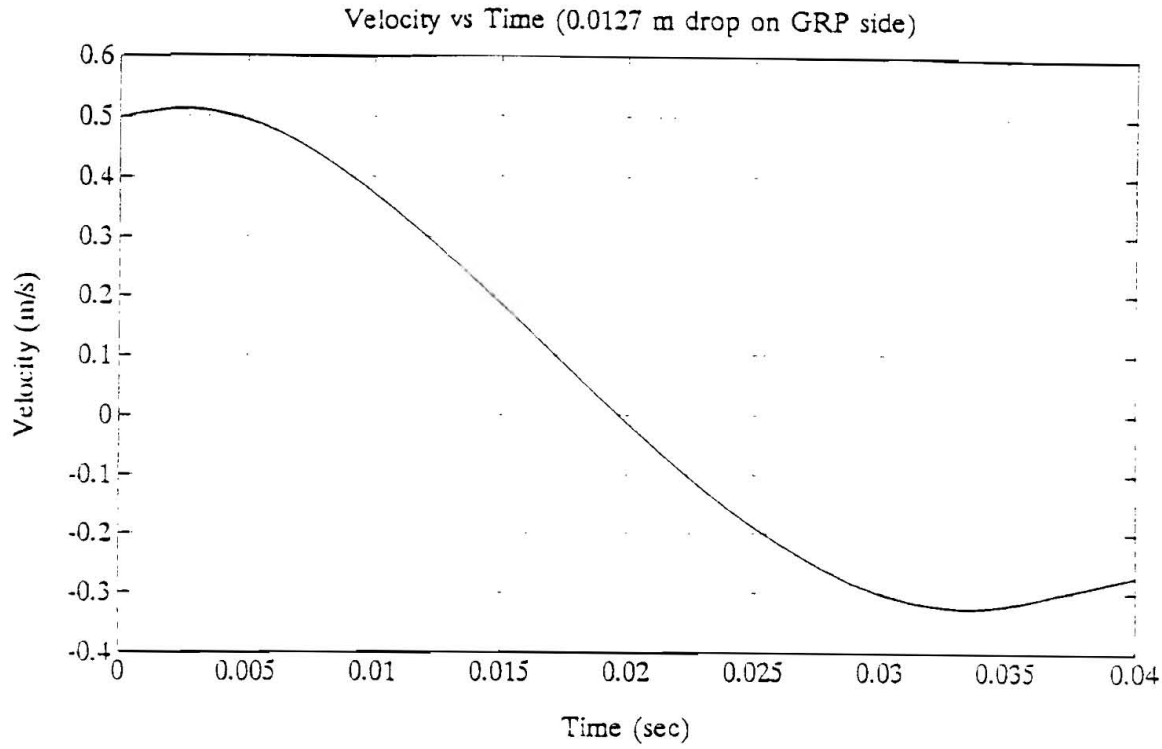
Velocity vs Time (0.0127 m drop on GRP side)
Velocity (m/s)
0.6
0.5
0.4
0.3
0.2
0.1
0
-0.1
-0.2
-0.3
-0.4
0
0.005
0.01
0.015
0.02
0.025
0.03
0.035
0.04
Time (sec)

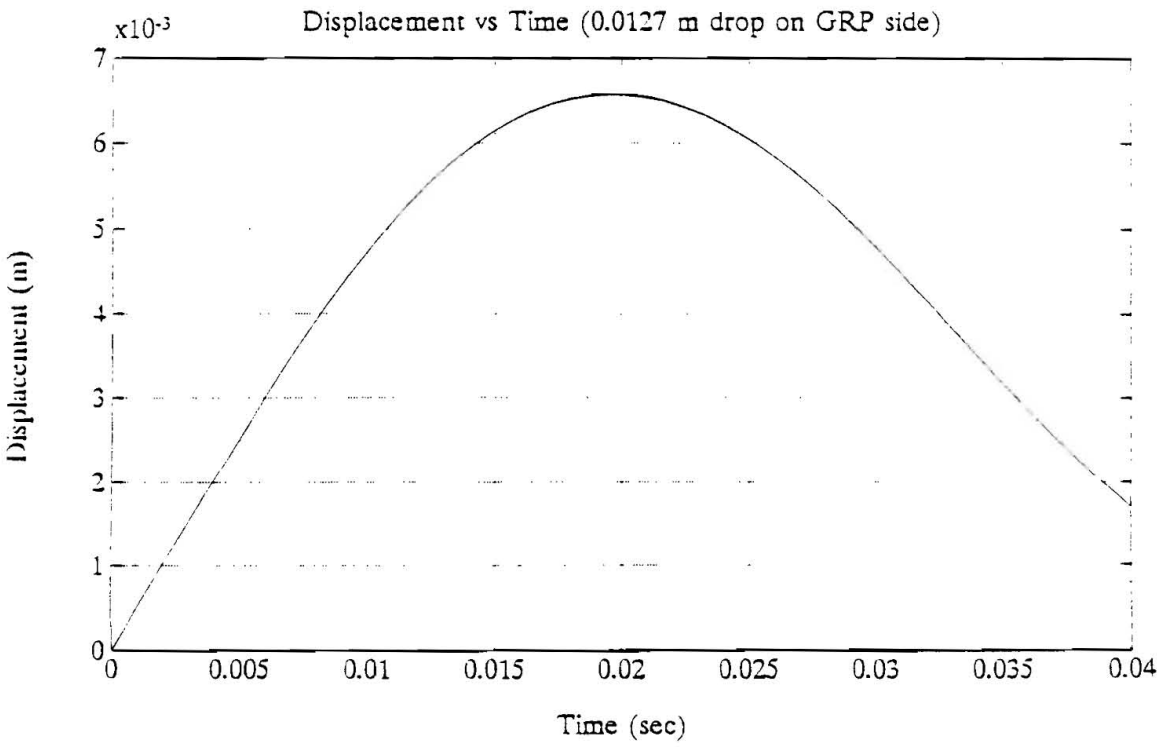
x10-3
Displacement vs Time (0.0127 m drop on GRP side)
Displacement (m)
7
6
5
4
3
2
1
0
0
0.005
0.01
0.015
0.02
0.025
0.03
0.035
0.04
Time (sec)

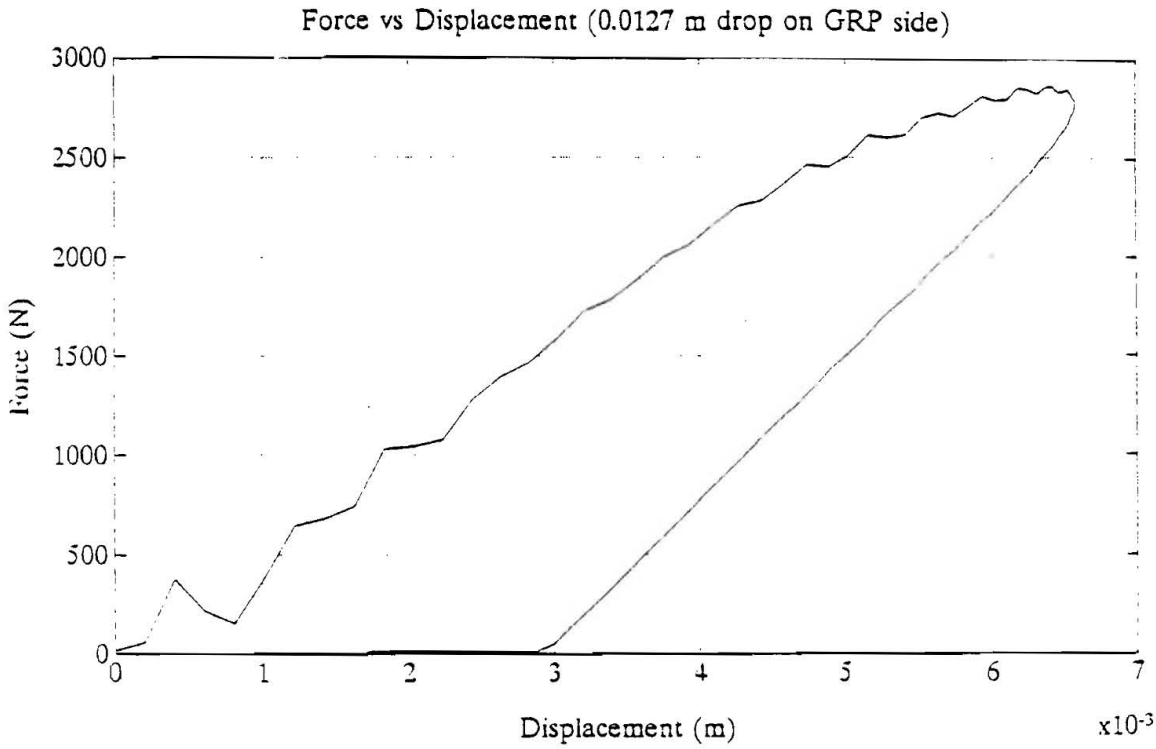
Force vs Displacement (0.0127 m drop on GRP side)
Force (N)
3000
2500
2000
1500
1000
500
0
0
1
2
3
4
5
6
7
Displacement (m)
x10-3

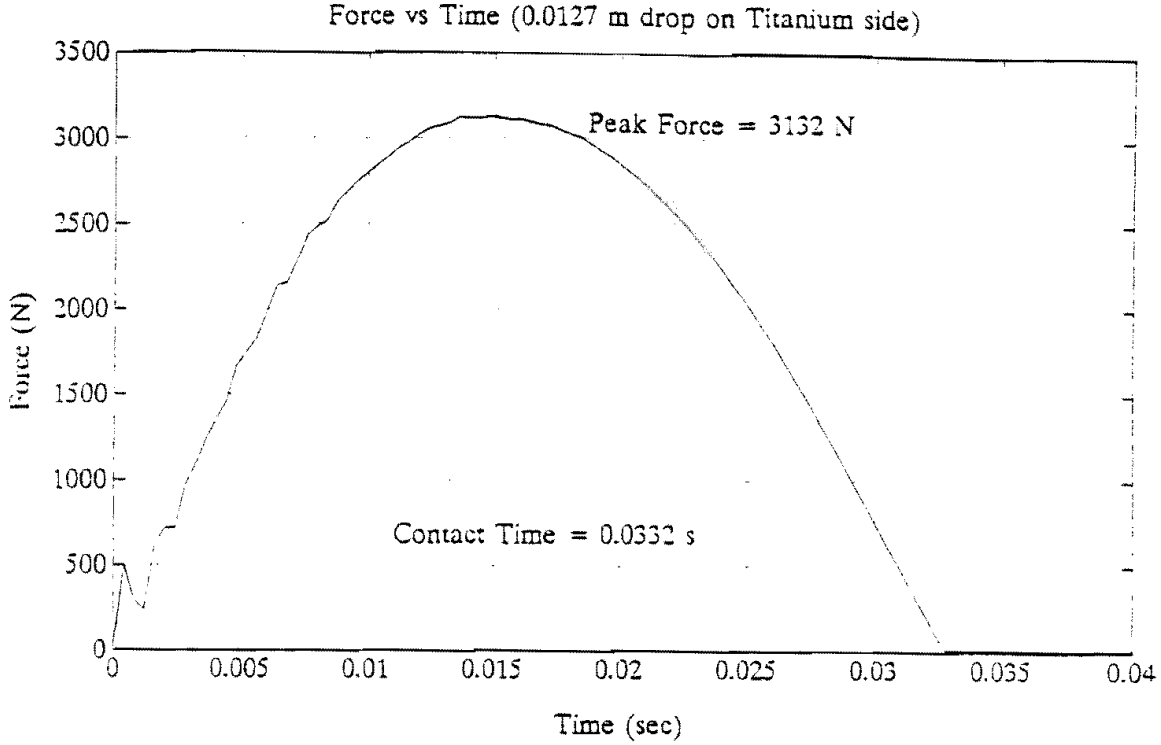
Force vs Time (0.0127 m drop on Titanium side)
Peak Force = 3132 N
Contact Time = 0.0332 s
Force (N)
Time (sec)
3500
3000
2500
2000
1500
1000
500
0
0.005
0.01
0.015
0.02
0.025
0.03
0.035
0.04

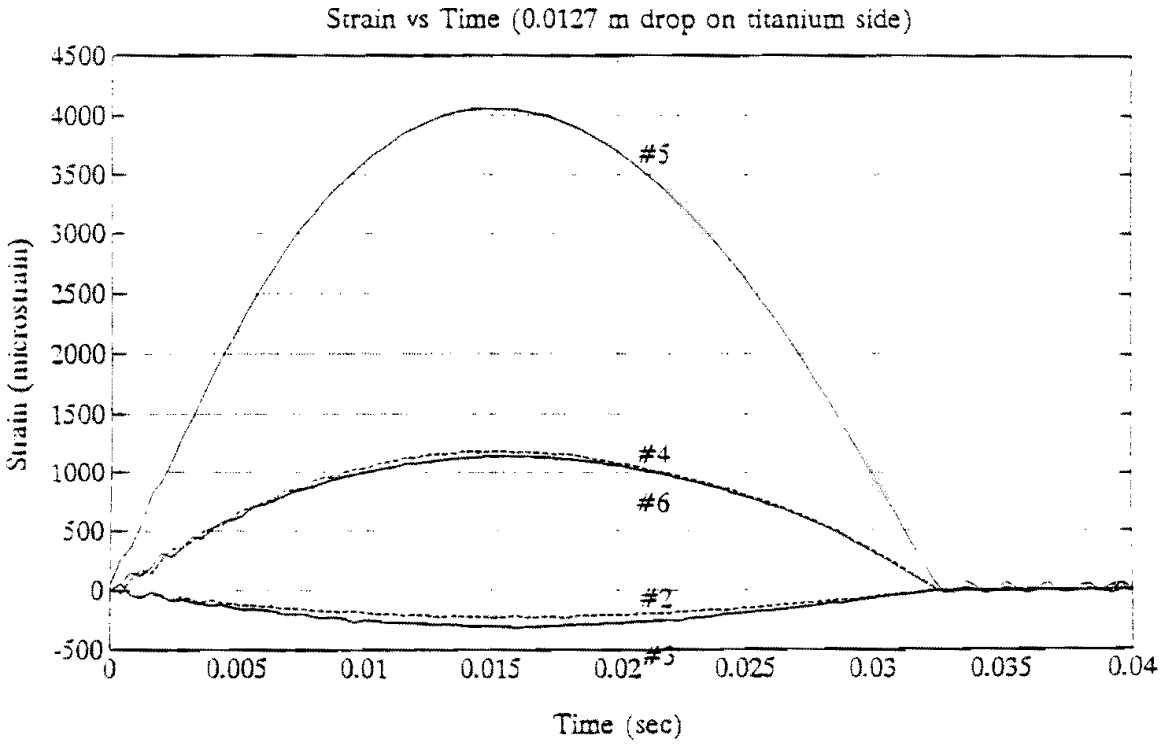
Strain vs Time (0.0127 m drop on titanium side)
#5
#4
#6
#2
#3
Strain (microstrain)
Time (sec)
4500
4000
3500
3000
2500
2000
1500
1000
500
0
-500
0
0.005
0.01
0.015
0.02
0.025
0.03
0.035
0.04

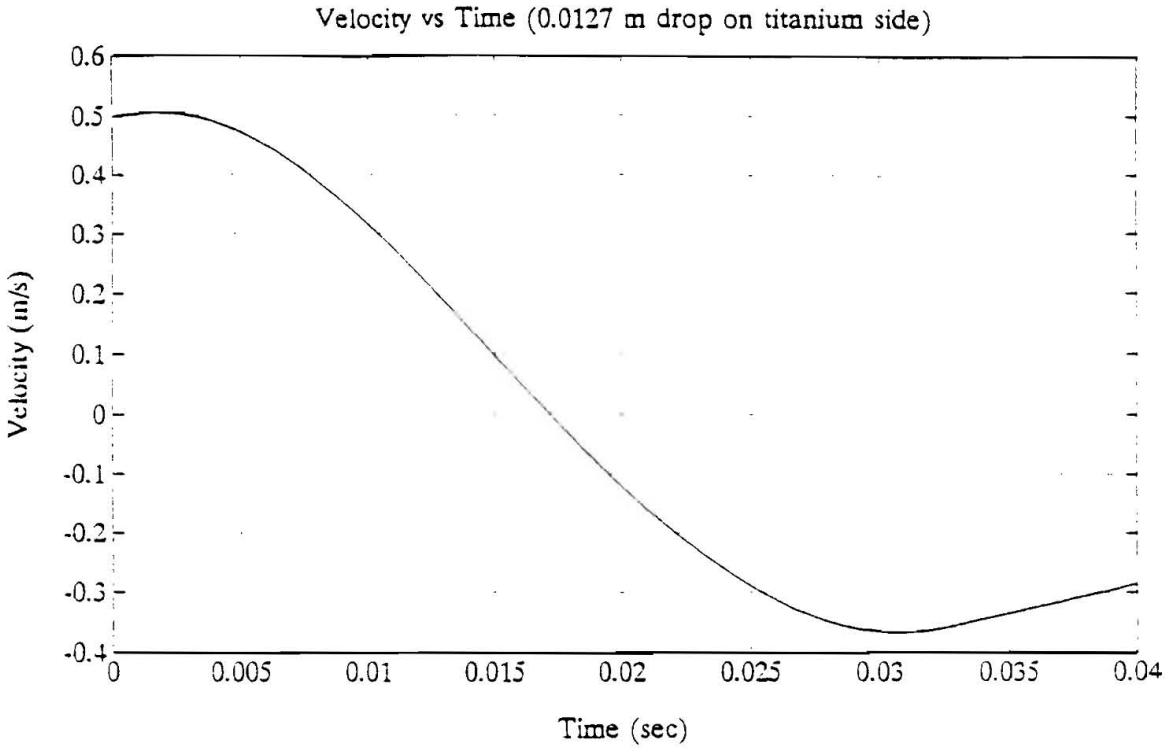
Velocity vs Time (0.0127 m drop on titanium side)
Velocity (m/s)
0.6
0.5
0.4
0.3
0.2
0.1
0
-0.1
-0.2
-0.3
-0.4
0
0.005
0.01
0.015
0.02
0.025
0.03
0.035
0.04
Time (sec)

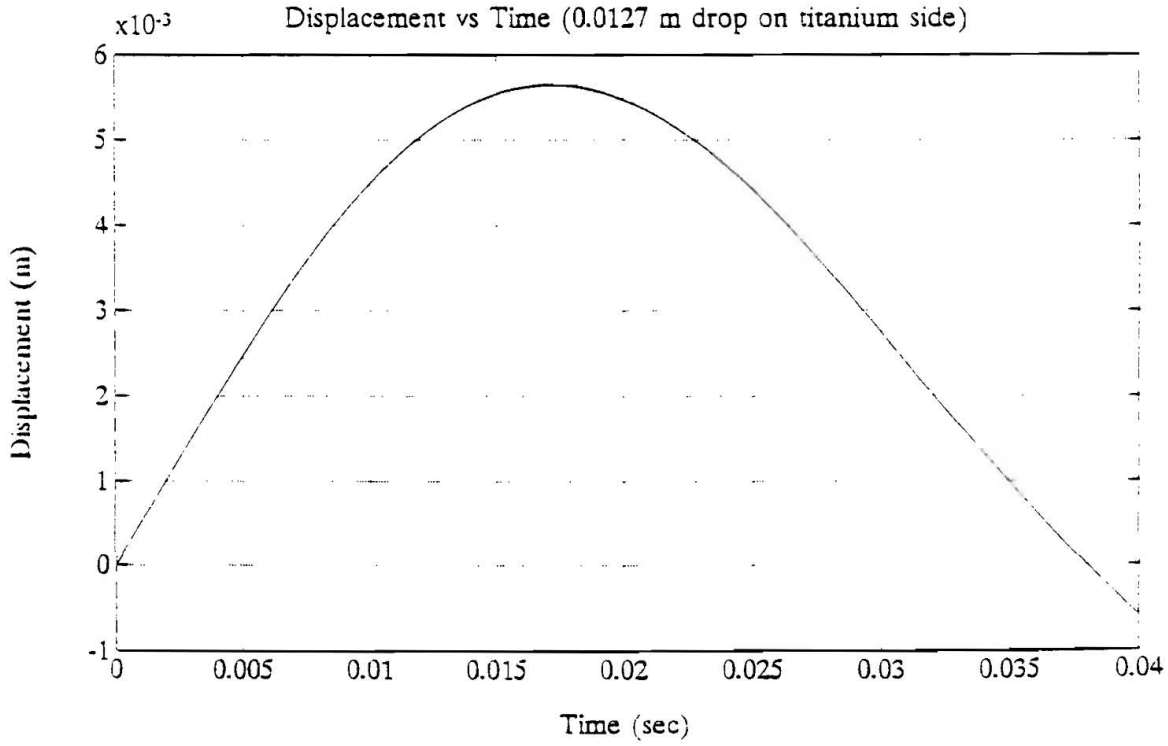
x10-3
Displacement vs Time (0.0127 m drop on titanium side)
Displacement (m)
6
5
4
3
2
1
0
-1
0
0.005
0.01
0.015
0.02
0.025
0.03
0.035
0.04
Time (sec)

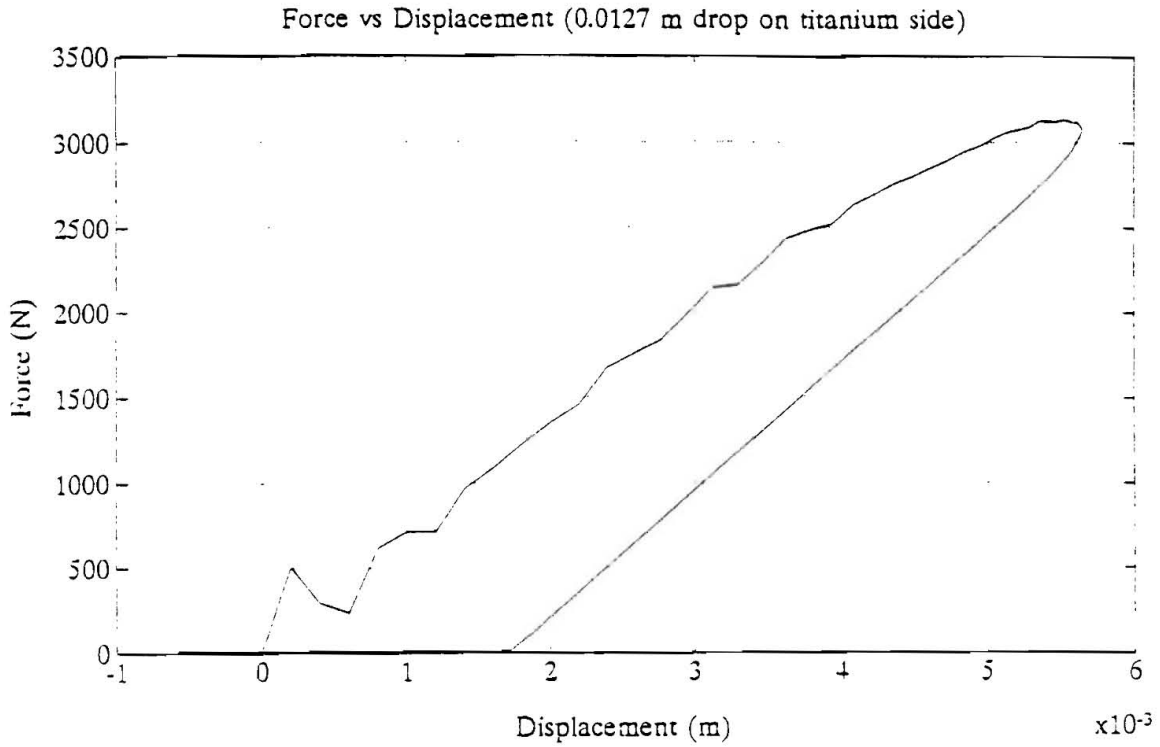
Force vs Displacement (0.0127 m drop on titanium side)
Force (N)
3500
3000
2500
2000
1500
1000
500
0
-1
0
1
2
3
4
5
6
Displacement (m)
x10-3

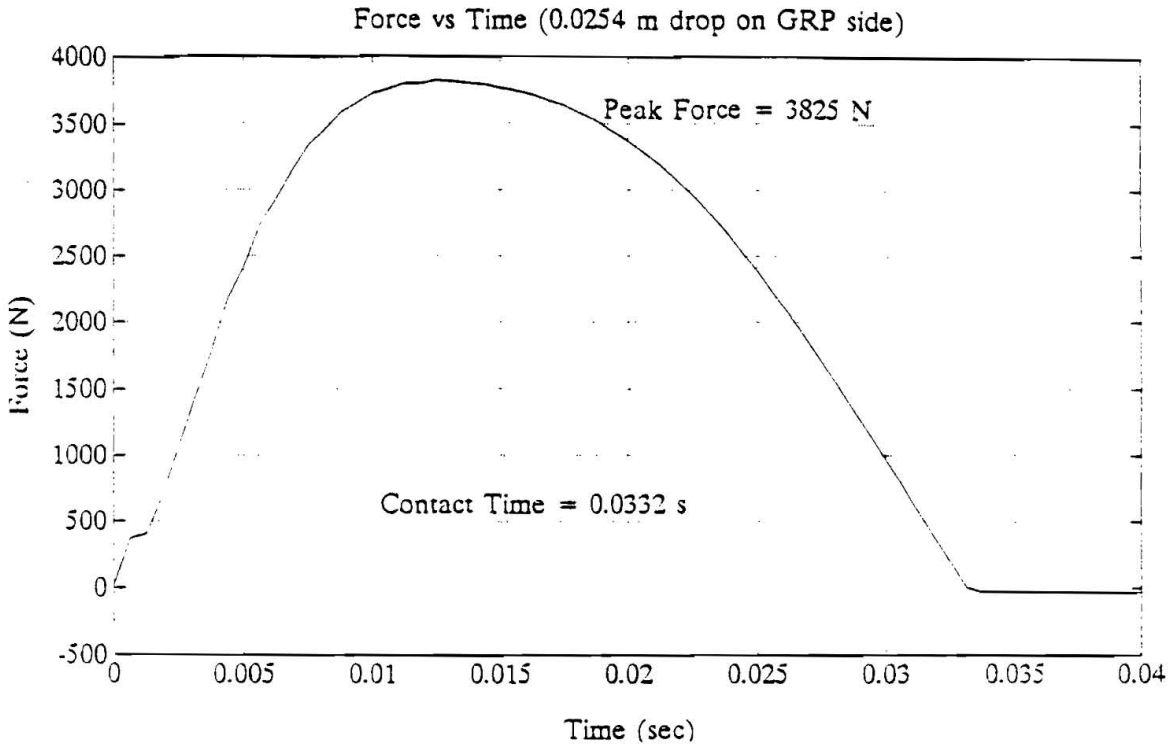
Force vs Time (0.0254 m drop on GRP side)
Peak Force = 3825 N
Contact Time = 0.0332 s
Force (N)
Time (sec)
4000
3500
3000
2500
2000
1500
1000
500
0
-500
0
0.005
0.01
0.015
0.02
0.025
0.03
0.035
0.04

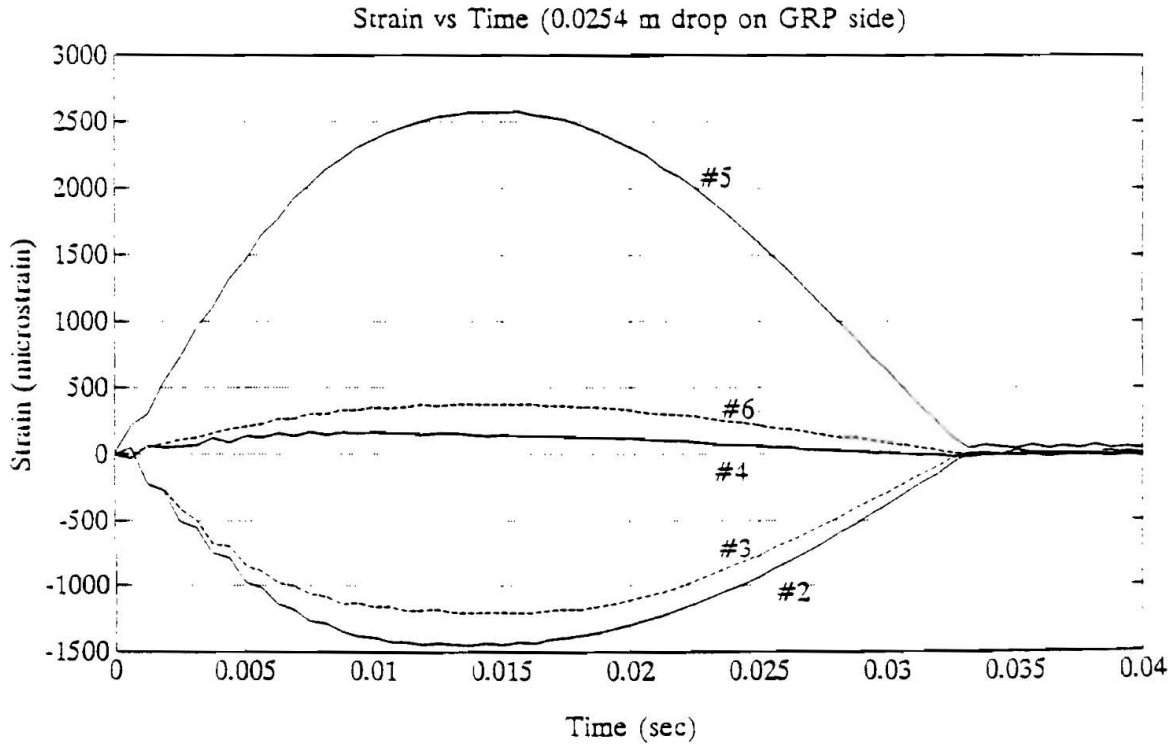
Strain vs Time (0.0254 m drop on GRP side)
Strain (microstrain)
Time (sec)
#5
#6
#4
#3
#2
3000
2500
2000
1500
1000
500
0
-500
-1000
-1500
0
0.005
0.01
0.015
0.02
0.025
0.03
0.035
0.04

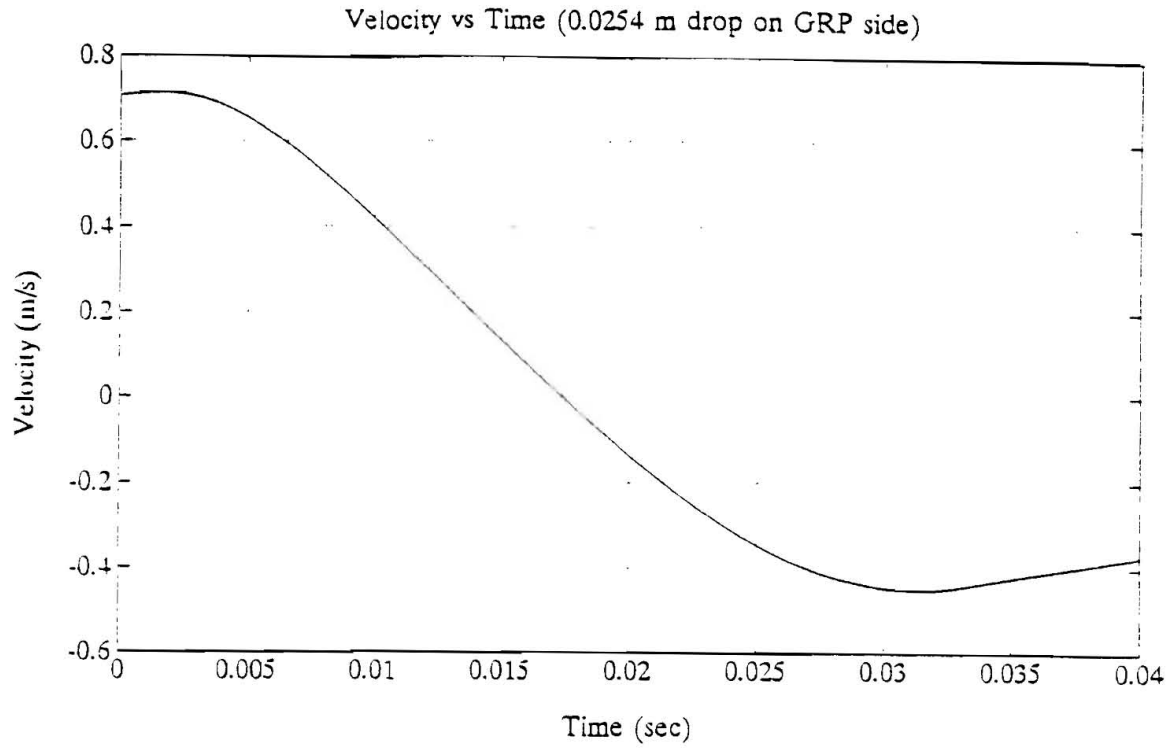
Velocity vs Time (0.0254 m drop on GRP side)
Velocity (m/s)
0.8
0.6
0.4
0.2
0
-0.2
-0.4
-0.6
0
0.005
0.01
0.015
0.02
0.025
0.03
0.035
0.04
Time (sec)

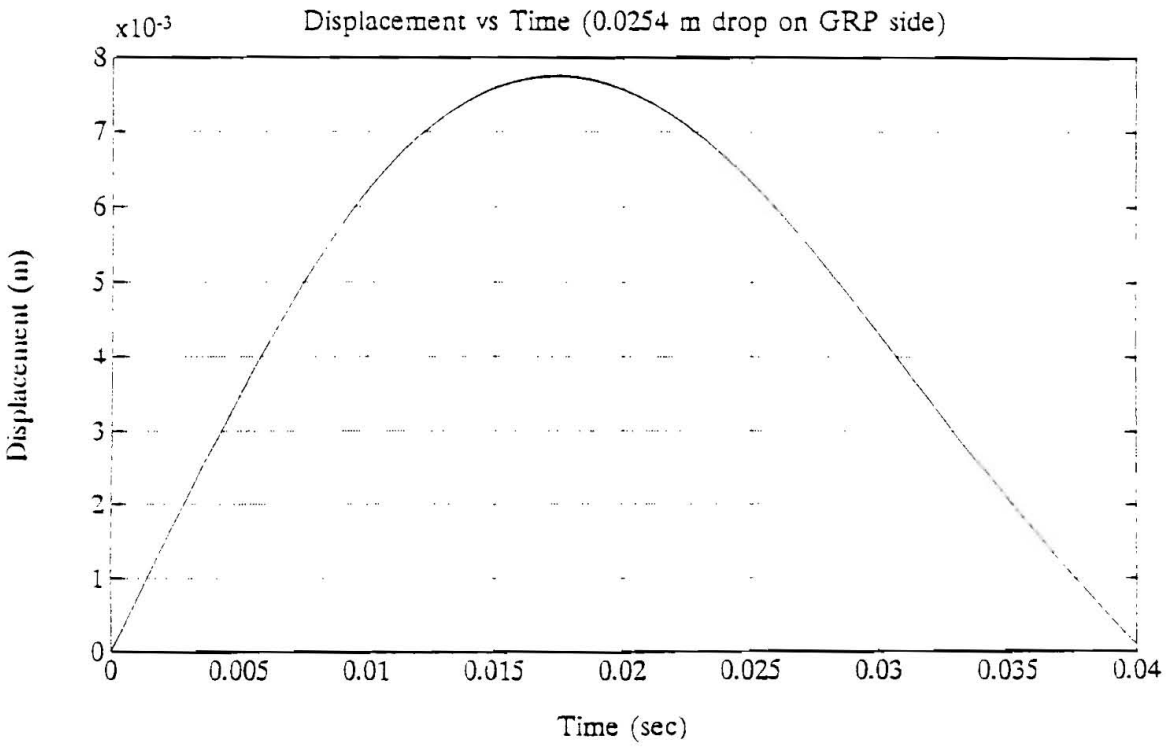
x10-3
Displacement vs Time (0.0254 m drop on GRP side)
Displacement (m)
8
7
6
5
4
3
2
1
0
0
0.005
0.01
0.015
0.02
0.025
0.03
0.035
0.04
Time (sec)

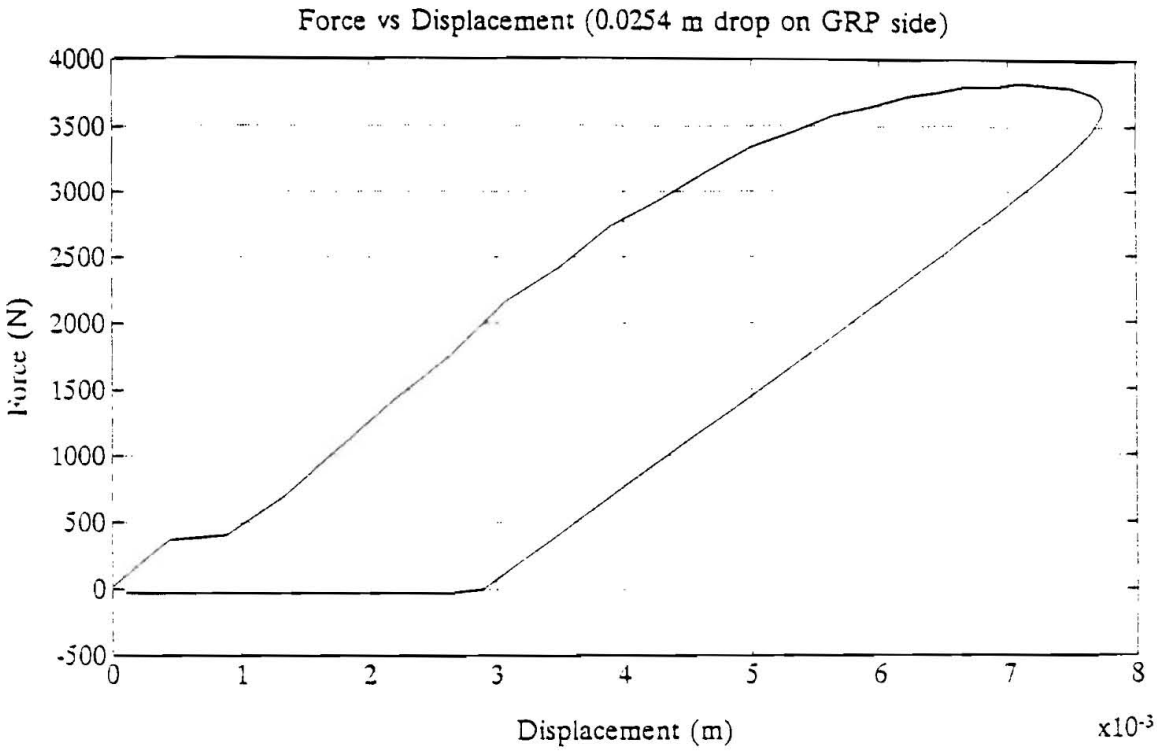
Force vs Displacement (0.0254 m drop on GRP side)
Force (N)
4000
3500
3000
2500
2000
1500
1000
500
0
-500
0
1
2
3
4
5
6
7
8
Displacement (m)
x10-3

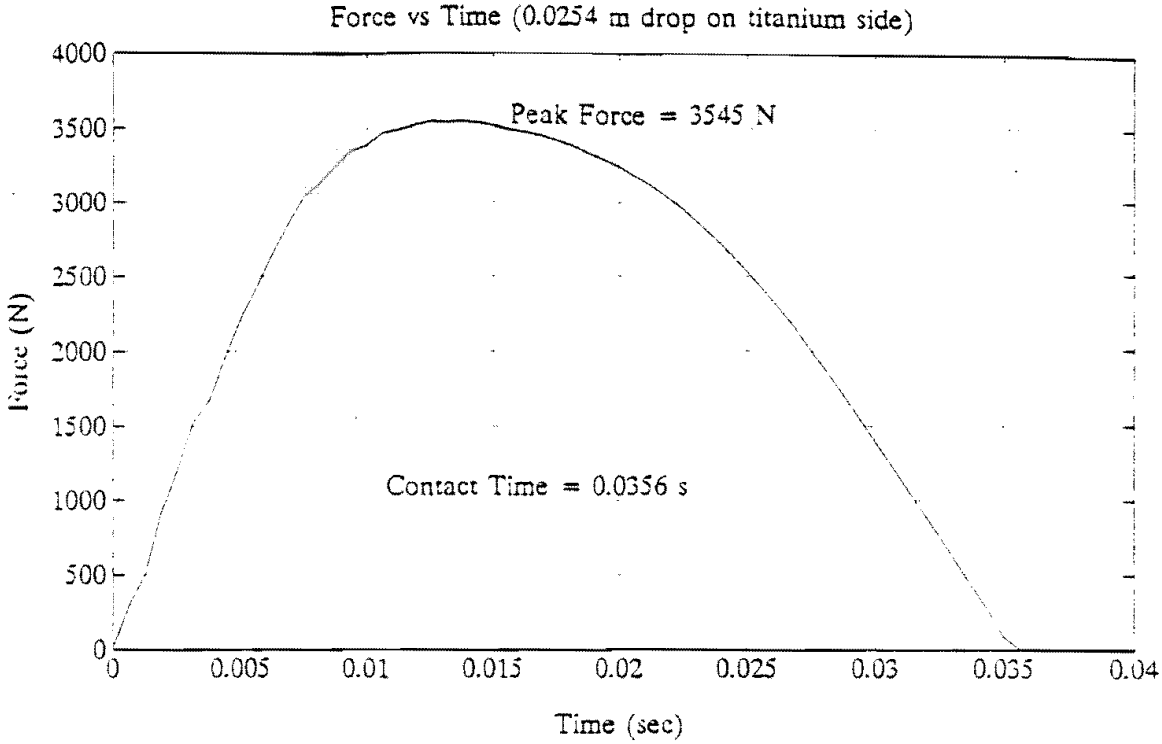
Force vs Time (0.0254 m drop on titanium side)
Peak Force = 3545 N
Contact Time = 0.0356 s
Force (N)
Time (sec)
4000
3500
3000
2500
2000
1500
1000
500
0
0
0.005
0.01
0.015
0.02
0.025
0.03
0.035
0.04

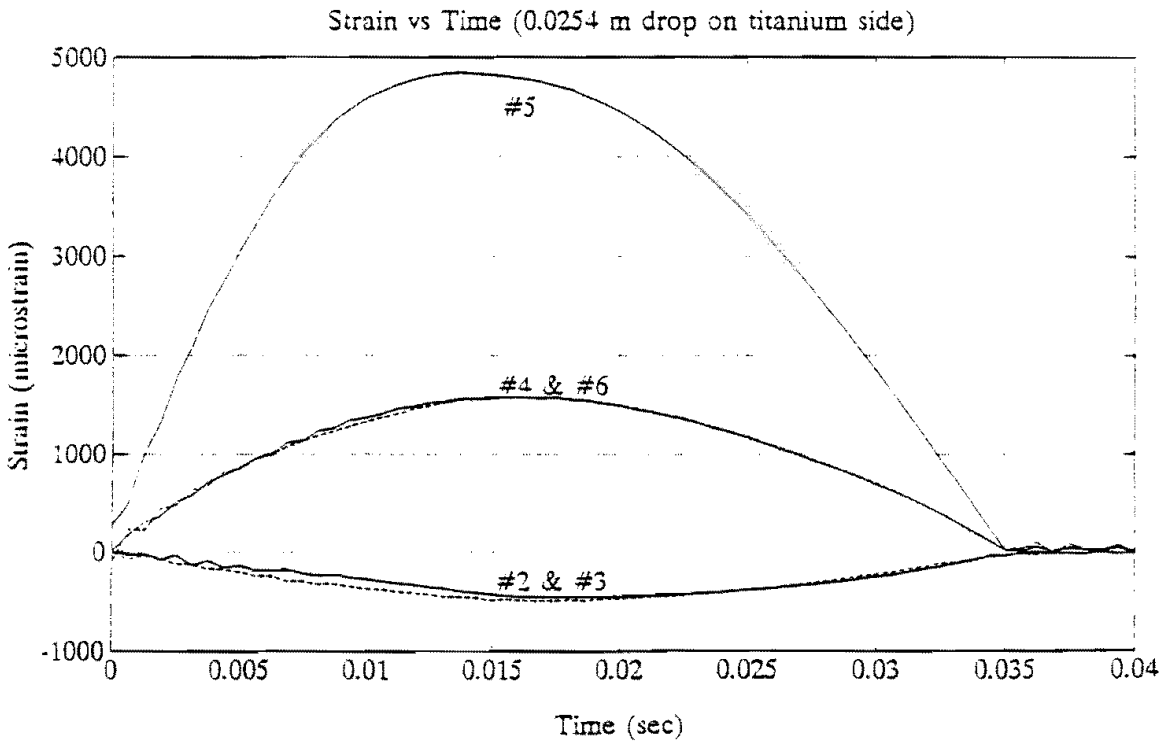
Strain vs Time (0.0254 m drop on titanium side)
#5
#4 & #6
#2 & #3
Strain (microstrain)
Time (sec)
5000
4000
3000
2000
1000
0
-1000
0
0.005
0.01
0.015
0.02
0.025
0.03
0.035
0.04

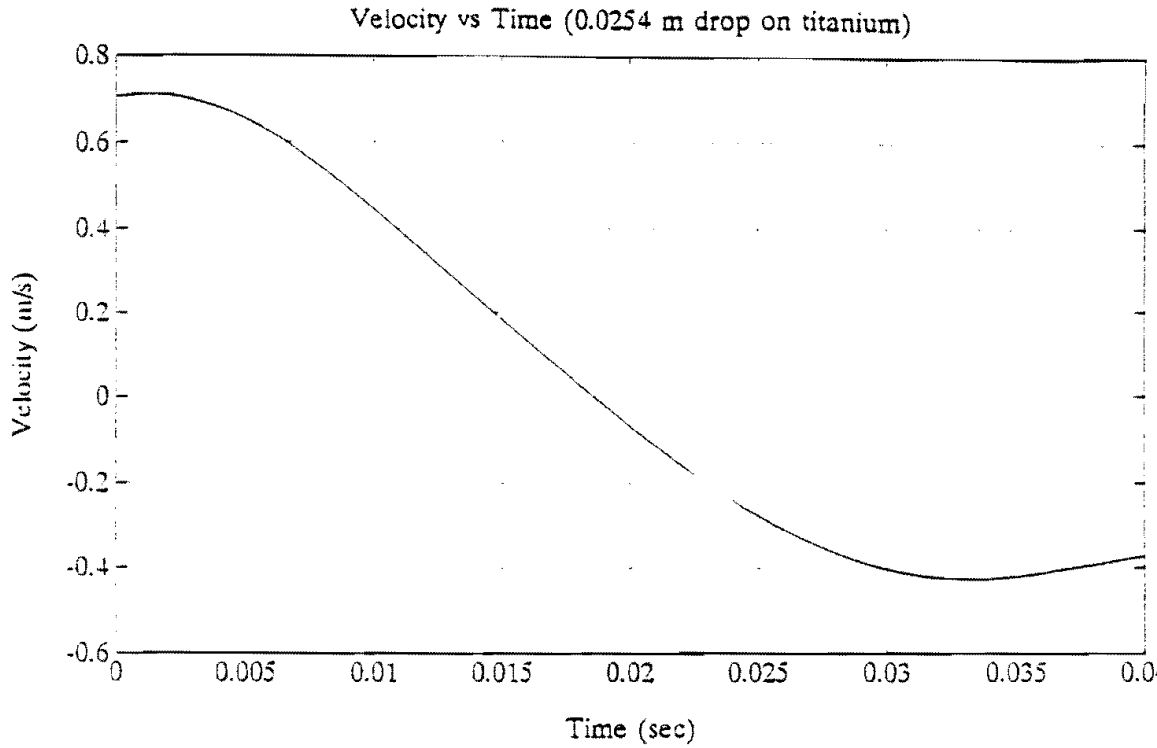
Velocity vs Time (0.0254 m drop on titanium)
Velocity (m/s)
0.8
0.6
0.4
0.2
0
-0.2
-0.4
-0.6
0
0.005
0.01
0.015
0.02
0.025
0.03
0.035
0.04
Time (sec)

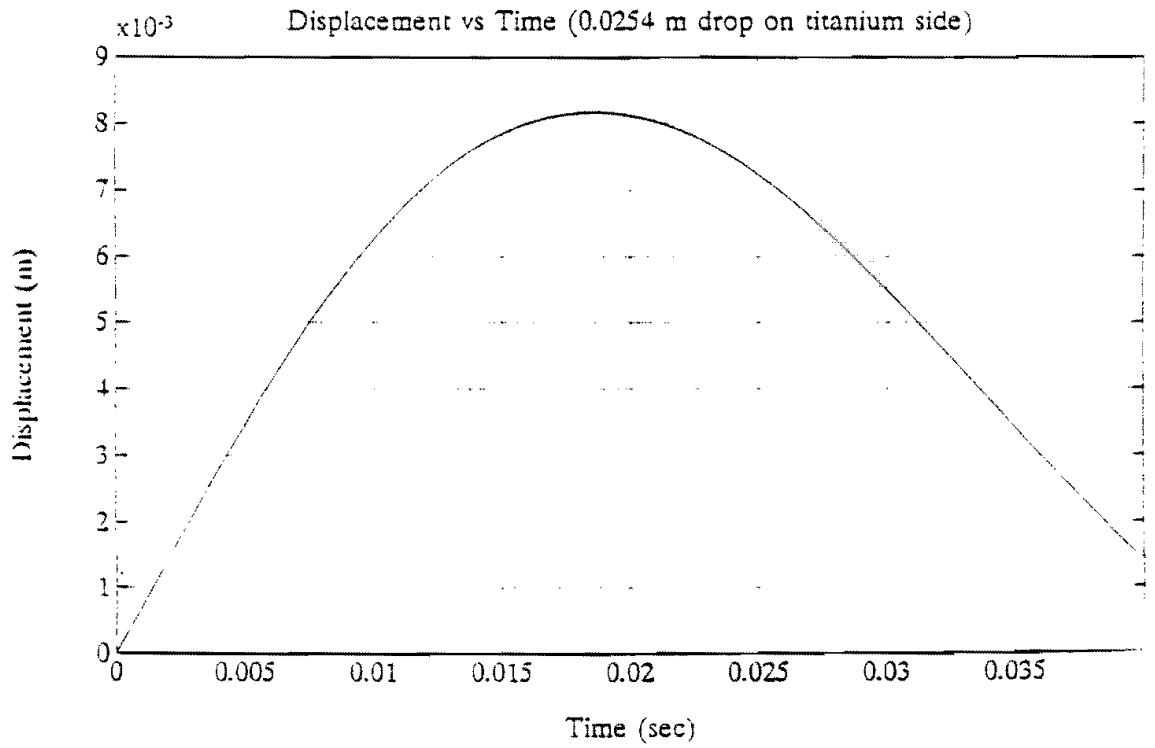
x10-3
Displacement vs Time (0.0254 m drop on titanium side)
Displacement (m)
9
8
7
6
5
4
3
2
1
0
0
0.005
0.01
0.015
0.02
0.025
0.03
0.035
Time (sec)

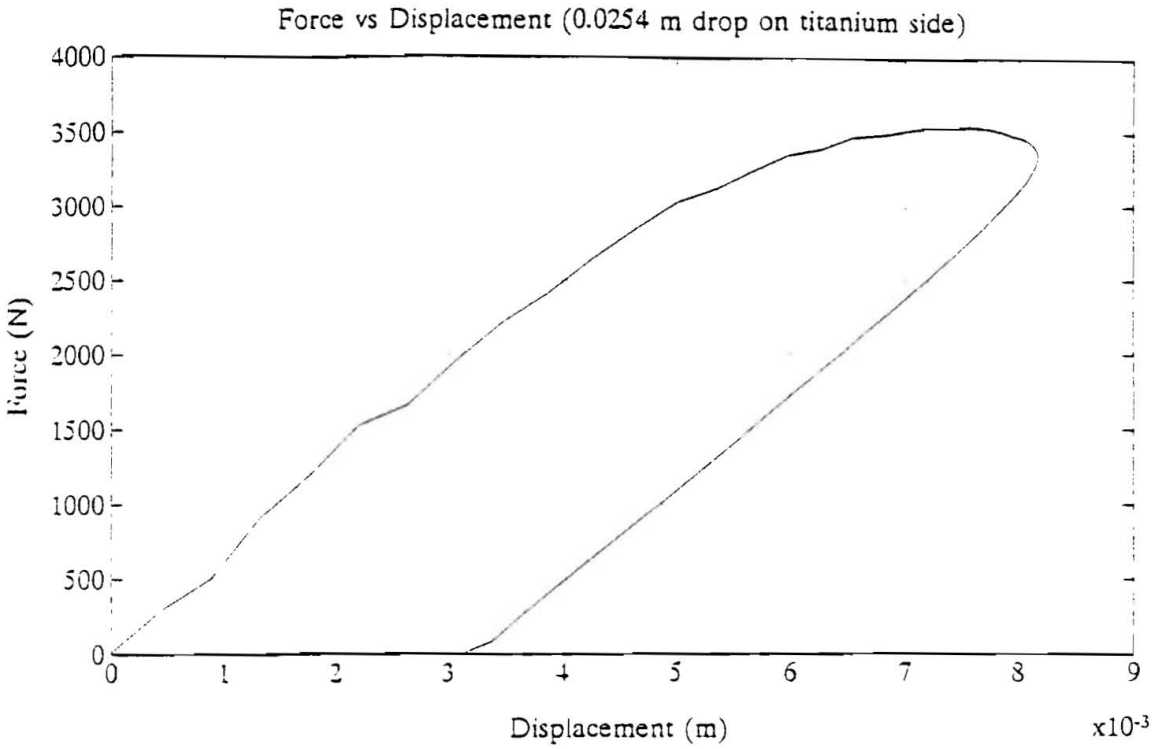
Force vs Displacement (0.0254 m drop on titanium side)
Force (N)
4000
3500
3000
2500
2000
1500
1000
500
0
0
1
2
3
4
5
6
7
8
9
Displacement (m)
x10-3

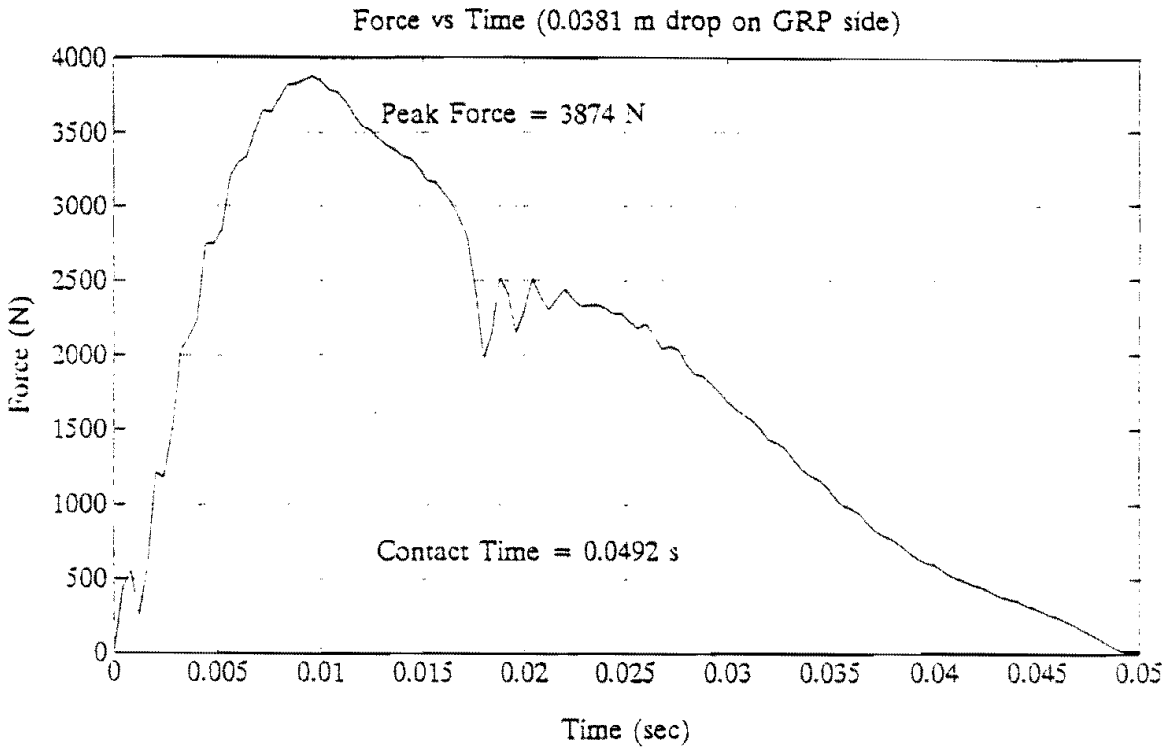
Force vs Time (0.0381 m drop on GRP side)
Peak Force = 3874 N
Contact Time = 0.0492 s
Force (N)
Time (sec)
4000
3500
3000
2500
2000
1500
1000
500
0
0
0.005
0.01
0.015
0.02
0.025
0.03
0.035
0.04
0.045
0.05

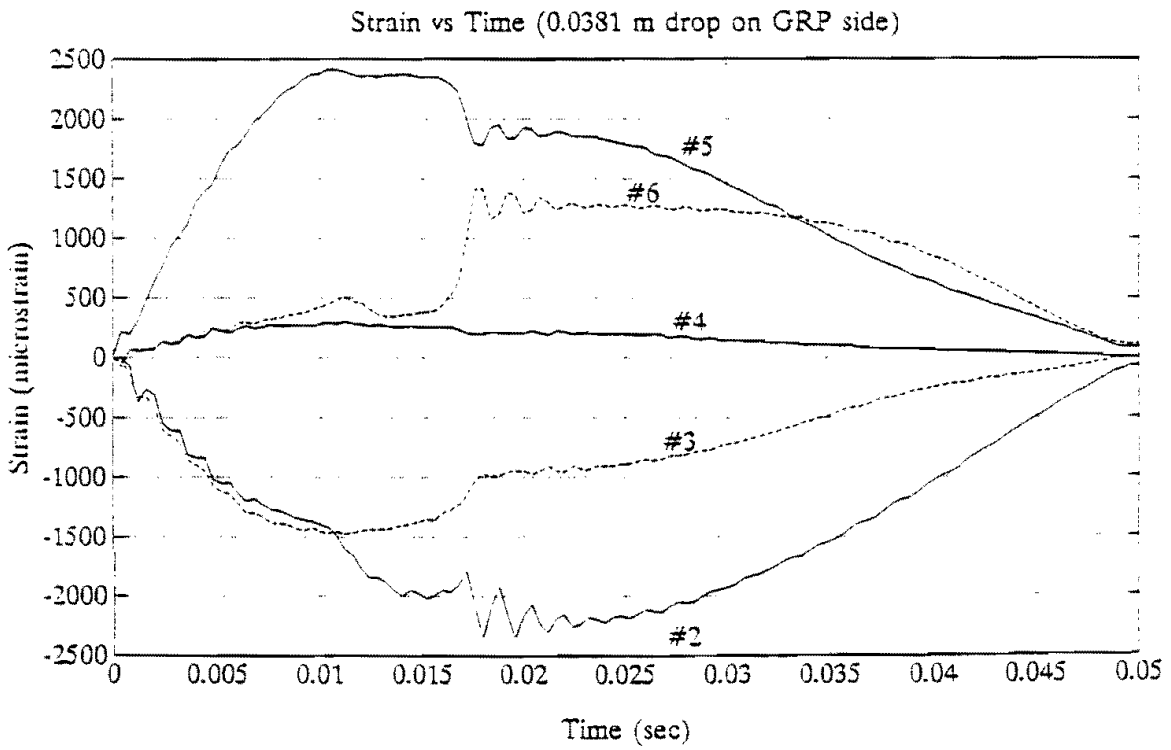
Strain vs Time (0.0381 m drop on GRP side)
#5
#6
#4
#3
#2
Strain (microstrain)
Time (sec)
2500
2000
1500
1000
500
0
-500
-1000
-1500
-2000
-2500
0
0.005
0.01
0.015
0.02
0.025
0.03
0.035
0.04
0.045
0.05

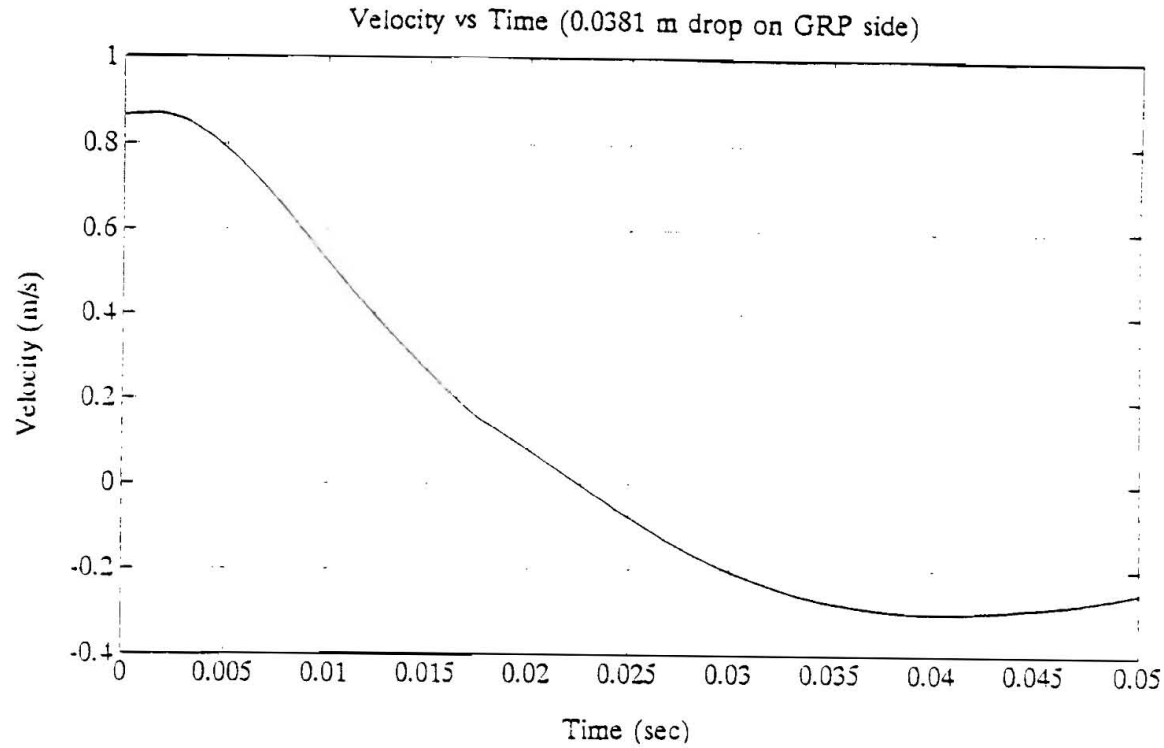
Velocity vs Time (0.0381 m drop on GRP side)
Velocity (m/s)
1
0.8
0.6
0.4
0.2
0
-0.2
-0.4
0
0.005
0.01
0.015
0.02
0.025
0.03
0.035
0.04
0.045
0.05
Time (sec)

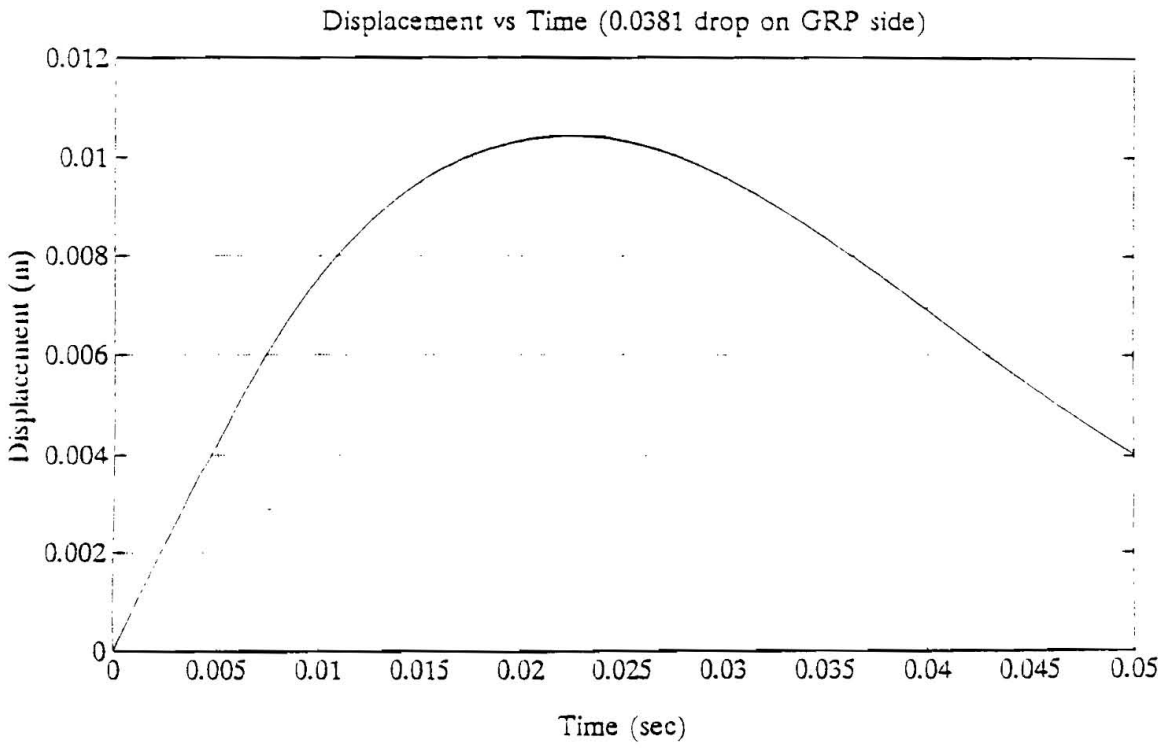
Displacement vs Time (0.0381 drop on GRP side)
Displacement (m)
0.012
0.01
0.008
0.006
0.004
0.002
0
0
0.005
0.01
0.015
0.02
0.025
0.03
0.035
0.04
0.045
0.05
Time (sec)

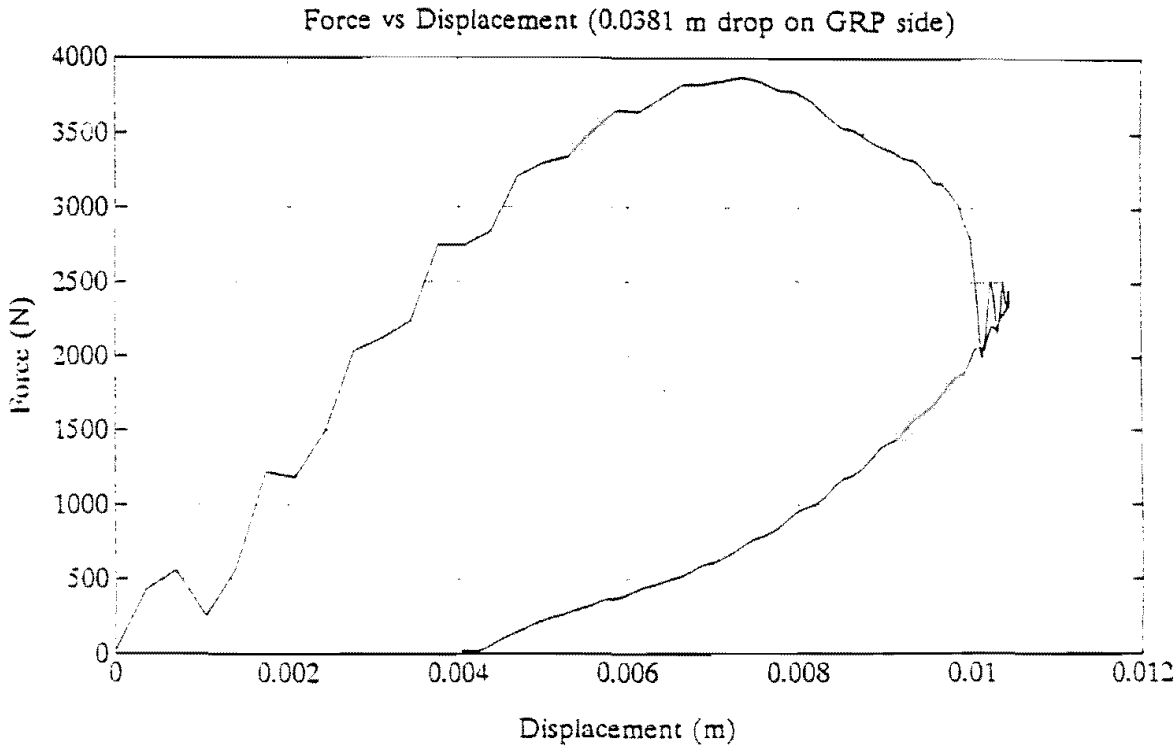
Force vs Displacement (0.0381 m drop on GRP side)
Force (N)
Displacement (m)
4000
3500
3000
2500
2000
1500
1000
500
0
0
0.002
0.004
0.006
0.008
0.01
0.012

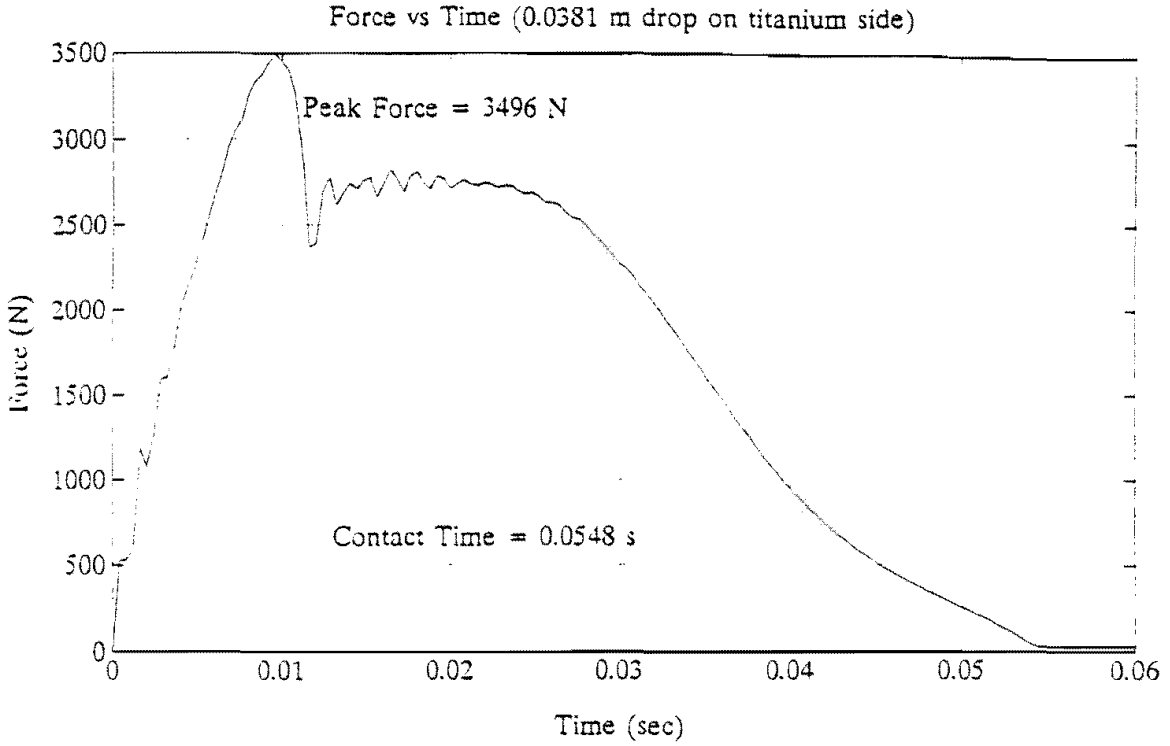
Force vs Time (0.0381 m drop on titanium side)
Peak Force = 3496 N
Contact Time = 0.0548 s
Force (N)
Time (sec)
3500
3000
2500
2000
1500
1000
500
0
0
0.01
0.02
0.03
0.04
0.05
0.06

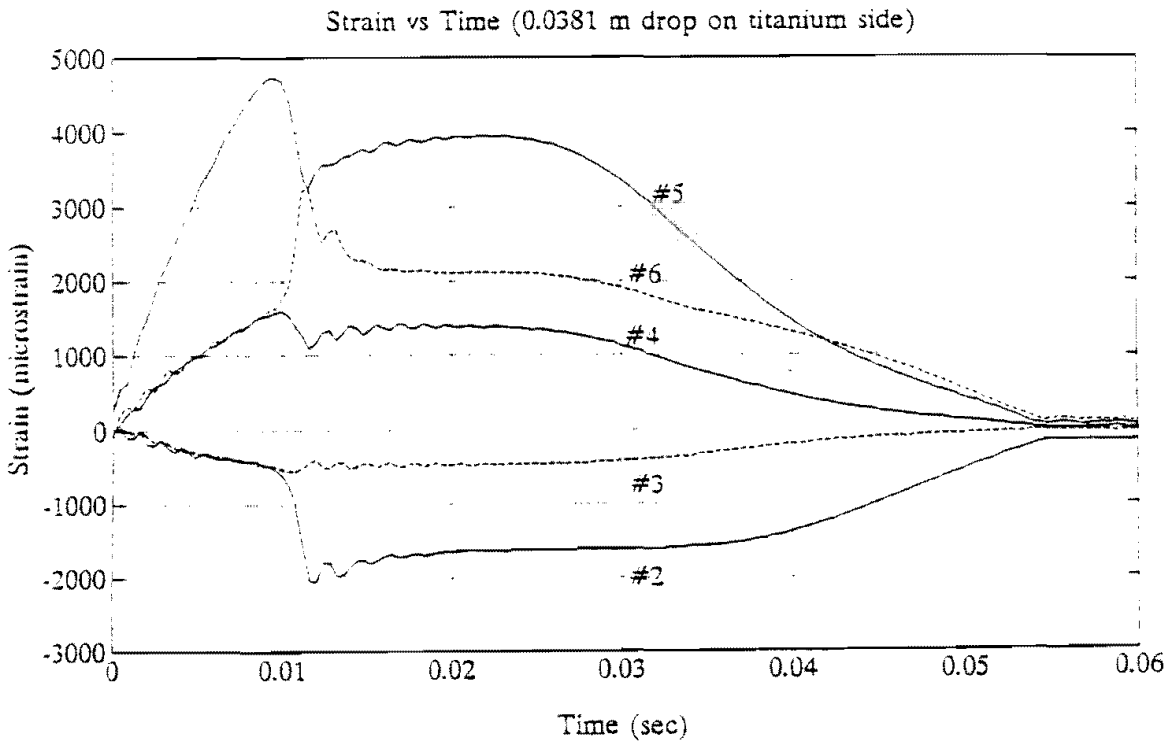
Strain vs Time (0.0381 m drop on titanium side)
#5
#6
#4
#3
#2
Strain (microstrain)
Time (sec)
5000
4000
3000
2000
1000
0
-1000
-2000
-3000
0
0.01
0.02
0.03
0.04
0.05
0.06

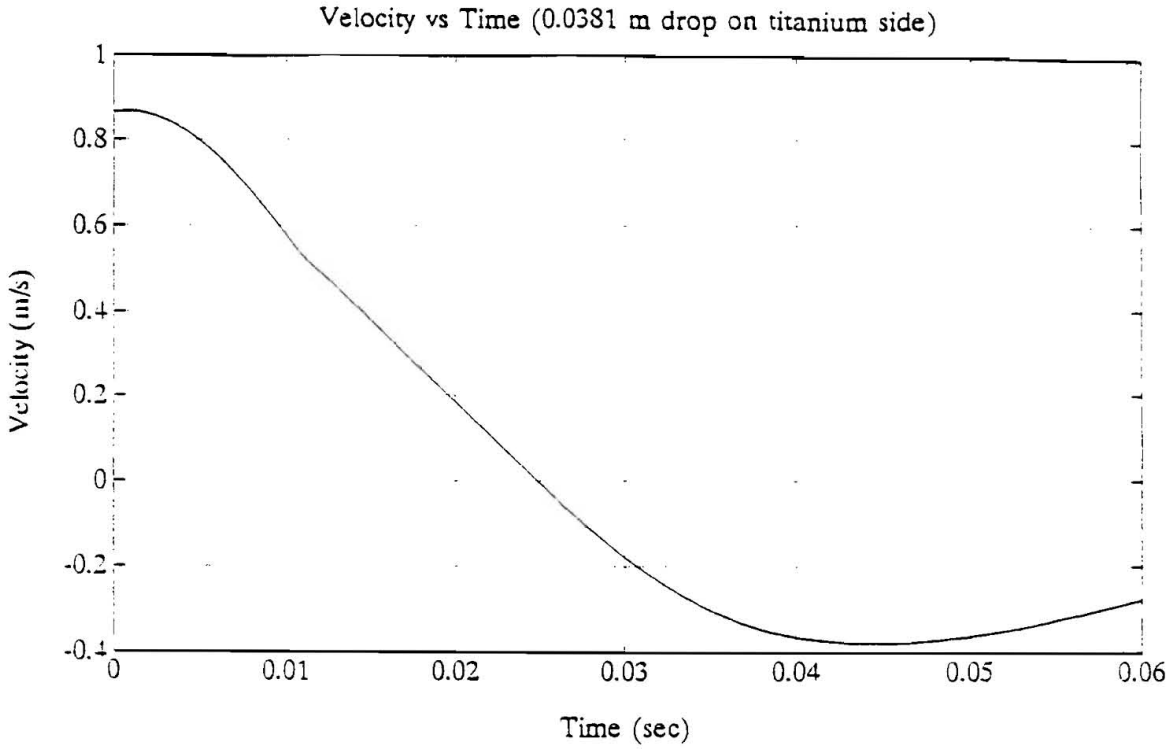
Velocity vs Time (0.0381 m drop on titanium side)
Velocity (m/s)
1
0.8
0.6
0.4
0.2
0
-0.2
-0.4
0
0.01
0.02
0.03
0.04
0.05
0.06
Time (sec)

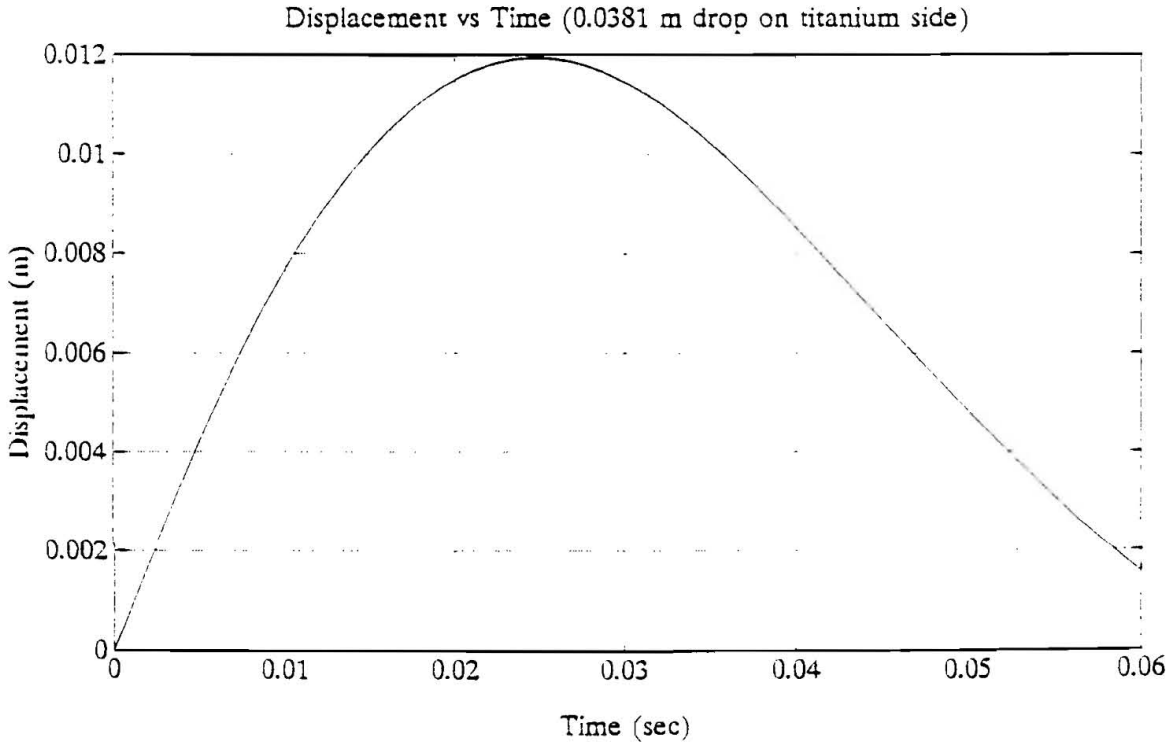
Displacement vs Time (0.0381 m drop on titanium side)
Displacement (m)
0.012
0.01
0.008
0.006
0.004
0.002
0
0
0.01
0.02
0.03
0.04
0.05
0.06
Time (sec)

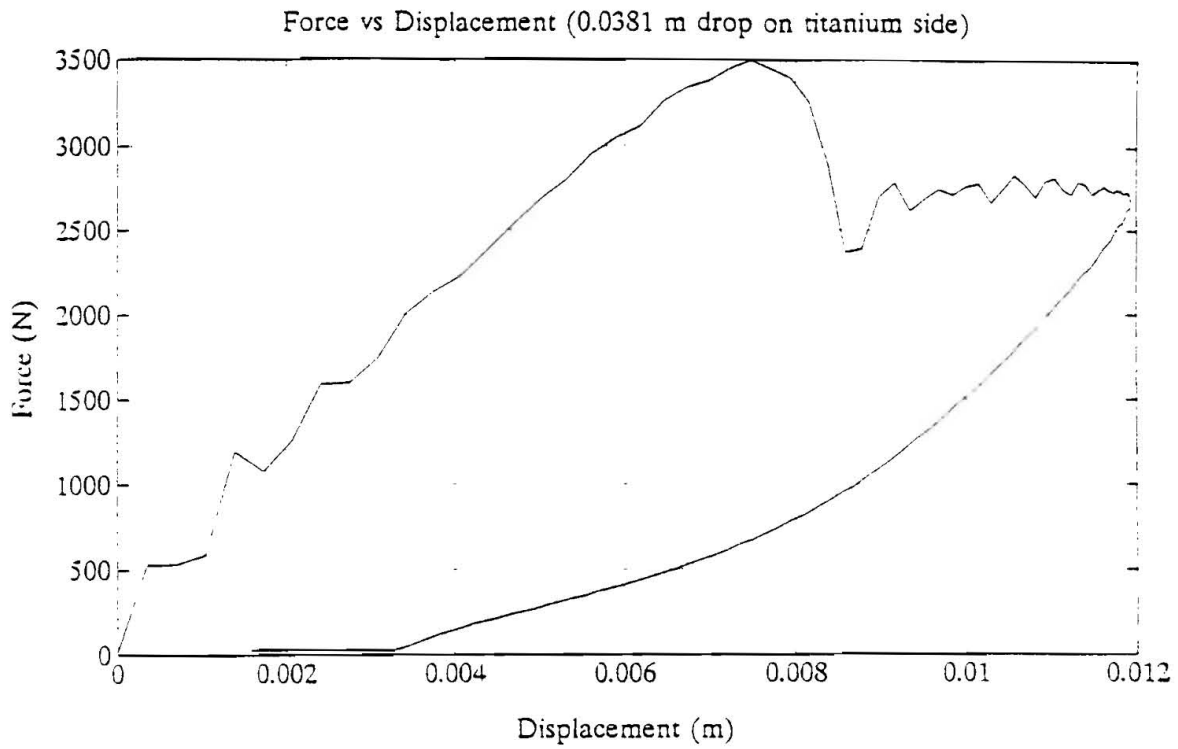
Force vs Displacement (0.0381 m drop on titanium side)
Force (N)
3500
3000
2500
2000
1500
1000
500
0
0
0.002
0.004
0.006
0.008
0.01
0.012
Displacement (m)

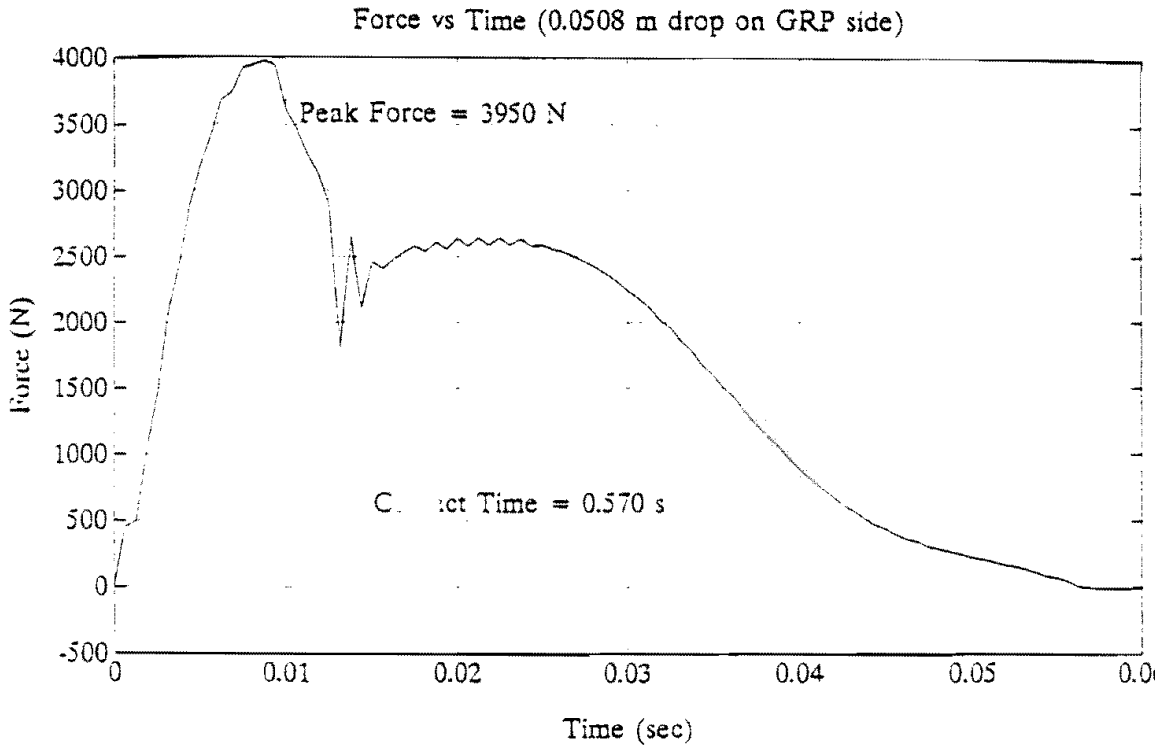
Force vs Time (0.0508 m drop on GRP side)
Peak Force = 3950 N
Force (N)
Time (sec)

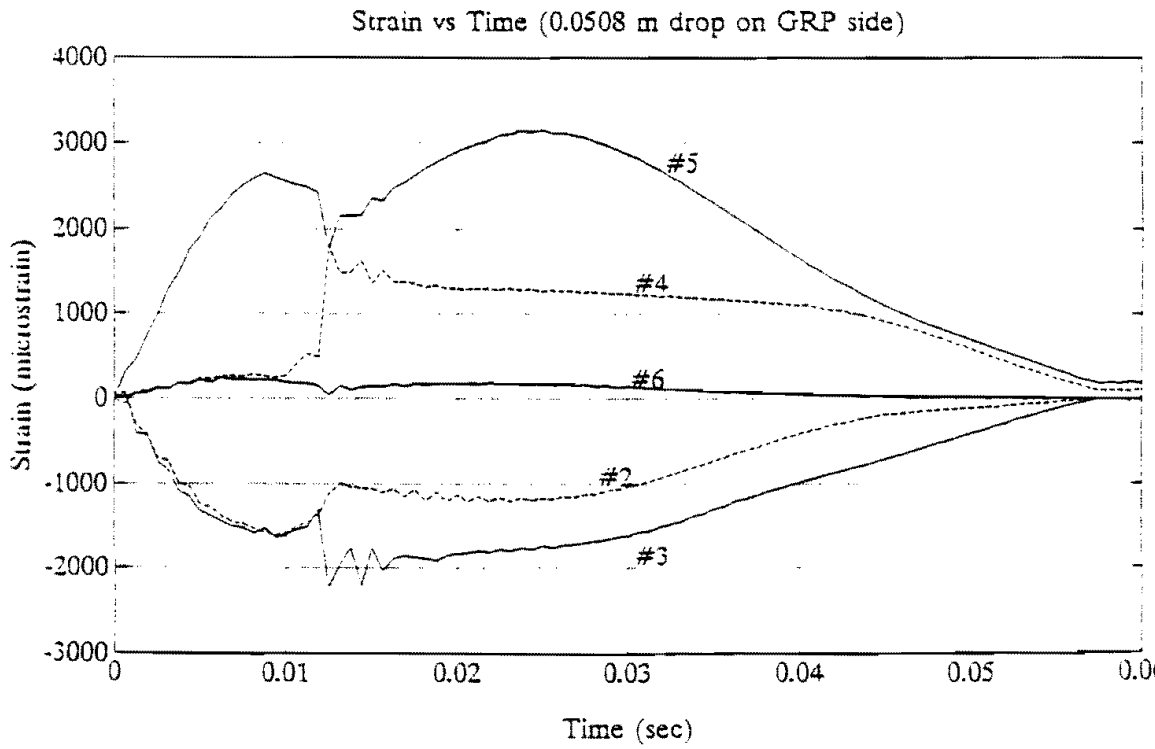
Strain vs Time (0.0508 m drop on GRP side)
#5
#4
#6
#2
#3
Strain (microstrain)
Time (sec)

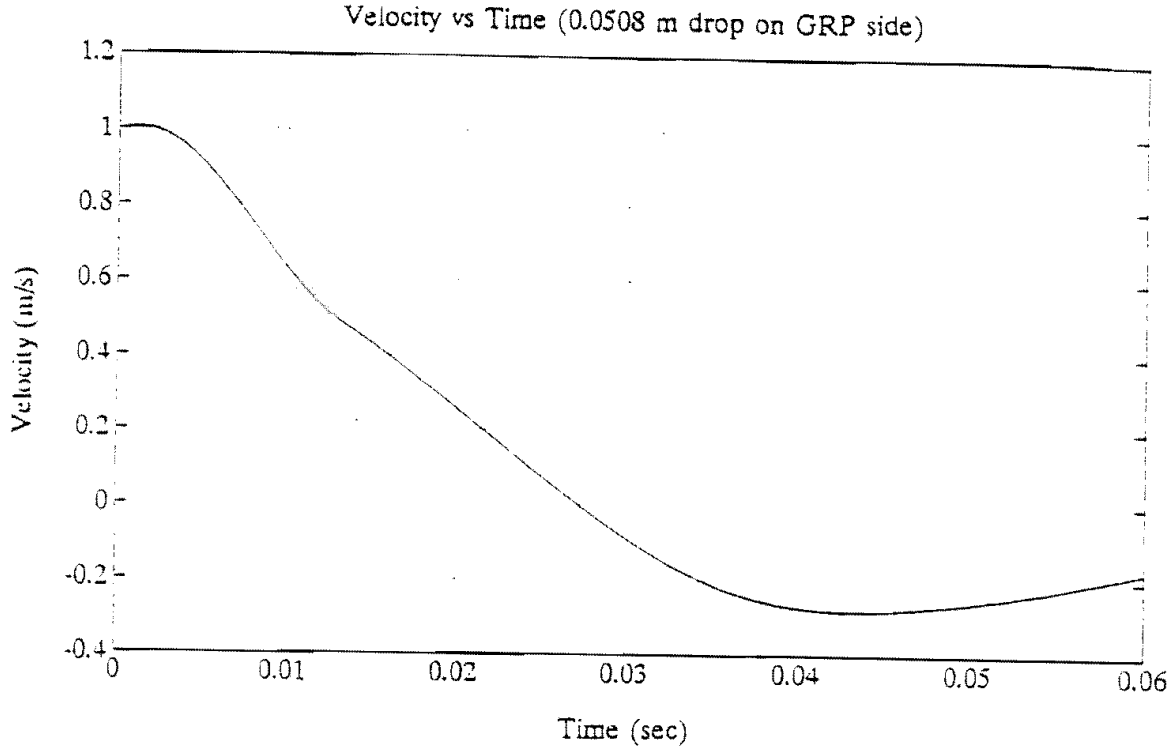
Velocity vs Time (0.0508 m drop on GRP side)
Velocity (m/s)
1.2
1
0.8
0.6
0.4
0.2
0
-0.2
-0.4
0
0.01
0.02
0.03
0.04
0.05
0.06
Time (sec)

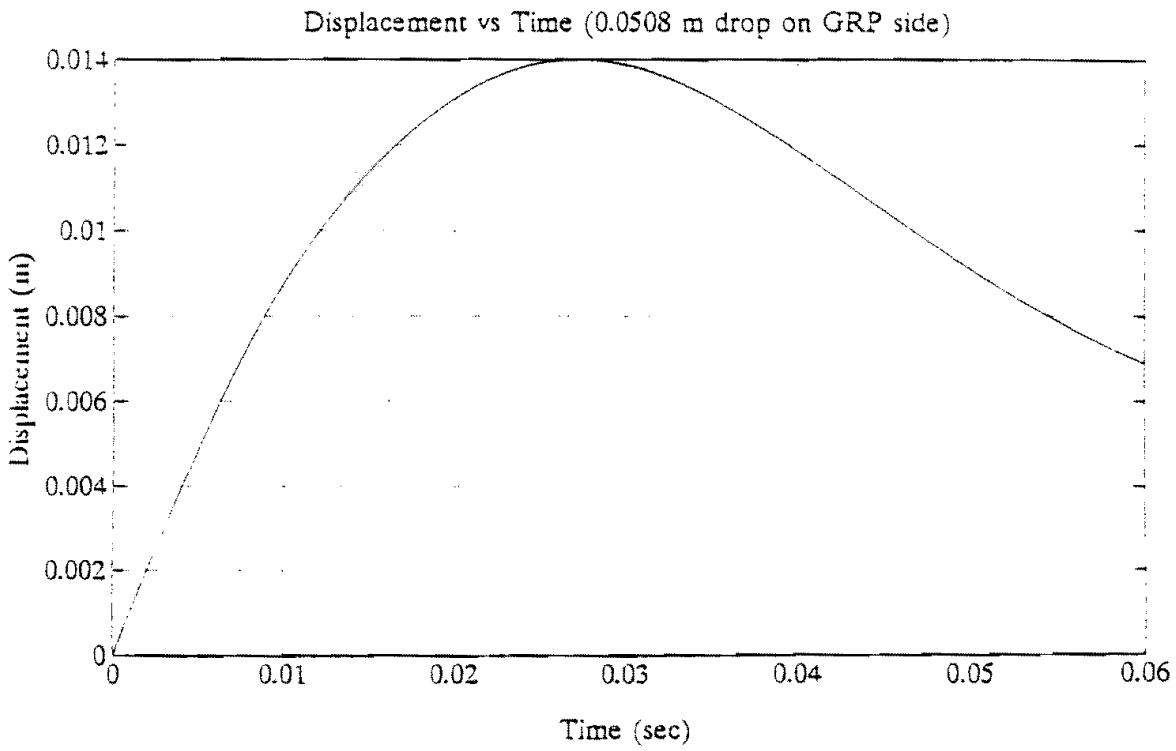
Displacement vs Time (0.0508 m drop on GRP side)
Displacement (m)
0.014
0.012
0.01
0.008
0.006
0.004
0.002
0
0
0.01
0.02
0.03
0.04
0.05
0.06
Time (sec)

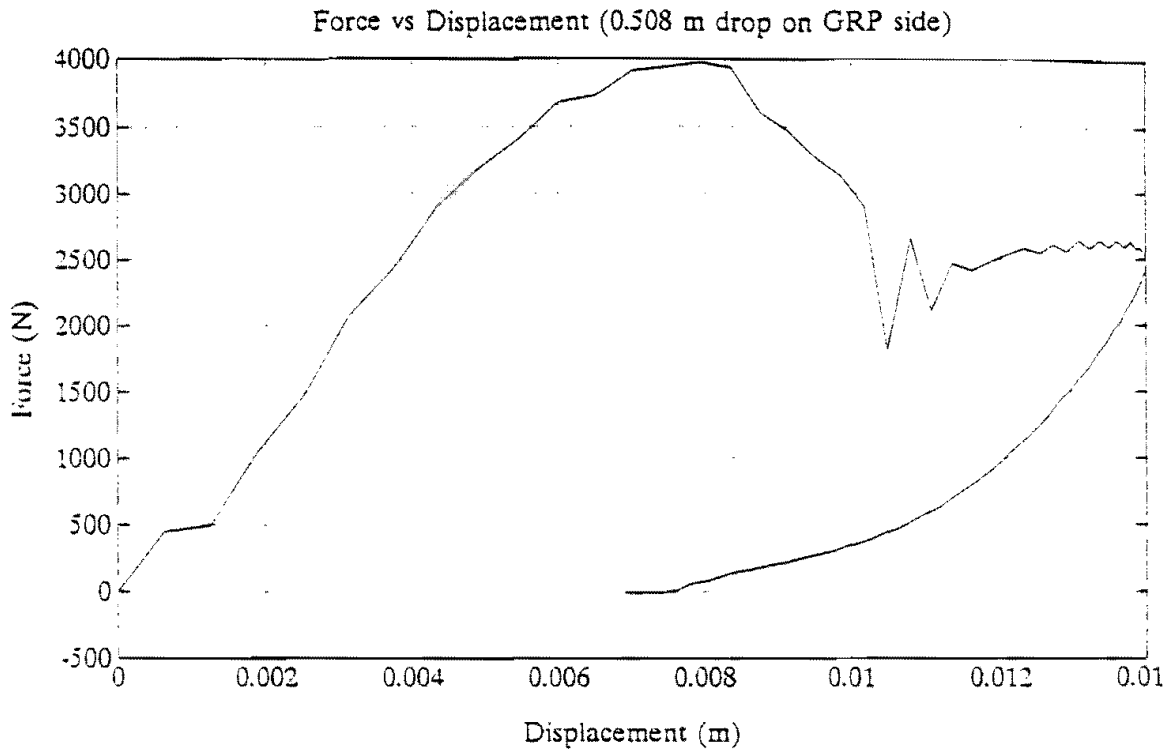
Force vs Displacement (0.508 m drop on GRP side)
Force (N)
4000
3500
3000
2500
2000
1500
1000
500
0
-500
0
0.002
0.004
0.006
0.008
0.01
0.012
0.014
Displacement (m)

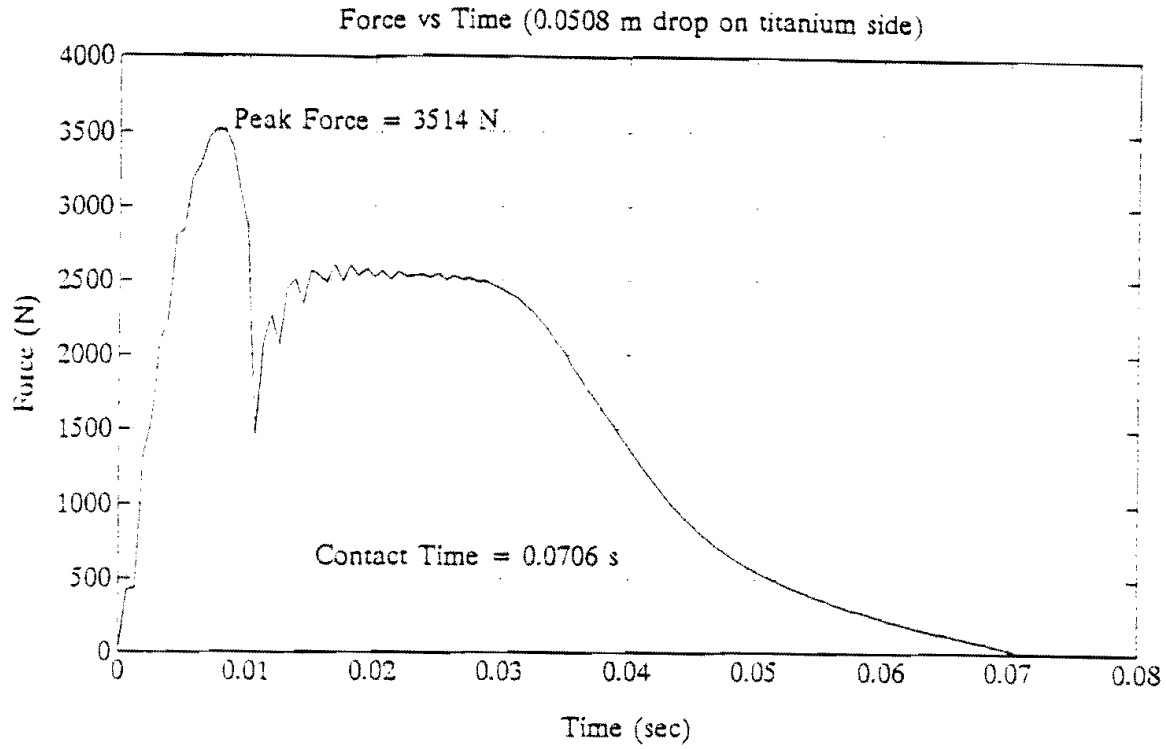
Force vs Time (0.0508 m drop on titanium side)
Peak Force = 3514 N
Contact Time = 0.0706 s
Force (N)
Time (sec)
4000
3500
3000
2500
2000
1500
1000
500
0
0
0.01
0.02
0.03
0.04
0.05
0.06
0.07
0.08

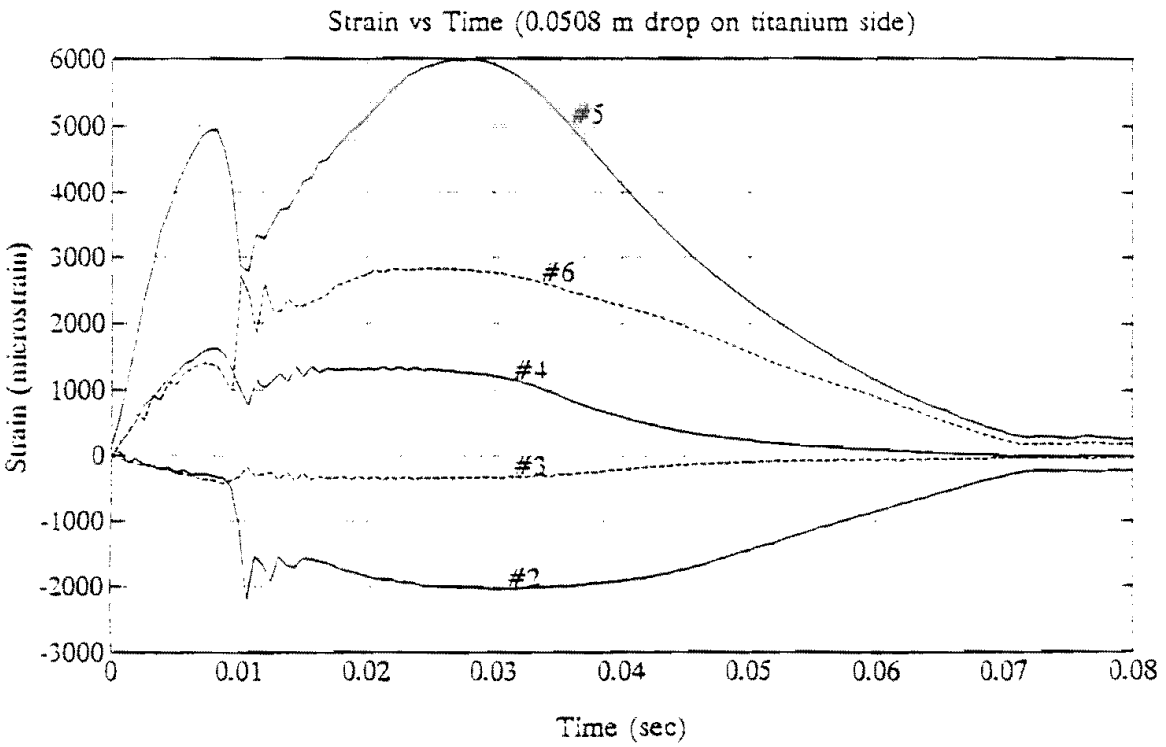
Strain vs Time (0.0508 m drop on titanium side)
#5
#6
#4
#3
#2
Strain (microstrain)
Time (sec)
6000
5000
4000
3000
2000
1000
0
-1000
-2000
-3000
0
0.01
0.02
0.03
0.04
0.05
0.06
0.07
0.08

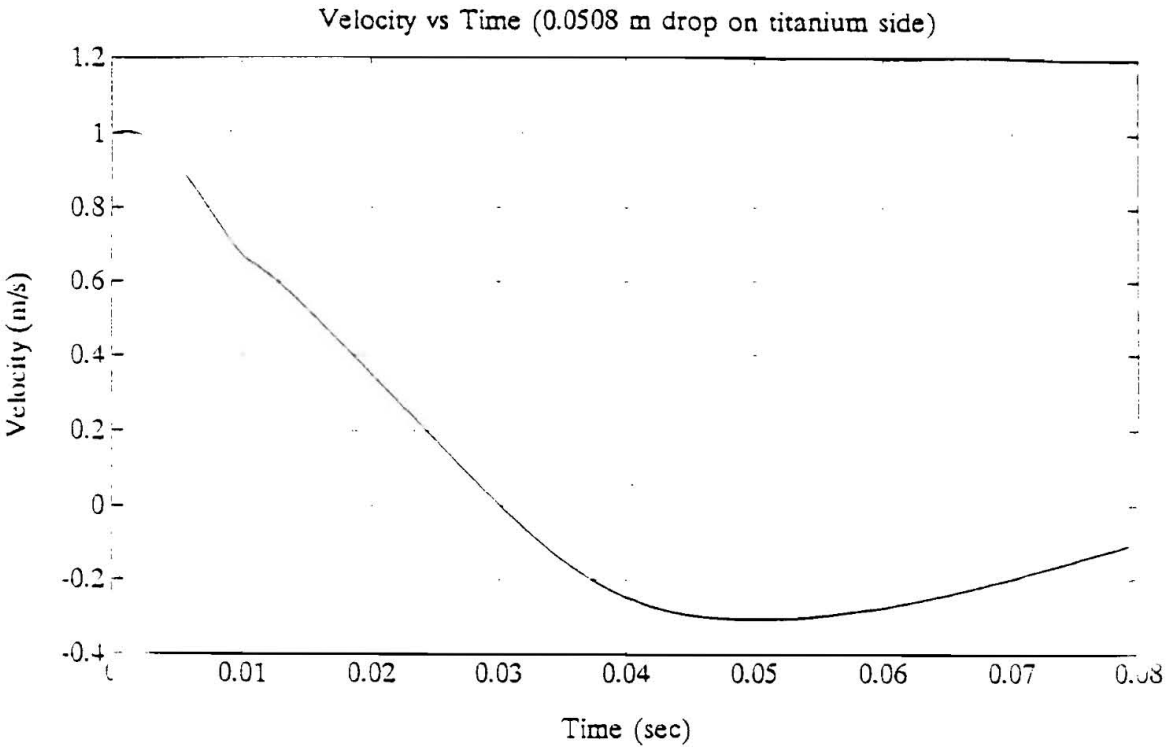
Velocity vs Time (0.0508 m drop on titanium side)
Velocity (m/s)
1.2
1
0.8
0.6
0.4
0.2
0
-0.2
-0.4
0.01
0.02
0.03
0.04
0.05
0.06
0.07
Time (sec)

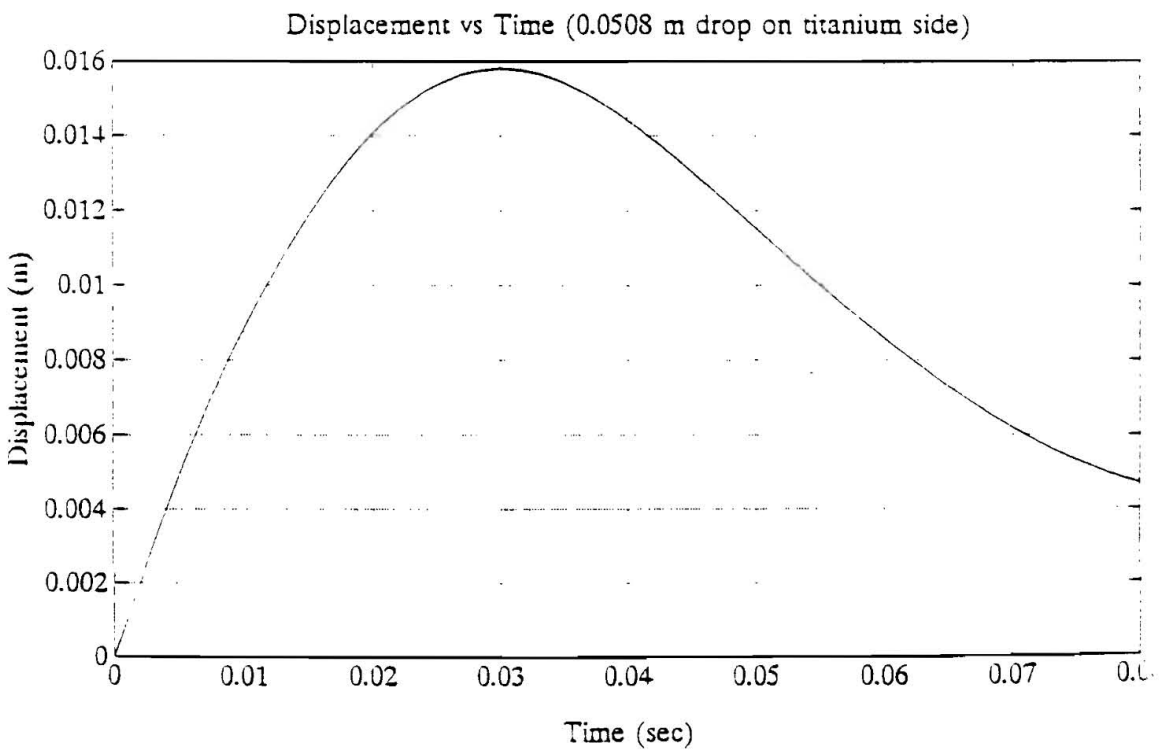
Displacement vs Time (0.0508 m drop on titanium side)
Displacement (m)
0.016
0.014
0.012
0.01
0.008
0.006
0.004
0.002
0
0.01
0.02
0.03
0.04
0.05
0.06
0.07
Time (sec)

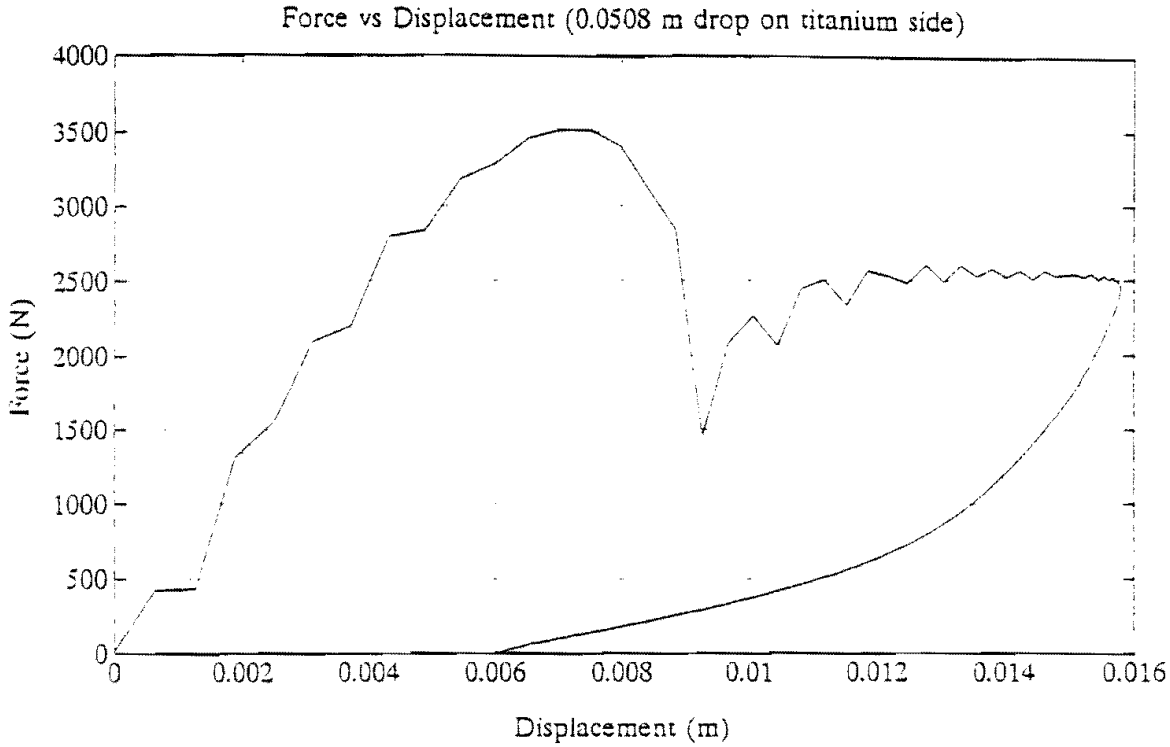
Force vs Displacement (0.0508 m drop on titanium side)
Force (N)
4000
3500
3000
2500
2000
1500
1000
500
0
0
0.002
0.004
0.006
0.008
0.01
0.012
0.014
0.016
Displacement (m)

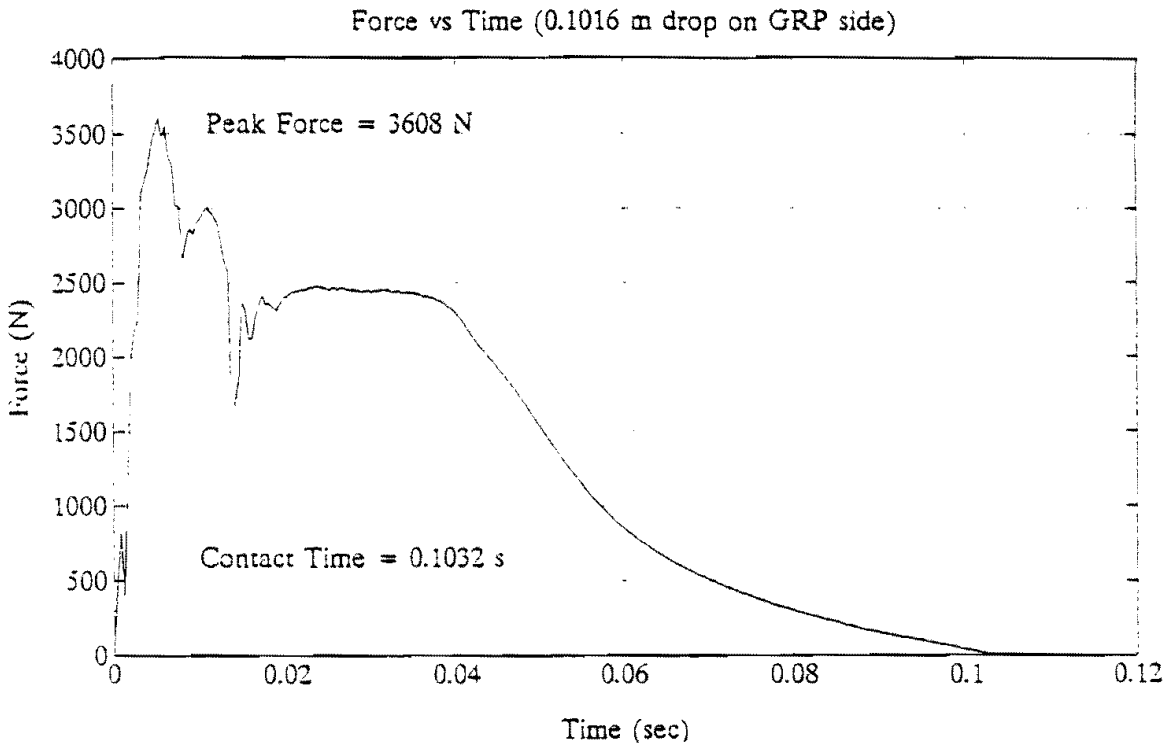
Force vs Time (0.1016 m drop on GRP side)
Peak Force = 3608 N
Contact Time = 0.1032 s
Force (N)
Time (sec)
4000
3500
3000
2500
2000
1500
1000
500
0
0.02
0.04
0.06
0.08
0.1
0.12

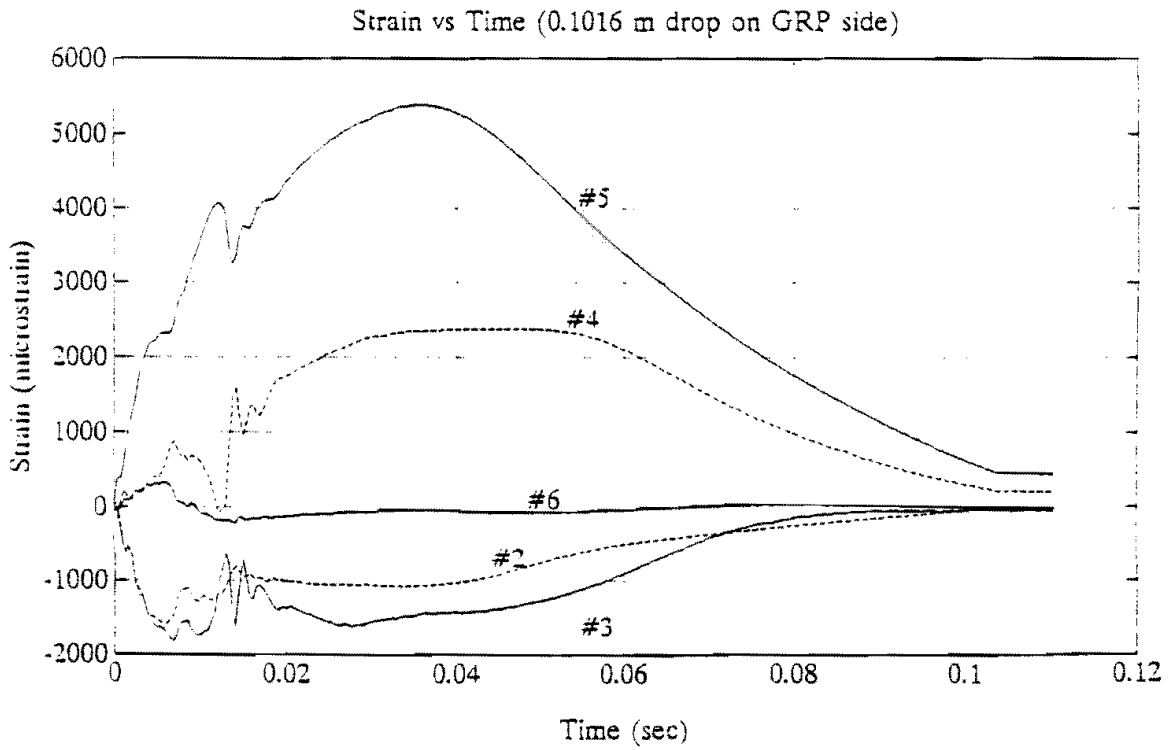
Strain vs Time (0.1016 m drop on GRP side)
Strain (microstrain)
Time (sec)
#5
#4
#6
#2
#3
6000
5000
4000
3000
2000
1000
0
-1000
-2000
0
0.02
0.04
0.06
0.08
0.1
0.12

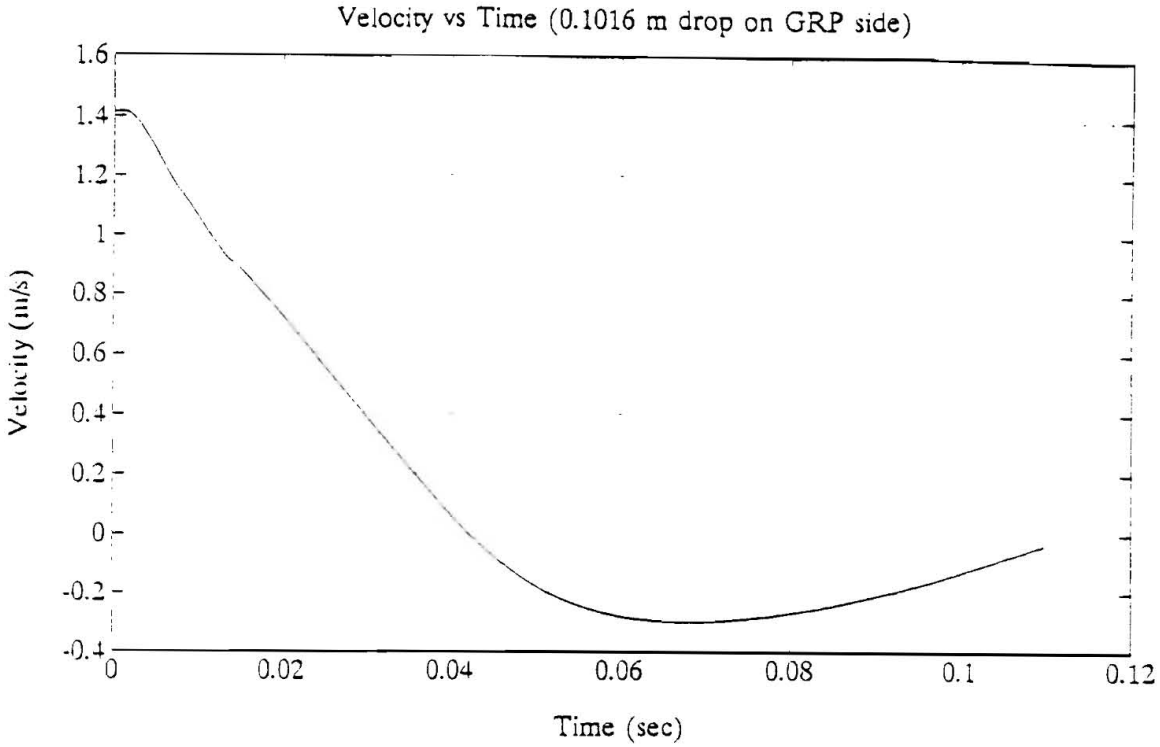
Velocity vs Time (0.1016 m drop on GRP side)
Velocity (m/s)
1.6
1.4
1.2
1
0.8
0.6
0.4
0.2
0
-0.2
-0.4
0
0.02
0.04
0.06
0.08
0.1
0.12
Time (sec)

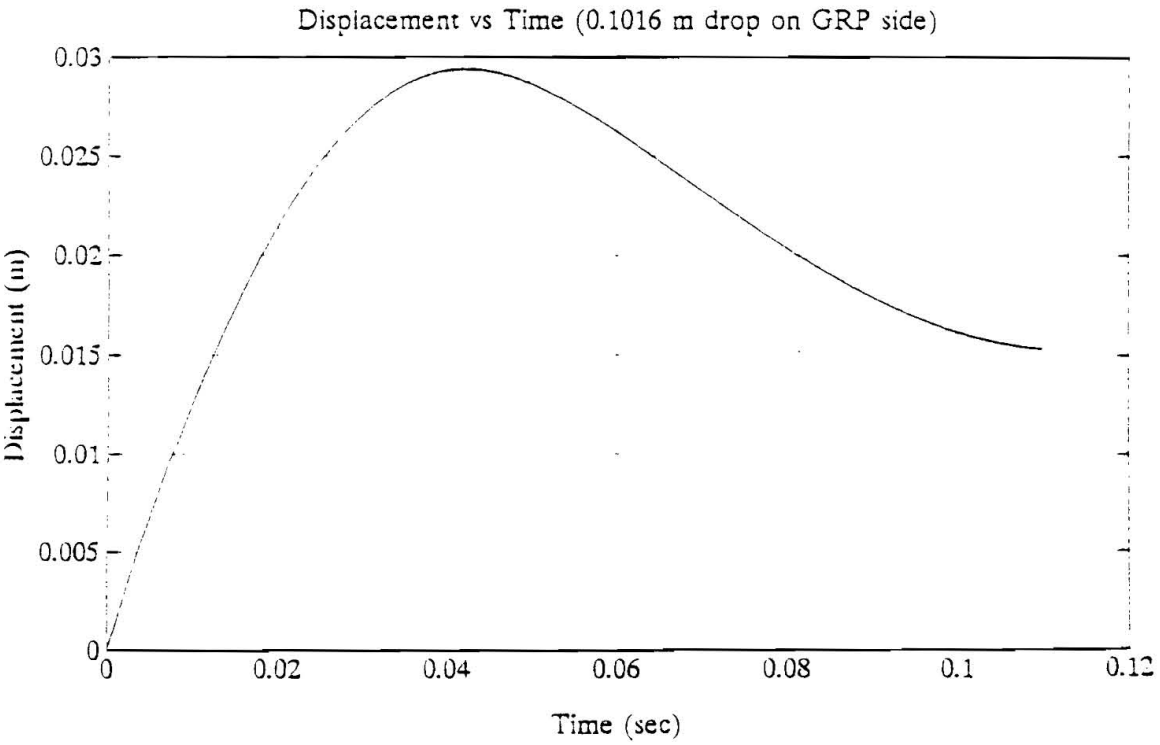
Displacement vs Time (0.1016 m drop on GRP side)
Displacement (m)
0.03
0.025
0.02
0.015
0.01
0.005
0
0
0.02
0.04
0.06
0.08
0.1
0.12
Time (sec)

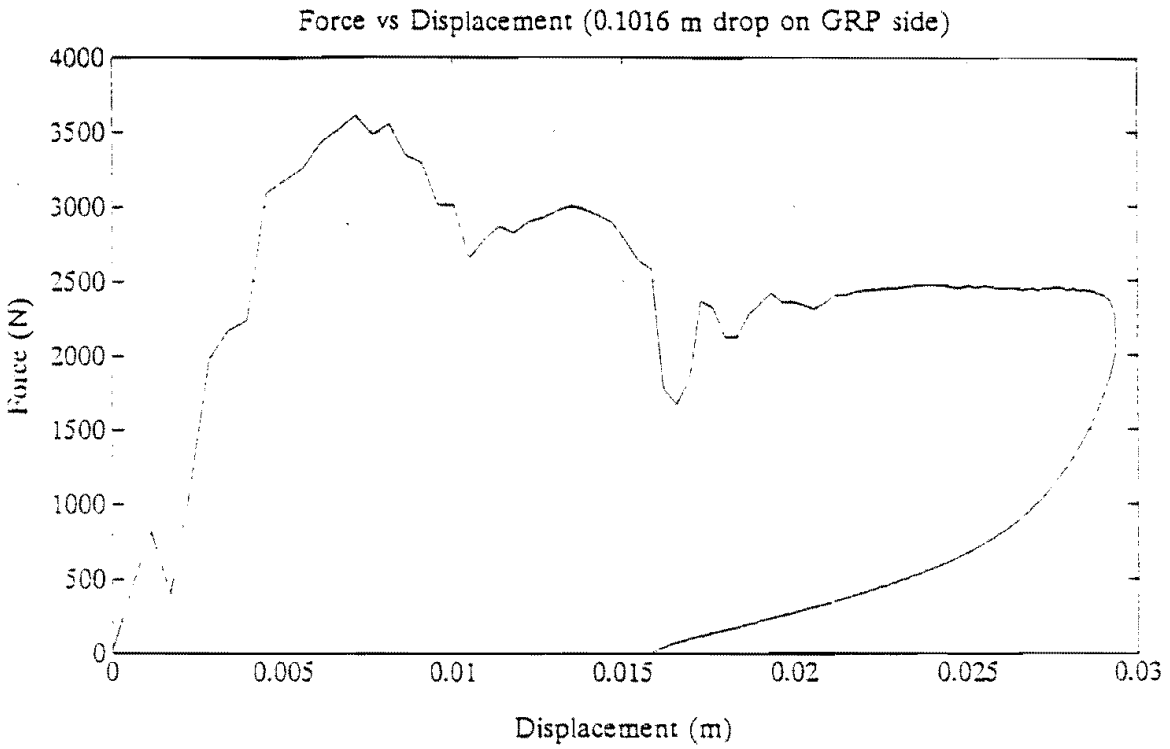
Force vs Displacement (0.1016 m drop on GRP side)
Force (N)
4000
3500
3000
2500
2000
1500
1000
500
0
0
0.005
0.01
0.015
0.02
0.025
0.03
Displacement (m)

LIST OF REFERENCES

1. Murphy, M. C., (1993) *A Study of the Structural Stability of an Unbalanced Sandwich Composite Configuration,* Master's Thesis, Naval Postgraduate School, Monterey, California.

2. Kim, C., and Jun, E., (1992) "Impact Resistance of Composite Laminated Sandwich Plates," *Journal of Composite Materials,* 26, 15.

3. Nemes, J. A., and Simmonds, K. E., (1992) "Low-Velocity Impact Response of Faom-Core Sandwich Composites," *Journal of Composite Materials,* 26, 4.

4. Lee, L. J., Huang, K. Y., and Fann, Y. J., (1993) "Dynamic Response of Composite Sandwich Plate Impacted by a Rigid Ball," *Journal of Composite Materials,* 27, 13.

5. Sioblom, P. O., Hartness, J. T., and Cordell, T. M., (1988) *"On Low-Velocity Impact Testing of Composite Materials,"* Journal of Composite Materials, 22, January.

6. Kelkar, A. D., Craft, W. J., and Sandhu, R. S., (1993) *"Study of Progressive Damage in Thin and Thick Composite Laminates Subjected to Low-Velocity Impact Loading,"* Recent Advances in Structural Mechanics, PVP-Vol 269/NE-Vol. 13, ASME.

7. David Taylor Research Center, DTRC-SME88/73, *Instrumented Impact Testing of Composite Materials,* by R. M. Crane and T. D. Juska, January 1989.

INITIAL DISTRIBUTION LIST

		No. Copies
1.	Defense Technical Information Center Cameron Station Alexandria VA 22304-6145	2
2.	Library, Code 052 Naval Postgraduate School Monterey CA 93943-5002	2
3.	Professor Y.W. Kwon, Code ME/Kw Department of Mechnical Engineering Naval Postgraduate School Monterey CA 93943-5000	2
4.	Department Chairman, Code ME/Kk Department of Mechnical Engineering Naval Postgraduate School Monterey CA 93943-5000	1
5.	Naval Enineering Curricular Office, Code 34 Naval Postgraduate School Monterey CA 93943-5000	1
6.	Dr. Vincent J. Castelli Naval Surface Warfare Center, Carderock Div. Composites and Resins Branch, Code 644 Annapolis MD 21402-5067	1
7.	Dr. Roger M. Crane Naval Surface Warfare Center, Carderock Div. Composites and Resins Branch, Code 644 Annapolis MD 21402-5067	1
8.	Dr. Y.D. Rajapakse Office of Naval Research Mechanics Division, Code 1132 800 North Quincy Street Arlington VA 22217-5000	1
9.	Mr. David Bonnani Naval Surface Warfare Center, Carderock Div. Code 1720.2 Bethesda MD 20084-5000	1

10. Dr. Phillip B. Abraham 1
Office of Naval Research
Mechanics Division, Code 1132
800 North Quincy Street
Arlington VA 22217-5000

11. Lt. Bryant Fuller 2
Puget Sound Naval Shipyard
Bremerton WA 98314-5001